

12-2010

Analyzing the Role of $\alpha v \beta 8$ Integrin in Glioma-Induced Angiogenesis

Jeremy H. Tchaicha

Follow this and additional works at: https://digitalcommons.library.tmc.edu/utgsbs_dissertations



Part of the [Cancer Biology Commons](#)

Recommended Citation

Tchaicha, Jeremy H., "Analyzing the Role of $\alpha v \beta 8$ Integrin in Glioma-Induced Angiogenesis" (2010). *The University of Texas MD Anderson Cancer Center UTHealth Graduate School of Biomedical Sciences Dissertations and Theses (Open Access)*. 90.

https://digitalcommons.library.tmc.edu/utgsbs_dissertations/90

This Dissertation (PhD) is brought to you for free and open access by the The University of Texas MD Anderson Cancer Center UTHealth Graduate School of Biomedical Sciences at DigitalCommons@TMC. It has been accepted for inclusion in The University of Texas MD Anderson Cancer Center UTHealth Graduate School of Biomedical Sciences Dissertations and Theses (Open Access) by an authorized administrator of DigitalCommons@TMC. For more information, please contact digitalcommons@library.tmc.edu.

CHAPTER 1:

Introduction and Background

Human CNS & Neurovascular Units

The human central nervous system (CNS) contains a rich vascular network consisting of billions of glia and neurons that have innumerable associations with blood vessels (1). Most notably, blood vessels function to deliver vital nutrients and oxygen to satisfy the metabolic demands of the brain, but also function to communicate with brain parenchymal cells. This fundamental communication has been correlated to proper CNS development and homeostasis (2). Blood vessels in the brain have unique structural and functional features known as the blood brain barrier (BBB). Endothelial cells lay the foundation for the BBB, which regulates the movement of molecules in and out of the brain parenchyma (3). The endothelial cells of the BBB are joined by adherens and tight junctions and lack the common fenestrations found in peripheral organ vascular beds (4). This barrier allows for the selective transport of oxygen and carbon dioxide via simple diffusion while nutrient transfer, i.e. glucose usually occurs via active transport (5).

The cellular interface between vascular and nervous systems, or the neurovascular unit (NVU), is crucial for the development and homeostasis of the BBB (6). The NVU is a multi-cellular complex made up of vascular, neural and glial cell types (Figure 1) (7). Ablumenally, the endothelial cells are surrounded by a basement membrane rich in extracellular matrix (ECM) proteins. Like other organs, smooth muscle cells and pericytes provide structural support for blood vessels in

the brain. Adjacent to the vascular/pericyte complex are the astrocytes and neurons. While astrocytes have many functions, they are best known for their support of the BBB integrity via their astrocytic endfeet (8). They are also important for regulating oxygen and nutrient provisions for the neural tissue. Neuronal interactions with astrocytes are essential to modulate rates of cerebral blood flow as required for proper nervous tissue homeostasis (6). The astrocytic endfeet interact with many ECM ligands present in the cerebral blood vessel's basement membrane through various cell-surface adhesion molecules, such as integrins (9).

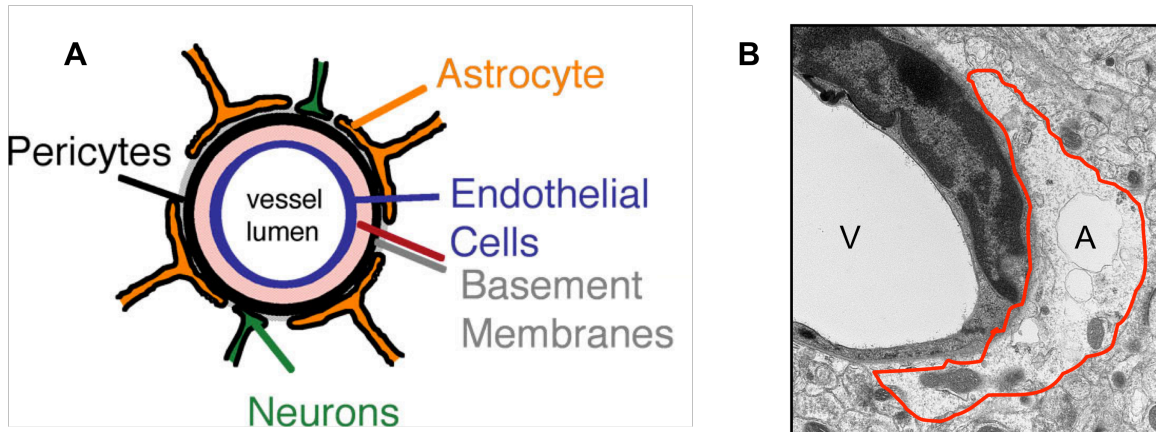


Figure 1. The Neurovascular Unit

(A) At the vascular lumen, endothelial cells are connected by tight junctions that form the BBB. Astrocytic endfeet play roles in tight junction maintenance and structural support. Neurons and NSCs also closely juxtapose the cerebral blood vasculature. This figure was adapted from McCarty et al. 2005 (4). (B) A 20,000x transmission electron micrograph illustrates the juxtaposition of an astrocyte (A-outline in red) to a cerebral blood vessel (V).

Integrins

Integrins are transmembrane glycoproteins that are comprised of a single (α) and beta (β) subunit that heterodimerize in the endoplasmic reticulum and golgi prior to arrival at the cell surface (Figure 2b) (10). These subunits form a non-covalent complex and contain small transmembrane and cytoplasmic domains and a large extracellular domain (11). In humans, there are 18 α subunits and 8 β subunits that lead to 24 heterodimeric combinations (Figure 2a) (10). The α subunits are generally larger than their β subunit binding partners (11). β subunits contain disulfide-rich bonds, an extracellular domain consisting of four repeats of forty amino acid cysteine-rich motifs and a relatively small cytoplasmic domain (11). Integrins are metazoan-restricted and are considered to be major adhesion receptors to ECM proteins although some are involved in cell-cell interactions (12). These two fundamental roles allow for cell attachment to the ECM as well as the ability to harbor those ECM signals intracellularly (13). Integrins regulate many cellular processes including, but not limited to, migration, proliferation, invasion and angiogenesis during normal embryogenesis and development (11) into adulthood (14). They have been implicated in a variety of diseases including many different types of cancer (15).

Integrins become activated in two different ways: inside-out or outside-in signaling (16). One commonality between the two signaling mechanisms is the necessity of the transmembrane domain to facilitate a signal across the cell membrane (17). Inside-out signaling involves an extracellular ligand binding its cognate receptor, which causes a structural change in the talin protein, leading to

binding at the NPxY motif of the β subunit's cytoplasmic tail (18). Furthermore, Kindlin-3 is essential for talin's role in integrin activation (19). The head region of talin, like many other integrin-recruited proteins, contains a FERM (Protein 4.1, Ezrin, Radixin, Moesin) domain that binds to and can activate integrins. Talin also links the integrin to the actin cytoskeleton upon interacting with alpha-actinin and vinculin (20). The intracellular signaling events that occur upon cytoplasmic interactions are very complex and some are cell-type specific (17). In the inactive state, integrin α and β subunits associate tightly with one another, but upon talin's interaction with the β subunit's cytoplasmic tail, a conformation change causes the alpha and beta extracellular domains to separate (10), allowing for increased affinity for ECM ligands (13). Conversely, outside-in signaling involves signals from the ECM to the inside of the cell. Upon binding to ECM ligands, integrins cluster in the membrane and signal inside of the cell (10). Both ways of signaling allow for cell anchorage to the ECM via cytoskeletal associations upon integrin activation.

Integrin ECM ligand specificity can be divided into four major groups: [1] laminin-binding, [2] collagen-binding, [3] leukocyte and [4] arginine-glycine-aspartate (RGD)-recognizing integrins (21). Laminin-binding integrins include $\alpha 3\beta 1$, $\alpha 6\beta 1$, $\alpha 6\beta 4$ and $\alpha 7\beta 1$, although these integrins do bind other ECM proteins (22). The α subunits are thought to be the major player in ligand-specificity (23). Although these three alpha subunits have significant sequence similarities to one another, their specificity is distinct based upon the β subunits they dimerize with at the cell surface. For instance, although $\alpha 6\beta 1$ and $\alpha 6\beta 4$ share the same alpha subunit, they tend to bind different laminins in the ECM (23). Based upon this

information, laminin-binding heterodimers retain higher affinities for different laminins present in the ECM (24).

Collagen-binding integrins include α subunits 1, 2, 10, 11 that all interact with $\beta 1$ to form heterodimers (25). Similar to most alpha subunits, their heads are created from a 7-bladed β -propeller domain that interacts with the α I-domain in specific locales (10). Structurally, these specific integrins are similar, but their affinity for certain subtypes of collagen is evident (26). For instance, $\alpha 1\beta 1$ preferentially binds Type IV collagen, whereas $\alpha 2\beta 1$ has increased affinity for fibrillar collagens (27) and play different roles in cellular processes, such as cell proliferation and matrix remodeling, respectively (28).

Leukocyte-expressed integrins include $\alpha 4\beta 7$, $\alpha E\beta 7$ and αL , αM , αX and αD , all of which bind $\beta 2$ (29). They play roles in naïve T-cell circulation, activation and eventual T cell homing and localization (30). In areas of infection or inflammation, leukocytes extravasate from the circulation heavily mediated by integrin expression. Integrins aid in immobilizing the leukocytes upon the infected site's endothelium and function to direct their migration across the endothelium's basement membrane to aid in the anti-inflammatory response (31). These integrins are expressed in other circulating immune cells and they also mediate cell-cell adhesion via counter receptors, such as V-CAM 1 and I-CAM 1.

Lastly, arginine-glycine-aspartate (RGD)-binding integrins include the αv subfamily of integrins ($\alpha v\beta 1$, $\beta 3$, $\beta 5$, $\beta 6$, $\beta 8$), $\alpha 5\beta 1$, $\alpha 8\beta 1$ and $\alpha 11\beta 3$ (29). The RGD tripeptide motif is present in a variety of ECM ligands including vitronectin, fibronectin and latent-associated peptide (LAP)-TGF β . The RGD motif interacts

with the α and β subunits where the arginine has affinity for the β -propeller component of the α subunit and the aspartate interacts with the von-Willebrand factor A-domain of the β subunit (32). LAP-TGF β s have the RGD tripeptide motif in the LAP portion of the inactive cytokine. Upon α v β 6 integrin binding of the motif, the inactive cytokine is activated allosterically (17). Similarly, α v β 8 integrin has been shown to bind the same motif and recruit metalloproteinases to aid in the cleaving of the pro-peptide into an active cytokine (33).

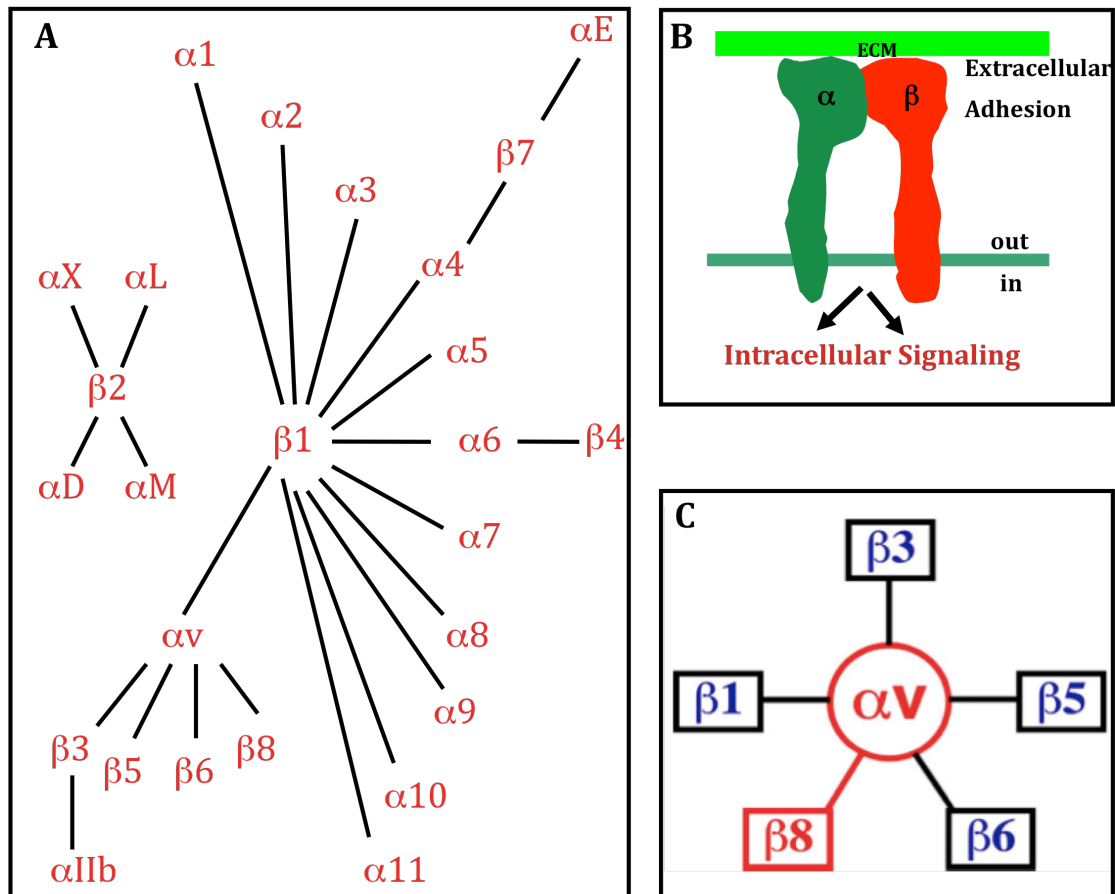


Figure 2. Mammalian Integrin Family

(A) The mouse and human integrin family trees are comprised of 18 α and 8 β genes that can form 24 heterodimeric combinations. This figure was adapted from Hynes et al. 2002 (29). (B) Integrins are comprised of a single α and single β subunit that are involved in extracellular adhesion and intracellular signaling. (C) Our laboratory focuses upon the αv subfamily of integrins, which binds with 5 different β subunits: $\beta 1$, $\beta 3$, $\beta 5$, $\beta 6$ and $\beta 8$. This dissertation examines the roles of $\alpha v\beta 8$ in glioma-induced angiogenesis.

α v Integrins

The primary group of RGD-binding integrins is the α v subfamily. As mentioned above, α v binds five different β subunits, β 1, β 3, β 5, β 6, β 8 (Figure 2c). α v integrins are broadly expressed throughout the body on a variety of different cell types. Some include epithelial, vascular and CNS cell types that indicates α v integrins' involvement in a multitude of cellular processes (34). To determine the necessity of the α v subfamily of integrins during various processes, ranging from development to birth, a mouse harboring a α v integrin null gene was created. It was evident that there were developmental issues concerning the loss of α v integrin, as neonates were not being born in the normal Mendelian ratios (1:2:1). Therefore, embryos were analyzed starting at embryonic day 8.5 (E8.5) until birth. It was shown that α v integrins are not required for normal development up to E9.5 as littermates wildtype, heterozygous or homozygous-null were morphologically and developmentally normal (35). Between E9.5 and E11.5, distinct defects start to arise in the α v-null embryos where they began to appear delayed in growth and development and affected mice continue to deteriorate and are eventually absorbed, mainly due to placental layering abnormalities. These affected mice continue to deteriorate and are eventually absorbed. The mice that pass this stage of development are born viable although they begin to develop bi-lateral intracerebral hemorrhage at E12.5, which gets progressively more severe towards birth. Intracerebral hemorrhage is first evident in the ganglionic eminence in the telencephalon and continues into the diencephalon and slowly into the cortex of the forebrain and midbrain. At birth, α v-null neonates display obvious signs of

hemorrhage, (Figure 3a) and also have cleft palates (35). The intracerebral hemorrhage, together with the inability of the neonates to feed, leads to their inevitable death (35). Conditional knockout strategies have demonstrated that the lack of expression on glia, and not the vascular endothelium, in the brain is the reason for the intracerebral hemorrhage (36). While these data are very intriguing, it is necessary to determine which $\alpha\beta$ heterodimer is responsible for these developmental and neonatal deficiencies.

αv -associated β subunits

The $\beta 1$ integrin subunit heterodimerizes with 10 different α subunits resulting in the largest integrin subfamily. Utilizing homologous recombination in embryonic stem cells, $\beta 1$ -null mice were created to further understand the necessities of this subunit in various developmental stages. Analysis of embryonic development reveals that $\beta 1$ integrin is not required during the blastocyst stage to E3.5. Although the blastocyst has the ability to implant into the uterine wall, they die afterwards at E6.5 (37). $\beta 3$ -null mice were generated and have been documented as being viable and fertile (38). In some instances, hemorrhage has been reported in $\beta 3$ mutants, although, it is believed that the absence of αIIb integrin expression is the reason for this phenotype (39). $\beta 5$ -null mice exhibit no obvious developmental pathologies and have the ability to reproduce normally (40). The $\beta 6$ subunit is expressed mainly on epithelia including the lung, skin and kidney (41). $\beta 6$ -nulls develop and reproduce normally, but have been shown to develop emphysema-like pathologies in the lungs and skin due to defective activation of latent TGF β s (42).

Lastly, $\beta 8$ subunit's primary site of expression is within the CNS (43). Similar to αv -null mice, $\beta 8$ -null mice develop two different subclasses of deficiencies. Embryonic lethality due to defective vascular development in the yolk sac and placenta has been documented in the majority of cases. The remaining minority consists of mice being born with severe intracerebral hemorrhage (Figure 3b,d), evident from the abnormally dispersed capillaries with hyperplastic endothelial cells (Figure 3f), and in some cases, a cleft palate (44). Based on the evaluation of the αv -binding β subunits, the specific heterodimer, $\alpha v\beta 8$, is responsible for the intracerebral hemorrhage observed in the complete αv knockout animals. Moreover, $\alpha v\beta 8$ interacts between perivascular neural cells and ECM ligands of the cerebral blood vessel basement membrane (45), giving further credence towards evidence that the heterodimer is responsible for those vascular pathologies.

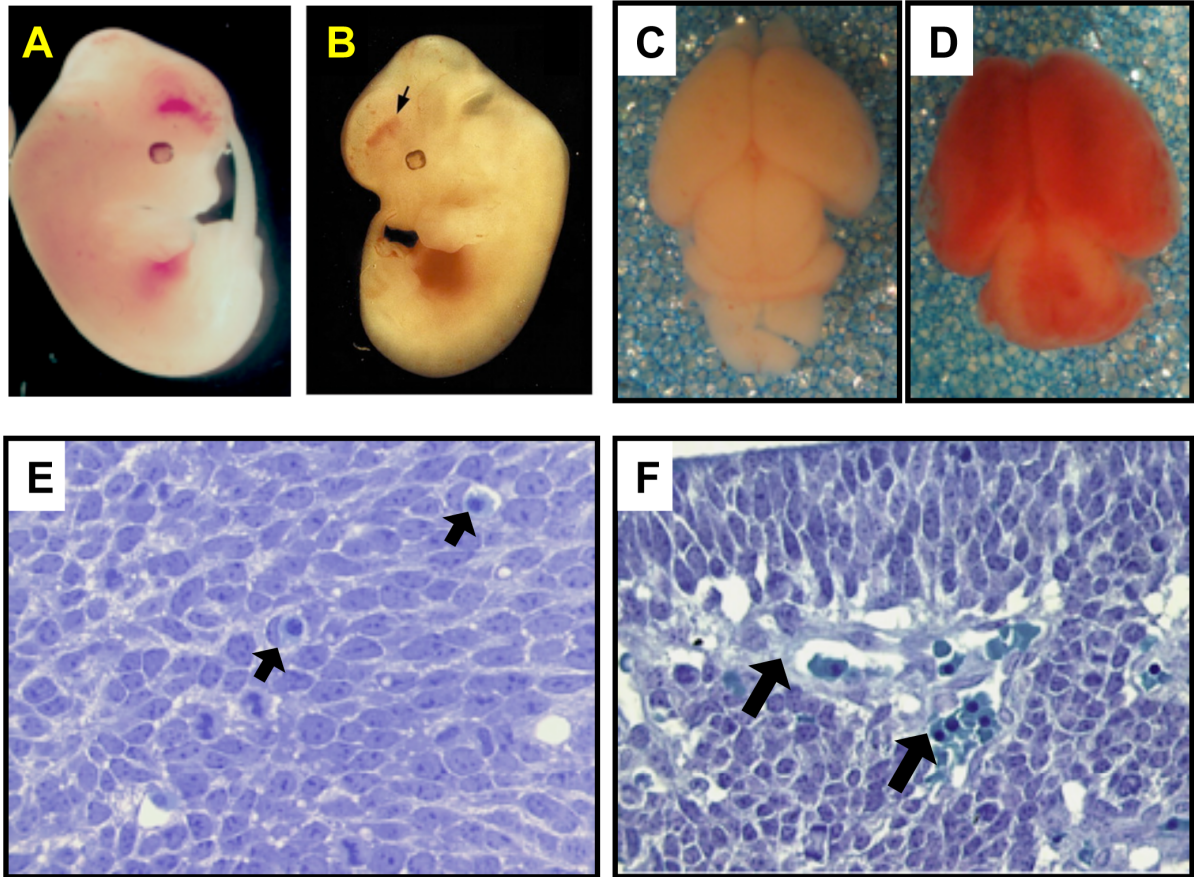


Figure 3. αv and $\beta 8$ Integrin Subunit Knockout Models

(A) $\alpha v^{-/-}$ and (B) $\beta 8^{-/-}$ neonates develop acute intracerebral hemorrhage at E11.5 (arrows). (C) Wild type animals develop normally while intracerebral hemorrhage becomes progressively more severe towards birth in both knockout mouse models ($\beta 8^{-/-}$ P1 neonate displayed **Fig. 3D**). (F) $\beta 8^{-/-}$ brain coronal sections reveal hemorrhage, endothelial hyperplasia and tortuous vasculature (arrows) compared to normal (E) wild type cerebral vasculature (arrows) (36).

α v β 8 Integrin

Moyle and colleagues first discovered the β 8 subunit in 1991 in rabbit and human tissues, where they showed it to have a unique polypeptide structure compared to other known β subunits. Human β 8 is comprised of a large extracellular domain and small hydrophobic transmembrane domain followed by a hydrophilic cytoplasmic domain. Northern blot analysis shows β 8 mRNA is expressed primarily in the brain with lower levels being detected in the ovary, uterus, kidney and placenta as well as several transformed cell lines (46). Initial studies of ECM ligand adhesion showed vitronectin as one ECM ligand that α v β 8 integrin has the ability to bind (47), although more recent studies would suggest otherwise. Using an affinity-based immunoprecipitation assay, Venstrom and Reichardt determined that the β 8 subunit can also bind laminin 1, collagen type IV and fibronectin (48). Furthermore, α v β 8 integrin has been shown to bind the RGD domain of LAP-TGF β 1 and 3 leading to bioactivation of the pro-peptide (49).

Aside from multiple ligand specificity, the β 8 cytoplasmic domain amino acid sequence is unique. All other β subunit cytoplasmic tails share homology containing one or two NPxY motifs that are binding sites for various phosphotyrosine-binding (PTB) domains. The α binding subunit cytoplasmic tails are quite different except for the GFFKR region that is the association site between the α and β subunits (10). Tyrosine phosphorylation in the NPxY motif of the β subunit cytoplasmic domain leads to interaction with intracellular proteins at the plasma membrane. A common PTB domain-containing protein that is recruited to the cytoplasmic tail of the β subunit is a protein known as talin. As previously

described, talin binds an NPxY motif present in most β subunit cytoplasmic tails, although $\beta 8$'s cytoplasmic tail lacks this common binding site (20). Yeast two hybrid technology identified $\beta 8$'s cytoplasmic domain as a binding partner for Band 4.1B. Other isoforms of Band 4.1s were also shown to have some interaction, although common cytoskeletal scaffolding proteins did not (50). Band 4.1 proteins have three specific functional domains, a FERM domain, a central spectrin/actin-binding domain and a C-terminal domain (CTD) (51). The CTD interacts with $\beta 8$'s cytoplasmic tail rather than the FERM domain that interacts with other β subunits (50).

Within the CNS, $\alpha v \beta 8$ integrin has been documented to be present in neurons in the brain and spinal cord as well as glia, such as astrocytes (48). Furthermore, conditional deletion using Cre-Lox technology revealed that the integrin is not required on vascular cells (Tie2-Cre) within the CNS. Ablation of $\alpha v \beta 8$ integrin in neurons did not lead to the intracerebral vascular pathologies evident in the complete αv and $\beta 8$ knockout animals, but conditional deletion in neuroepithelia (i.e. GFAP+ astrocytes), recapitulated the intracerebral hemorrhage (52). These data suggest that it is the interaction between the astrocyte and the cerebral blood vasculature that is responsible for the phenotype upon $\alpha v \beta 8$ integrin loss (49). Moreover, $\alpha v \beta 8$ integrin mediates contact and communication events between perivascular glial cells and ECM components of the vascular basement membrane (45). Upon integrin ablation, several vascular pathologies arise including the aforementioned intracerebral hemorrhage as well as vascular thrombosis, edema and endothelial hyperproliferation. When $\beta 8$ integrin knockouts

were first generated, they were created on a C57BL/6J and 129/Sv background that did not allow for the knockouts to survive post-natally (44). Upon backcrossing onto an ICR/CD1 mixed genetic background, 50% of $\beta 8^{-/-}$ neonates survive to adulthood and some live as long as 5 months post-natally, although they develop severe neurological defects. Furthermore, $\alpha v\beta 8$ integrin regulates neurogenesis and neurovascular homeostasis in the adult mouse brain (14). The most striking aspect of the complete αv and $\beta 8$ knockout mouse models are the vascular abnormalities, which strongly resemble those vascular pathologies characterized in human high-grade glioma. Since it is the distinct expression of $\alpha v\beta 8$ integrin on the glial cell that controls the vascular pathologies in the knockout models, and given the fact that glial cells are putative cells of origin for gliomas, it becomes necessary to investigate the involvement of $\alpha v\beta 8$ integrin in human high-grade gliomas.

Glioma

Glioma is an extremely deadly cancer affecting nearly 30,000 patients in the United States annually (53). These tumors represent the most common type of primary brain cancer where the most advanced cases epitomize some of the most fatal forms of cancer (54). Regardless of recent progress in cancer diagnosis and treatment, glioblastoma multiforme (GBM), the highest grade of glioma, becomes highly invasive with an innate ability to elude modern surgical, radio- and chemotherapeutic interventions (55). Therefore, determining the basic cellular and molecular events contributing to glioma-induced angiogenesis and progression may lead us to new therapeutic strategies to remedy or inhibit this disease.

The World Health Organization (WHO) has developed a scoring pattern for different subtypes of glioma ranging from Grade I to IV. There are several tumor types that arise from various CNS cell types, including astrocytes, oligodendrocytes and ependymal cells (Figure 4a) (56). A large majority of research has been focused upon tumors of the neuroepithelia that arise from these cell types. In general, Grade I tumors are considered to be clinically benign because of their low proliferative potential and their ability to be managed with surgical resection with minimal tumor recurrence. Grade II tumors comprise infiltrative cells which often recur post-surgical resection, even though they also retain a low proliferative potential. Grade III, anaplastic astrocytomas, for example, are often a result of grade II tumor's increase in malignancy. This grade of tumor is best known for their regions of nuclear atypia and enhanced mitotic activity. Lastly, grade IV tumors, or GBM, are highly malignant and mitotically active, often characterized for their pseudopalisading necrotic and angiogenic pathologies (56). Upon diagnosis with GBM, the median survival rate remains a dismal 9-12 months, even with the previously described clinical interventions, while patients diagnosed with grade II or grade III gliomas have been documented as surviving on average 10-15 years and 2-3 years, respectively (57).

Putative Cell of Origin in Glioma

The cell of origin for gliomas still remains a controversial subject as tumors have been documented as having astrocytic, oligodendroglial, ependymal or mixed components (58). Most of the cells found in the brain are fully differentiated and non-proliferative, therefore the cell of origin is thought to be one that maintains its ability to proliferate and/or differentiate (59). More recently, it has been hypothesized that GBMs may arise and/or recur from neural stem cells (NSCs) that undergo genetic mutations in tumor suppressor genes and oncogenes (57). Three routes have been established for the propagation of gliomas: [1] the neural stem cell (NSC); [2] the glial progenitor (maintains the ability to differentiate into astrocytes and oligodendrocytes) and [3] the fully differentiate glial cell (Figure 4b) (60). NSCs are located in two specific locations in the brain; the subventricular zone (SVZ) of the lateral ventricle and the subgranular zone of the dentate gyrus of the hippocampus (57). These cells retain self-renewal capacities and have the ability to differentiate into the cell types found in the brain, thus the attraction of targeting them with therapies. Due to the high degree of cell proliferation, the germinal regions in the SVZ have often been thought to be the source of gliomas as opposed to other niches harboring more fully differentiated, non-proliferative cell types (61). Non-neoplastic cells that transform and produce astrocytic- and oligodendrocytic-based gliomas or mixed oligoastrocytomas are likely direct descendants of a common NSC. For many years, the astrocyte had been thought to be the source of most gliomas, although recent evidence involving the cancer stem cell (CSC) has become a hot topic (62). There are two CSC hypotheses in the field that are of

ongoing debate: 1) the stochastic model identifying every cell having the same ability to acquire somatic mutations and produce tumor lesions and 2) the hierarchical model whereby a distinct subset of cells (<5%) having the ability to produce tumor (63). The latter of the two is currently the more accepted model.

Figure 4: Glioblastoma Multiforme Tumor Formation

(A) CNS cell types likely originate from a common neural stem cell (NSC). The NSC differentiates into either neural or glial progenitors. The neural progenitors give rise to neurons while the glial progenitors give rise to astrocytes, oligodendrocytes, and ependymal cells. **(B)** Tumors of the CNS are thought to arise from a variety of different sources (dashed arrows). A brain cancer-propagating cell can give rise to fully differentiated cancer progeny or a progenitor cell type, while both can create CNS tumors, such as GBM. **(C)** Genetic pathways leading to primary and secondary GBMs are different based on their specific alterations. Primary and secondary GBMs have common loss of chromosome 10q while p53 mutations are more common in secondary GBMs. (*) Represents specific genetic alterations that are significantly different between the two paths to GBM. This figure was adapted from Hadjipanayis et al. 2010 (A, B) and Ohgaki et al. 2007 (C) (54, 60).

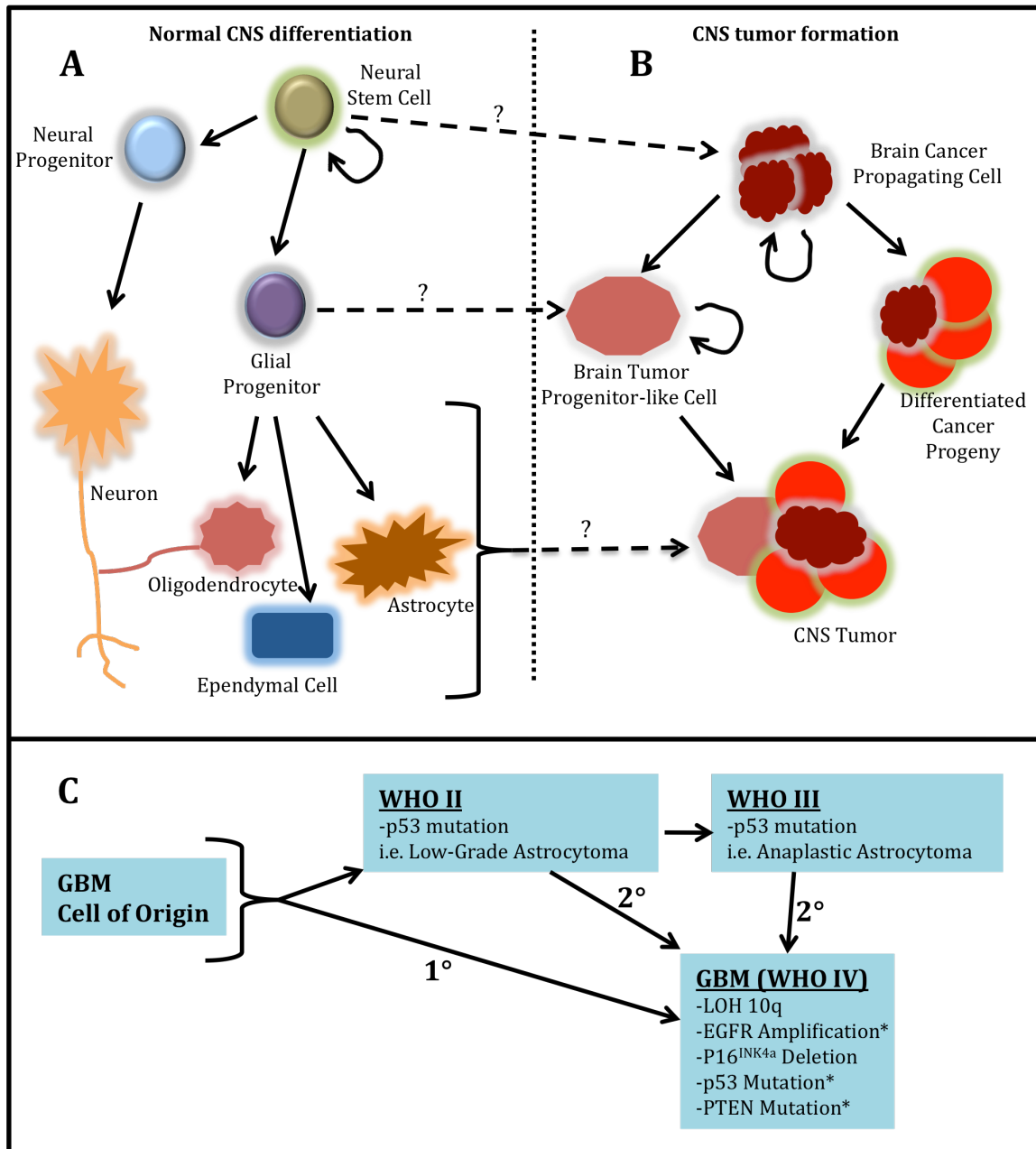


Figure 4

Molecular Pathologies in Glioma

There are two different routes for GBM to arise, primary and secondary. About 90% of GBMs arise *de novo* (1°) without any prior evidence of malignancy while the other 10% (2°) arise from lower grade II or III gliomas (Figure 4c) (54). Gliomagenesis has been a widely studied area to make it possible for more effective interventions to eradicate the disease upon patient diagnosis. As with many tumor types, there's a rich body of literature focused upon molecular and cellular alterations in glioma. Many gene expression profiles and chromosomes are commonly altered, often correlating with histological grade and clinical prognosis (53). It is common to observe overexpression of a variety of growth factors (i.e. PDGF, FGF2) and their cognate receptors (53, 64). Overexpression of growth factors and their receptors commonly leads to induced amplification of downstream proteins, such as Ras and Akt, involved in cell proliferation and survival (65). Also, the p53 protein is often mutated, affecting cell cycle control (66). Furthermore, in grade III anaplastic astrocytomas, additional disruptions of cell cycle control machinery are evident with INK4a/Arf deletion leading to loss of inhibition of cyclin-dependent kinase 4 (CDK4) and MDM2, respectively. This loss of inhibition causes an inhibition of retinoblastoma (Rb) and p53, respectively (53). p53 mutations along with mutations in neurofibromatosis 1 (Nf1) has also led to tumors of various grades (67). The cancer genome atlas (TCGA) has identified somatic mutations or deletions in Nf1 in nearly 25% of a 206-glioma patient sample size, therefore suggesting a role for the molecule as a potent tumor suppressor (67). Moreover, in grade IV gliomas, there are additional alterations that supplement the already

serious changes evident in lower grade gliomas. These include common loss of chromosomal region 10q22-25, which harbors many tumor suppressor genes, particularly PTEN (phosphatase and tensin) (68). PTEN acts as the key component in the negative feedback loop of Akt where it inhibits the functional activation of Akt via dephosphorylation of PIP3 to PIP2 (69). Additionally, epidermal growth factor receptor (EGFR) is amplified or hyperactivated via mutation in 30-50% of GBMs leading to signal transduction activation of intracellular protein cascades, such as the MAPK, JNK and Akt pathways, involved in pro-survival and pro-proliferative cellular processes (70). Together, a majority of the changes in cell signaling become important players in the development of a high grade gliomas (68).

Conversely, recent data from TCGA has identified mutations of isocitrate dehydrogenase 1 and 2 (IDH1/2) in about 12% of secondary GBMs where it has increased the overall rate of survival of patients as compared to those patients harboring wild type IDH1/2 (71). This non-biased approach has implicated mutations in these molecules as having pro-survival effects rather than the alternative, providing nearly two- to three-fold higher median survival rates for patients diagnosed with anaplastic astrocytoma or GBM (72). Collectively, TCGA analysis has provided further understanding of the molecular alterations that occur in glioma, which in turn, may lead to the development of effective therapeutics to potentially prolong survival of diagnosed patients.

Clinical treatment of Glioma

Currently, standard first line treatment for GBM is surgical resection and acute radiotherapy (RT) alongside simultaneous temozolomide (TMZ) treatment, followed by adjuvant treatment of patients with the same chemotherapeutic (73). This concomitant approach allows for modest improvement in overall median survival rates from 12 months to 14.6 months compared to patients treated with radiotherapy alone (74). Indeed, there are subsets of patients that survive past 2 years post-diagnosis, but with RT and TMZ dual therapies, the percentage of these patients increase from 10% to 26% (74). Newly diagnosed GBM patients exhibiting promoter methylation of the MGMT gene have been documented to respond best to the RT/TMZ combined therapeutic regimen, increasing overall survival to 23 months (75). Although these numbers are encouraging, further efforts are ongoing to acutely treat patients based more so on their molecular signatures in their tumors, although the main obstacle of treatment has and continues to be the blood brain barrier (76). More recently, advancement in therapies has commenced in the development of anti-angiogenic agents. Bevacizumab, an anti-VEGF-A humanized monoclonal antibody, has been recently approved by the FDA for patients with a recurring GBM (77). While the data supporting this decision was quite encouraging, the use in newly diagnosed patients is frowned upon as it may cause issues in areas of surgical wounds. Other anti-VEGF therapies have been established based on the knowledge of VEGF receptors. Previously, soluble decoy receptors for VEGF have shown poor *in vivo* pharmacokinetics, including low affinity for the growth factor and minimal half-life, therefore, further research was performed

to overcome those shortcomings. This research led to the development of a more potent VEGF blocker, VEGF-Trap, which maintained high affinity for the growth factor while increasing *in vivo* pharmacokinetics of previously documented soluble decoy molecules (78).

Furthermore, other anti-vascular agents have been examined for glioma, although limited response has been documented and many of the drugs are still in pre-clinical development. Other than the aforementioned soluble receptors and bevacizumab, angiogenesis is also being targeted intracellularly where drugs such as cediranib, vatalanib, and sunitinib target cytoplasmic receptor tyrosine kinase activity of the VEGF receptors 1-3 and cKIT. In addition, sorafenib, pazopanib and vandetanib target the same intracellular tyrosine kinase activity of EGFR and PDGFR α , respectively (79). Possible anti-VEGF therapies concomitant with radiotherapy may be the best route to treat patients based upon their genetic prognostic indicators, especially those recurrent patients. Further research is ongoing targeting these highly angiogenic tumors to prolong overall patient survival with minimal side effects while also addressing the invasive phenotype of high-grade glioma cells that are often the source of tumor recurrence post-VEGF therapy.

Mouse Model	Experimental Model	Glioma Subtype
Nude (Athymic)	Intracranial injection of human glioma cell lines, transformed rodent/human astrocytes & 1° GSCs	Astrocytoma/GBM
RCAS/N-tva	Intracranial injection of RCAS oncogenic vectors, infection and transformation of nestin expressing cell types.	Astrocytoma/GBM
RCAS/G-tva	Intracranial injection of RCAS oncogenic vectors, infection and transformation of GFAP expressing cell type.	Astrocytoma/GBM
Nf1-/-;p53-/-	Germline deletion followed by LOH at the Nf1 & p53 loci.	Astrocytoma/GBM

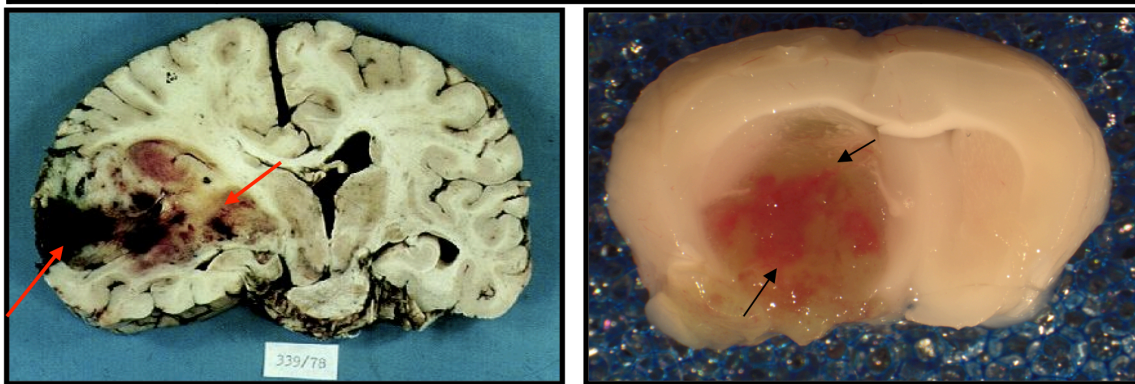


Figure 5: Mouse Models of Astrocytoma/GBM

Table: A partial list of mouse models that mimic human astrocytoma/GBM that are developed from known glioma-associated genetic alterations (66, 80, 81). Gross pathologies of a coronal section of a human GBM (bottom-left, red arrows) are recapitulated by intracranial implantation of a GFP-labeled human glioma cell line into athymic mice (bottom-right, black arrows). Pathologies include intratumoral hemorrhage, thrombosis and edema (arrows).

Animal models of Glioma

Animal models of cancer have long been the flagships for understanding tumor biology in a dynamic setting. The most common of these is the use of immunocompromised (nude) mouse models, including orthotopic and non-orthotopic xenografts (Figure 5 Table). Orthotopic models involve the implantation of a cell type into its normal microenvironment within the same species while xenograft models allow for the use of different species, such as the injection of a human cell line into a mouse. Collectively, these models have been the most beneficial in recapitulating the human disease *in vivo* as oppose to transgenic models (Figure 5) (82).

Genetically engineered mice (GEM) have also been used to study gliomas. A model with germline mutations of neurofibromatosis 1 and p53 (Nf1^{-/-};p53^{-/-}) leads to the development of astrocytomas, ranging from low to high grade (Figure 5 Table) (66). Additionally, an RCAS/tva model allows for the cell type-specific induction of tumors utilizing an avian retroviral delivery system to initiate loss of tumor suppressors and/or overexpression of oncogenes that have been associated with glioma (Figure 5 Table) (81). Additional inducible models are available where specific cell types can be targeted for conditional deletion of tumor suppressors or activation of potent oncogenes. The GFAP-CreERT2 or Nestin-CreERT2 have been used to conditionally delete a gene of interest, such as p53, Nf1 and PTEN, where they are flanked with loxP sites to allow for cre recombinase activity to conditionally inactivate them upon exposure to tamoxifen (83, 84). Furthermore, an additional model was created utilizing the S100 β promoter to transgenically express

a transforming homologue of EGFR, which resulted in low-grade oligodendrogliomas (85). Collectively, multiple models have been established to evaluate specific genes in the development of glioma.

Glioma and Integrins

Integrins are known to play critical roles in normal and neoplastic cell adhesion and motility. The interaction between the ECM, which is a major component of the CNS microenvironment, is essential for integrin function, and integrins promote the invasion and migration of glioma cells throughout the brain parenchyma (86). Furthermore, normal brain tissue versus GBM tissue was analyzed for integrin expression using immunohistochemistry. GBM tissue displayed increased overall integrin expression as compared to normal tissue (87). Moreover, the necessity of integrins in GBM has become evident based on preclinical studies, as therapeutics have been developed to act as antagonists, i.e. cilengtide (88). Cilengtide has been used in the clinic to target those patients with RGD-overexpressing integrin profiles, such as $\alpha v \beta 3$ and $\alpha v \beta 5$ integrins. These integrins contribute to adhesion and migration of tumor cells (89). Abnormal cell-ECM interactions can often be a source of gliomagenesis, especially in its early stages. This interaction allows for anchorage to perivascular regions in the brain promoting tumorigenesis (90). Similar to many primary tumor populations, gliomas start out as a relatively avascular lesion, which require the co-option of the pre-existing vascular network to progress as well as migrate to other non-hypoxic regions of the brain (91). Additional to tumor cells adhering ECM components of

the vascular basement membrane, they are also known to direct their migration along white-matter tracts (57). These two methods of migration are often the reason for GBM recurrence post-therapy and poor prognosis upon initial diagnosis (92).

Integrins have been implicated in the onset and progression of gliomas for many years (93). The fibronectin receptor, $\alpha 5 \beta 1$, is considered to be a pro-angiogenic integrin that is overexpressed in both tumor-associated endothelial cells and gliomas, alike (94, 95). Laminin is most concentrated around the vascular basement membrane. Laminin-binding integrins, $\alpha 3 \beta 1$ and $\alpha 6 \beta 1$, are commonly expressed in glioma cell lines and are often mediators of migration as well (96). Limited research has been focused upon the αv subfamily of integrins in relation to gliomagenesis, although data surrounding the role of $\alpha v \beta 3$ and $\alpha v \beta 5$ integrins has been obtained. Both integrins are expressed in endothelial cells and glioma cells, but have been shown to be concentrated along the tumor periphery, suggesting their roles in invasion (97). Moreover, glioma growth and invasion was reduced upon exposure to a small molecule peptide against $\alpha v \beta 3$ integrin (98). Conversely, when $\beta 3^{-/-}$ astrocytes were immortalized and transformed *ex vivo* and implanted back into the brain, significantly larger tumors resulted, suggesting the role of $\alpha v \beta 3$ integrin as a possible tumor suppressor (99). Perhaps, $\alpha v \beta 3$ integrin expression at the periphery plays a fundamentally different role in overall tumor biology as opposed to ubiquitous expression throughout the tumor. Nevertheless, these data suggest the role of αv integrins in glioma biology; however limited research has unraveled the roles for other $\alpha v \beta$ heterodimers.

Aside from the obvious invasive nature of gliomas, microvascular proliferation and other angiogenic pathologies mark high-grade gliomas (100). During gliomagenesis, especially at early stages, tumor cells often co-opt the intratumoral vasculature, disrupting the cohesive nature of the BBB, leading to leaky or hemorrhagic vessels that allow increased nutrient and oxygen delivery (101). As the tumors progress, they become hypoxic and nutrient-dependent, thus relying upon angiogenesis to remedy their situation. Angiogenesis is defined as the physiological process from which new blood vessels are created from pre-existing ones (102). Although the role of $\alpha v \beta 8$ integrin has yet to be established in glioma, there are multiple reason for studying its probable involvement. First, $\alpha v \beta 8$ integrin is expressed in NSCs and astrocytes within the brain, both of which have been documented as putative sources of gliomas (14, 50, 58). Second, $\alpha v \beta 8$ integrin has also been documented in several glioma cell lines and primary tissues, both at the mRNA and protein levels (103). Third, upon αv and $\beta 8$ integrin ablation in the CNS, vascular pathologies ensue that mimic high-grade glioma vascular pathologies (35, 52). Fourth, GBM stem cells, much like non-neoplastic stem cells, reside in areas of vascular niches, both of which express $\alpha v \beta 8$ integrin (14, 104). These results suggests that the integrin may play an unknown role in gliomagenesis as it plays significant roles in regulating neurovascular homeostasis within the adult brain (14).

Collectively, the data in regard to integrin biology and gliomagenesis is clear although limited focus has been placed upon $\alpha v \beta 8$ integrin. Understanding the functional role of $\alpha v \beta 8$ integrin during glioma-induced angiogenesis may prove pivotal in the discovery of a more specific therapeutically targeted approach to the

disease alongside increased prevention and early diagnosis. As current treatments for high-grade gliomas are few and inefficient, it is essential to determine novel therapeutic target genes, which could help in prolonging or eradicating the progression of glioma. In this dissertation, we will analyze the roles that $\alpha\beta8$ integrin plays in the onset and progression of GBM in regard to tumor growth and angiogenesis. Moreover, we will substantiate the known role of $\alpha\beta8$ integrin in regard to homeostatic control of the BBB, by focusing on its potential role in the glioma setting.

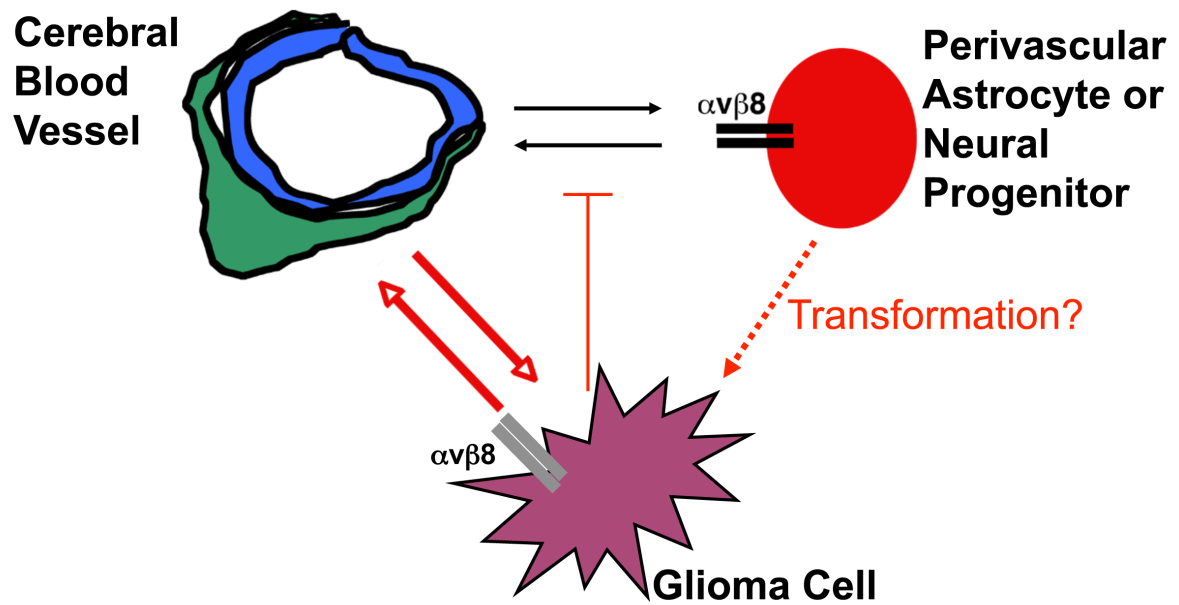


Figure 6: Working Model

Expression of $\alpha v\beta 8$ integrin on perivascular astrocytes or neural progenitors is essential for proper cell-cell communication within the NVU and allows for normal CNS development and homeostasis (14). During a transformation event (red, dotted arrows), the glioma cell either loses expression or function of $\alpha v\beta 8$ integrin, which leads to the inhibition of normal vascular homeostasis. This defect allows for the exploitation of the cerebral blood vasculature resulting in an increase in tumor grade and worse overall patient prognosis.

Specific Aims

Integrins are cell surface receptors for various ECM ligands that play roles in cell adhesion and signaling pathways. Improper integrin function regulation is known to lead to the development of many CNS diseases, together with cancer. Glioblastoma multiforme (GBM) remains the most frequently diagnosed and malignant form of adult brain cancer. Despite recent progress in cancer diagnosis and treatment, the median survival rates of patients have not changed over the past several decades. Integrins have been shown to play fundamental roles in GBM proliferation and malignancy. The main pathological hallmarks include pseudopalisading necrosis, increased mitotic index and microvascular proliferation associated with vascular hemorrhage, edema and thrombosis. A gap in knowledge exists between these pathologies and the molecular pathways driving them. Consequently, we have initiated studies to investigate how the role of a specific integrin, $\alpha v \beta 8$, functionally contributes to blood vessel abnormalities in GBM.

Therefore, we hypothesize that abnormal $\alpha v \beta 8$ integrin expression and/or function contributes to the angiogenesis pathologies in malignant brain tumors. To test this hypothesis, the following specific aims were developed:

- 1) Determining functional roles for $\alpha v \beta 8$ integrin in glioma-induced angiogenesis using an orthotopic mouse model of astrocytoma**
- 2) Elucidate the functional roles for $\alpha v \beta 8$ integrin in glioma-induced angiogenesis during the pathogenesis of human gliomas**

CHAPTER 2:

Materials and Methods

Transgenic & Immunocompromised Mice

$\beta 8^{+/-}$ mice (44) were obtained from the Mutant Mouse Regional Resource Center (Portland, ME). Mice were backcrossed for several generations onto an ICR/CD-1 mixed genetic background (Jackson Laboratories). $\beta 8$ heterozygote's were crossed to generate $\beta 8^{+/+}$, $\beta 8^{+/-}$ and $\beta 8^{-/-}$ progeny. Genotypes of the progeny were confirmed by PCR using ear snips. Genomic DNA was isolated by digesting ear snips in 100 μ g/ml proteinase K (USB Scientific, Cleveland, OH) in STE overnight at 55°C. Next, the mixture is added to the same volume of 100% EtOH where the DNA precipitates out of solution and is dissolved for 30 minutes at 37°C in 1X TE while being shaken at 1400 RPM. The following PCR primers were used to confirm $\beta 8$ status, as previously described (44):

Wild-type primers:

- 1) 5'ATTATCTGGTTGATGTGTCAGC3'
- 2) 5'AGAGAGGAACAAATATCCTTCCC3'

Mutant primers:

- 1) 5'AGAGGCCACTTGTGTAGCGCCAAG3'
- 2) 5'GGAGGCATACAGTCTAAATTGT3'

Neo PCR conditions were as follows using Mango-Taq (Bioline, Taunton, MA):

Denature - **Step 1**: 95°C for 5'

Denature - **Step 2a***: 95°C for 45"

Annealing - **Step 2b***: 58°C for 30"

Extension – **Step 2c***: 72°C for 1'

***Repeat Steps 2a-c**, 30 times

Extension – **Step 3**: 72°C for 10'

PCR Products:

Wild-type: 330 base pairs

Mutant (neo cassette only): 450 base pairs

Heterozygote: Both 330 and 450 base pair products

Male NCR^{nu/nu} mice were purchased from Jackson Laboratories (Bar Harbor, ME) and used for all experiments involving intracranial injections of transformed mouse cells and human glioma cell lines.

Isolation and Purification of Primary Astroglia

Wild type and $\beta 8^{-/-}$ neonatal (P0-P3) brains were removed and immersed in sterile, cold Hank's Balanced Salt Solution (HBSS). Olfactory bulbs and hindbrain are snipped away from the cerebral cortices. The neocortices were dissected from the hippocampus and other internal structures. Meninges were carefully removed away from the freshly isolated cortices and minced in fresh HBSS. The homogenized cortices were double-checked for residual meninges and then allowed to digest in 150 units/ml collagenase (Worthington, Lakewood, NJ) and 40 μ g/ml DNase I (Sigma, St. Louis, MO) in HBSS for 30 minutes at 37°C. The cortical tissue was pelleted and triturated using a glass borosilicate pipette tip in low

glucose DMEM (Sigma, St. Louis, MO) supplemented with 10% FCS (Hyclone, Logan, UT) and passed through a 50 μ m sterile filter. The single-cell mixture was plated onto a tissue culture flask that was coated in 10 μ g/ml murine laminin (Sigma, St. Louis, MO) and allowed to grow for 7-10 days at 37°C/5% CO₂. Once the flask was confluent, the contaminating neurons, oligodendrocytes and fibroblasts were shaken off of the astroglial monolayer overnight at 250 RPM at 37°C. Next day, the media was changed and astroglia were solely left behind evident by their robust GFAP staining pattern (>95%+). All as previously described (36).

Immortalization and Transformation of Murine Astroglia

To generate retroviral stocks, 293T Phoenix cells were transfected with pLXSP-puro-E6/E7 and pLXSN-neo-^{G12V}H-Ras (80). Primary astroglial cells were transduced with the E6/E7 retroviral supernatant and cells were selected in growth media containing 1 mg/ml puromycin for 5 days. Puromycin-resistant clones were pooled and transduced with ^{G12V}H-Ras retrovirus supernatant, and selected after 10 days in G418 (900 mg/ml). To analyze integrin expression in passaged cells, semi-confluent monolayers of cells were trypsinized and split 1:5 onto new dishes. After reaching 80-90% confluence the procedure was repeated.

Isolation of Primary GBM Cell Lines

Dr. Frederick Lang resected the primary GBM tissue sample from patients at M.D. Anderson Cancer Center. The tissue was placed in phosphate buffered saline

(PBS) and put on ice. Tissue was brought into the lab and minced. Homogenized tissue was digested in the same collagenase/DNase I solution in HBSS for 30 minutes at 37°C. The resulting tissue was pelleted and triturated in nude DMEM-F12 (Mediatech, Manassas, VA) with a glass borosilicate pipette and passed through a 50 µm filter. This single-cell suspension was grown in a T-75 flask in DMEM-F12 with B-27 supplement and 20 ng/ml of EGF and bFGF (Invitrogen, Carlsbad, CA). Upon spheroid formation, accutase (Sigma, St. Louis, MO) was used to passage the cells.

Adherent Human Cell Lines and Culture Conditions

U87, LN18, and LN229 cell lines were purchased from ATCC (Manassas, VA). U251 cells were kindly a gift of Dr. Oliver Bögl and SNB-19 cells were a kind gift of Dr. Dimpy Koul, both at MDACC. All cell lines were grown in DMEM/F12 (Mediatech, Manassas, VA) supplemented with 10% fetal bovine serum and antibiotics. Normal human astrocytes were purchased (Lonza) and grown in their proprietary media. Transformed human astrocytes were kindly donated to us from Dr. Russel Pieper at UCSF.

Intracranial injections of Transformed Astroglia and Human Glioma Cell Lines

Nude mice were anesthetized and a single incision was made from the anterior pole of the skull to the posterior ridge. A hole was drilled over the target brain structure to expose the brain. We targeted the striatum for cell implantation using the following stereotactic coordinates, all relative to the bregma: 1.5 mm

rostral, 1.5 mm anterior, and 4 mm below the pial surface. An automated micropump (Stoelting Instruments) was used to dispense cells in 3 to 5 ml PBS over a five-minute period. Transformed mouse astroglia cultured for less than four passages after transformation were used for the experiments. In the Kaplan-Meier survival studies 2.5×10^4 transformed mouse cells and 5×10^4 transformed human astrocytes were injected, and animals were monitored until development of tumor-induced neurological phenotypes, ranging from weight loss to ataxia. In other experiments, nude mice were stereotactically injected with $1-5 \times 10^5$ wild type or $\beta 8^{-/-}$ transformed cells and tumor-bearing animals were perfused with 4% PFA/PBS. Brains were coronally sliced at 1 mm intervals and paraffin-embedded tissue was serially sectioned at 7 mm intervals. Human intracranial xenograft tumors were generated by injecting 5×10^5 U87 or SNB19 cells into the striatum of immunocompromised mice.

Rescuing $\beta 8$ Integrin Expression in $\beta 8^{-/-}$ Transformed Astroglia and U87 Cells

Transformed $\beta 8^{-/-}$ astroglia and U87 human glioma cell lines were transfected with empty vector (pcDNA4.0-V5) or vector containing the full-length human $\beta 8$ integrin cDNA (pcDNA4.0- $\beta 8$ V5) (36). Stable transfectants were selected in zeocin (300 μ g/ml) for 10 days, and integrin overexpression was confirmed by immunoblotting lysates with anti- $\beta 8$ or anti-V5 antibodies.

Isolation of CD31+ Intratumoral Endothelial Cells

Mice harboring 21 day-old intracranial tumors derived from $\beta 8^{-/-}$ (+ vector) or

$\beta 8^{-/-}$ (+ $\beta 8V5$) transformed astroglial progenitors were sacrificed. Tumors were then microdissected from the brain and dissociated into a single cell suspension using neural tissue dissociation media (105). CD31-expressing cells were sorted using a rat anti-mouse CD31 antibody (BD Biosciences), magnetic beads coated with goat anti-rat secondary antibody (Miltenyi Biotec, Inc.), and a BioMag magnetic separation unit (Polysciences, Inc.)

Antibodies for Immunofluorescence, Immunohistochemistry and Immunoblotting

An affinity-purified anti- αv rabbit polyclonal antibody was generated by our group using a synthetic peptide (CKRVRPPQEEQEREQLQPHENGEGTSEA) corresponding to a region of the chicken αv cytoplasmic domain. The anti- $\beta 8$ integrin antibody used for all immunoblotting has been described previously (36, 50). The following antibodies were purchased: rabbit anti- $\beta 1$ integrin, rabbit anti- $\beta 5$ integrin, rabbit anti-nestin, and rat anti-mouse CD133 (Chemicon), rat anti-mouse CD34 mAb (Genetex), chicken anti-Nestin IgY (Neuromics), rat anti-mouse CD31 and rat anti-mouse αv -PE mAbs (BD Biosciences), Texas-Red conjugated anti-Phalloidin, rabbit anti- β -actin pAb, mouse anti-laminin (Sigma), rabbit anti-GFAP pAb (DAKO), rabbit anti-pSmad3 mAb (Epitomics), rabbit anti-GFP (Abcam) and anti-Ras and anti-E7 antibodies (Santa Cruz Biotech). Mouse anti-VEGF, rabbit anti-Desmin, as well as rabbit anti-pSmad2 and tSmad2/3 antibodies were purchased from Cell Signaling Technologies. The anti-V5 mAb was purchased from Clontech Laboratories. Secondary antibodies were goat anti-rabbit, goat anti-

chicken, goat anti-rat and goat anti-mouse, all conjugated to Alexa488 or Alexa594 (Molecular Probes). Secondary HRP-conjugated sheep anti-mouse, goat anti-rabbit and donkey anti-chicken IgY antibodies were purchased from Jackson ImmunoResearch Labs. For quantitation of blood vessel densities, digital images were captured from sections stained for CD34 immunofluorescence. Mean fluorescence intensity was calculated using ImageJ software. Two investigators, who were blinded to the genotypes for each sample, analyzed fluorescent sections.

Cell Surface Biotinylation of Integrin Subunits

Cells were grown to confluence in normal growth media. First, cells were washed once with PBS. Next, cell monolayers or GBM neurospheres were incubated in 0.1 mg/ml of EZ Link Sulfo NHS LC biotin for 30 minutes at 37°C. After the incubation, the cells were washed twice with PBS and once with TBS. Cells were then lysed in NP40 Lysis buffer + protease inhibitors for 15 minutes at 4°C. Next, mixture was centrifuged at high speed for 15 minutes at 4°C, after which being assayed for protein concentration. For each integrin subunit analyzed, a proper same-species IgG control was used. Lysates were split evenly, in terms of protein concentration, among the integrin subunits that were being assayed.

First, lysates were blocked with the 2°-agarose beads (pre-mixed with NP40 lysis buffer) for 30 minutes at 4°C while tumbling. Next, mixture was centrifuged at 1000xg for 1 minute at 4°C. Blocked lysates were removed and put into a fresh, chilled microfuge tube with their respective primary antibody and tumbled overnight at 4°C. Next day, 2°-species specific agarose beads are added to each incubating

lysate for 45 minutes tumbling at 4°C. Mixtures were centrifuged and supernatant is removed. Agarose bead containing integrin subunit was washed three times for 15 minutes while tumbling at 4°C. After the last wash, agarose pellets were incubated with 2X SDS-PAGE, non-reducing, gel loading buffer for 10 minutes at 95°C. Supernatant samples were run on a 7.5% SDS-PAGE gel, transferred onto PVDF and blocked with 5% BSA. Next, membranes were incubated with ABC complexes (chromagen) for 30 minutes. Then, membranes were thoroughly washed twice with TBST for 10 minutes followed by a 10-minute wash with TBS. Afterwards, westerns were visualized via chemiluminescence substrates.

Immunoblotting

Cells were lysed in either NP40 buffer + protease inhibitors (for non-phosphorylation-related experiments) or RIPA buffer + protease inhibitors & phospho-protease inhibitors (for phosphorylation-related experiments) and proteins were quantified via BCA assay (Pierce). 10µg of total protein was separated by SDS-polyacrylamide gel electrophoresis and transferred to Immobilon P transfer membrane (Millipore). The membranes were washed in Tris-HCl-buffered saline (10 mM Tris-HCl, 150 mM NaCl, pH 8) + 0.1% Tween20 (TBST). Next, membranes were blocked in 5% nonfat milk in TBST for 1 hour at room temperature. Blots were probed overnight in 5% nonfat milk with specific antibodies at relevant dilutions (see Antibodies section). Blots were washed three times with TBST for 5 minutes. Proper species-specific secondary antibodies conjugated to horseradish peroxidase were diluted 1:1000 in 5% nonfat milk and incubated with the blots for 1 hour at

room temperature. Again, blots were washed three times with TBST and developed with chemiluminescence substrates. β -actin antibody (1:5000) was used as a loading control (Sigma).

Immunostaining

Frozen Samples

Animals were anesthetized and cardiac perfused with 4% paraformaldehyde (PFA) in PBS. Brains were removed and sliced at 2mm coronal sections and placed into fresh 4% PFA for 2 hours at 4°C. Next, sections were placed in 9% sucrose for 2 hours followed by an overnight incubation in 18% sucrose at 4°C. Sections were then placed into OCT and frozen on dry ice and stored in -80°C. The MDACC histology core performed sectioning onto positively charged slides and H&E staining of resulting sections.

Paraffin Samples

Animals were anesthetized and cardiac perfused with 4% paraformaldehyde (PFA) in PBS. Brains were removed and post-fixed overnight in 4% PFA at 4°C. Next day, 2mm coronal section and placed into histology cassettes and submitted to MDACC's histology core for processing and standard paraffin embedding. 7 μ m-unstained sections were processed and 1 was H&E-stained.

Immunofluorescence (frozen)

Frozen slides were removed from -80°C and allowed to thaw to room temperature for 20 minutes. Samples were rehydrated with PBS for 5 minutes. Blocked for 30 minutes at room temperature in 10% serum of the species that the 2°

antibodies were created (PBS). Next, primary antibodies were diluted in the blocking solution per manufacturers' spec sheet overnight at 4°C. Next day, sections were washed twice with PBS +0.1% Tween20 for 5 minutes each followed by a single wash with PBS for 5 minutes. Secondary antibodies conjugated to AlexaFluor 488 or 594 were diluted in 10% blocking solution (1:250) and added to the sections for 1 hour at room temperature followed by the same washing procedure. Sections were then mounted in VectaShield mounting media + DAPI and visualized on a Zeiss microscope. This process was also performed on paraffin sections, see augmented protocol below.

Immunostaining (Paraffin)

Paraffin sections were placed on a 60°C heat block for 30 minutes. Sections were then de-paraffinized in standard xylene/alcohol solutions. Sections were rehydrated in with PBS. Slides were then submersed in either of two antigen retrieval solutions, 1) Citrate, pH=6 or 2) Targeted Antigen Retrieval, pH=9 (DAKO) and incubated at 95°C for 30-45 minutes. Sections were cooled to room temperature. Samples are rehydrated with PBS for 5 minutes. Blocked for 30 minutes at room temperature in 10% serum of the species that the 2° antibodies were created (PBS). Next, primary antibodies were diluted in the blocking solution per manufacturers' spec sheet overnight at 4°C. The following day, sections were washed twice with PBS +0.1% Tween20 for 5 minutes each followed by a single wash with PBS for 5 minutes. Next, sections were blocked for endogenous peroxidases with 0.3% hydrogen peroxide in PBS for 10 minutes. Then, sections were washed three times with PBS. Sections were incubated in biotin conjugated

secondary antibodies for 1 hour. Sections were washed twice with PBS +0.1% Tween20 for 5 minutes each followed by a single wash with PBS for 5 minutes. Then, sections were incubated in ABC chromagen (Vector) complexes for 30 minutes. Sections were washed three times in PBS followed by DAB peroxidase substrate incubation (Vector) for about 5-10 minutes. Next, sections are rinsed in water and counterstained with hematoxylin (Vector). Finally, sections are mounted with a xylene-based mounting medium (Richard Allen Scientific).

Immunocytochemistry (Coverslips)

Glass coverslips were coated with 10 µg/ml murine laminin cultured from murine sarcoma basement membrane (Sigma) for 1 hours. Coverslips were rinsed twice with PBS and 25,000 – 100,000 cells were plated per well. Once cells grew to the desired confluence, they were rinsed once with PBS and then fixed on ice with 4% PFA for 10 minutes. Next, coverslips were washed again with PBS and permeabilized with PBS + 0.5% NP40 for 10 minutes at room temperature. Coverslips were washed with PBS and blocked in 10% serum of the species in which the secondary antibody was produced. After blocking, primary antibody was incubated atop the coverslip overnight at 4°C. Next day, coverslips were washed twice with PBS +0.1% Tween20 for 5 minutes each followed by a single wash with PBS for 5 minutes. Coverslips were incubated in fluorescent-conjugated secondary antibodies and mounted in vectashield mounting medium + DAPI and imaged under the Zeiss microscope.

Fluorescence Activated Cell Sorting (FACS)

Green fluorescence protein (GFP) sorting

Primary GBM cell lines and transformed human astrocytes were transduced with lentiviral constructs were washed with PBS and detached with trypsin (adherent cells) or accutase (neurospheres). Cells were sorted by MDACC's FACS core facility on the BD FACS ARIA flow cytometer (BD Biosciences). GFP+ populations were sorted and used in various experiments.

Traditional FACS

Various cell types were washed with PBS and incubated in a Phycoerythrin (PE)-conjugated α v-recognizing antibody and/or an Allophycocyanin (APC)-conjugated CD133-recognizing antibody ($\sim 10\mu\text{L}/10^6$ cells) for 30 minutes on ice in the dark. Proper IgG-isotype and mock controls were performed to validate primary antibody's specificity. Next, cells were washed with a FACS wash buffer (2% FBS or BSA, 2mM EDTA, 1% antibiotics in PBS) twice. PE/APC-labeled cells were then sorted on the BD FACS ARIA flow cytometer by the MDACC core facility. Analysis was focused on evaluating α v integrin expression in specific cell types as well as sorting α v high and low, and in some instances CD133+, populations for intracranial injection.

***In vitro* Proliferation Assay**

Cells were plated at 25,000 cells/well into 12 well plate, each cell type were performed in triplicate. Using trypan blue exclusion solution and a hemocytometer, cells were counted at 24, 48, 72 and 96 hours post-plating.

Soft Agar Assays

A 1% solution of sterile DNA-grade agarose was mixed with 2X DMEM medium, and the 1X base solution was added to 6-well dishes and solidified. The transformed mouse and human astroglia (20,000 cells/ml in 2X media) were mixed with a 0.7% agarose solution, and 5,000 cells were added to the base agarose. The plates were incubated at 37°C for 14 days. Cells were fixed with 4% PFA/PBS, stained with 0.1% crystal violet and mean colonies were counted.

Luciferase Reporter Assays

Mink lung epithelial cells stably transfected with a PAI1-Luciferase plasmid (106) were seeded onto poly-lysine-coated 6-well plates at 4×10^5 cells per well. Twelve hours later media was removed and serum-free media was added for 24 hours. Conditioned media from wild type and $\beta 8^{-/-}$ transformed astroglial progenitor cells pre-incubated for 12 hours with or without 10 ng/ml LAP-TGF β 1 (R&D Systems) was collected and added to MLECs for 12 hours. Cell lysates were then prepared and luciferase substrates were added and quantified using an Enhanced Luciferase Assay Kit (BD Biosciences).

Semi-quantitative Reverse Transcriptase PCR (RT-PCR)

RNA/cDNA Preparation

Cells were harvested and 0.5 ml of Trizol reagent (Invitrogen) was added and pipetted up/down. This mixture incubated for 10 minutes at room temperature. Next, mixture was centrifuged for 10 minutes in the cold room. The soluble fraction

was transferred to a new microfuge tube and to it 100µL of chloroform was added, homogenized and incubated at room temperature for 10 minutes. Next, mixture was centrifuged for 15 minutes in the cold room. The top phase was transferred to a fresh microfuge tube where 250µL of isopropanol was added for 10 minutes at room temperature. Samples were centrifuged and the supernatant was removed left with the RNA pellet. The pellet was washed with 70% EtOH followed by another centrifugation step. The pellet was dried with a vacuumfuge and dissolved in 50µL of water. Next, absorbance readings determined the concentration of the cRNA.

5µg of cRNA was used to produce cDNA according to protocols of SuperScript II Reverse Transcriptase kit (Invitrogen). Resulting cDNA was treated with RNase A to remove any residual cRNA in the sample.

***In vitro* analysis of TGFβ gene expression (cDNA)**

The expression of TGFβ isoforms was determined by RT-PCR. The following primers were used to look at three TGFβ isoforms:

TGFβ1

(Forward) 5'-GCTACTGCCGCTTCTGCT-3'

(Reverse) 5'-GCCCTGTATTCCGTCTCC-3'

TGFβ2

(Forward) 5'-TACTACGCCAAGGAGGTT-3'

(Reverse) 5'-AATTATTAGACGGCACGAA-3'

TGFβ3

(Forward) 5'-GCAAAGGGCTCTGGTAGT-3'

(Reverse) 5'-GTCTCCATTGGGCTGAAA-3'

The primers along with the Platinum Taq DNA Polymerase High Fidelity kit (Invitrogen) were used to determine isoform expression. GAPDH cDNAs were amplified by PCR in the same reaction mixture and carried out by an initial denaturation at 94°C for 2 min, followed by 35 cycles of denaturation at 94°C for 30 seconds, annealing at 55°C for 30 seconds, and extension at 68°C for 1 minute. A final elongation step was carried out at 68°C for 10 min.

Vascular Endothelial Growth Factor A (VEGF-A) gene expression

cDNAs were generated in the same way as for the TGF β isoform studies. VEGF-A isoforms were amplified by RT-PCR using primers in the mouse VEGF cDNA amplification kit (R&D Technologies). Kit positive controls were amplified by PCR in the same reaction mixture and carried out by an initial denaturation at 94°C for 5 min, followed by 35 cycles of denaturation at 94°C for 45 seconds, annealing at 55°C for 45 seconds, and extension at 72°C for 45 seconds. A final elongation step was carried out at 72°C for 10 min. The kit produces bands at 613, 541 and 410 basepairs for VEGF-188, -165 and -120, respectively. Positive control product size is 235 bp.

Lentiviral shRNA Cloning/Transduction

For lentiviral-mediated stable knockdown of human β 8 integrin, DNA oligonucleotides were synthesized (Integrated DNA Technologies) to generate shRNA stem loops. Three separate regions of the human β 8 integrin cDNA were targeted. The following three sequences were BLAST-searched to confirm minimal homology with other genes (**bold**=loop):

1: 5'-GCAAAGGCTGCTCAGTTGATT**CAAGAGAT**CAACTGAGCAGCCTTTGC-3'

- Targets the 3' β 8 ORF

2: 5'-GTATGGCATACCTACAGGGTT**CAAGAGACC**CTGTAGGTATGCCATAC-3'

- Targets the 5' β 8 ORF

3: 5'-GCAAAGGCTGCTCAGTTGATT**CAAGAGAT**CAACTGAGCAGCCTTTGC-3'

- Targets the β 8 UTR

Three separate regions of the human α v integrin cDNA were targeted. The following sequences were BLAST-searched to confirm minimal homology with other genes (**bold**=loop):

1: 5'-GTCCCATCAGTGGTTTGGATT**CAAGAGAT**CCAAACCACTGATGGGAC-3'

- Targets the 3' α v ORF

2: 5'-GTTGGCAGATCTTCCTAAGTT**CAAGAGACT**TAGGAAGATCTGCCAAC-3'

- Targets the 5' α v ORF

3: 5'-GAGGAGTCTCGAGTCCTGATT**CAAGAGAT**CAGGACTCGAGACTCCTC-3'

- Targets the α v UTR

Non-Targeting (NT) Sequence (provided by Bar-Eli lab lentiviral core):

5'- TTCTCCGAACGTGTCACGT-3'

The α v and β 8 oligonucleotides were annealed into the pLB lentiviral gene-transfer vector (107), using the HpaI and XhoI restriction sites. Highly competent *E. coli* (DH5 α – Invitrogen) were transformed with the annealed lentiviral vector and grown overnight at 37°C on ampicillin-resistant LB-agar. Many bacterial colonies were isolated and grown in LB-broth (+amp) overnight at 37°C at 225 RPM. DNA

was isolated from the bacteria via a Midi plasmid DNA purification kit (Qiagen). Lone Star DNA sequencing company verified proper insertion and lengths of inserts. Lentiviruses were produced by transfecting 293-FT cells with pLB transfer vectors (α v, β 8 and NT) in combination with plasmids encoding gag/pol and VSV-G envelope proteins. Next day, the media is changed and fresh growth medium is added. The following day, lentiviral media is harvested, filtered to remove cellular debris and concentrated using centrifugation concentrators (Fisher). Appropriate cells are plated at 50-70% confluence into 6 well plates and transduced with the lentivirus + polybrene (Sigma) overnight. Next day, viral-containing medium is aspirated off and fresh normal growth media is added. Knockdown is verified via western blot. A target of 70% or higher knockdown is most desirable.

Invasion Assays

Matrigel invasion assay chambers (BD - 8 μ M pores) were pre-incubated in media containing no chemoattractant. 10% FBS in normal growth medium was added to the lower well to act as the chemoattractant for the 50,000 cells transformed human astrocytes plated above the Matrigel-coated insert. Invasion occurred over a 24 hour period at 37°C. Next day, the inserts were removed, the matrigel swabbed away and the invaded cells on the opposite side from their initial placement were stained with crystal violet. The stain was solubilized in 2% SDS and an absorbance reading at OD=570nm was measured.

Live Migration Assays

Transformed human astrocytes were plated at 100,000 cells/well onto murine laminin coated coverslips. At 100% confluence, with a p-10 pipette tip, a wound or scratch was made down the middle of the coverslip. Over 36 hours, at increments of 30 minutes, pictures were taken with the Olympus Inverted Imaging Microscope. Movies were visualized and migration rates were determined.

VEGF/TGF β ELISAs

300,000 cells were plated into 6-well plates at the same densities and were allowed to condition the media for 48 hours. Each cell type was assayed in triplicate. Media was harvested and filtered to remove cellular debris. Kit and unconditioned medias were used as controls. Colormetric ELISAs were used to quantify VEGF (R&D Systems) and TGF β (eBioscience) presence in conditioned medias.

Statistical Analyses

Student's t-test was used to determine statistically significant differences. The Wilcoxon Rank Sum Test was used for analysis of Kaplan-Meier survival results.

CHAPTER 3: Specific Aim 1

Determining Functional Roles for $\alpha v\beta 8$ Integrin in Glioma-Induced Angiogenesis using an Orthotopic Mouse Model of Astrocytoma

Introduction

Grade IV astrocytomas, or glioblastoma multiformes (GBMs) are the most common and fatal form of primary brain cancer and are noted for their hallmark angiogenic pathologies (108). More specifically, blood vessels in GBMs exhibit endothelial cell hyperplasia, glomeruloid-like tufts, and show signs of edema and hemorrhage owing to the breakdown of the intratumoral blood brain barrier (102). Over the last several decades, the median survival rate for GBM-diagnosed patients has remained at 9-12 months (57) due to the poor efficacy of standard clinical intervention (55).

Our laboratory has shown previously that $\alpha v\beta 8$ integrin is a key regulator of angiogenesis in the embryonic mouse brain (35, 36, 44, 52, 109). Upon genetic ablation of αv or $\beta 8$ integrin genes in neural progenitors and astrocytes, but not endothelial cells, intracranial vascular phenotypes develop as a result of defective integrin-mediated activation of LAP-TGF β s (33, 49). Combined TGF β 1 and TGF β 3 loss leads to severe intracerebral hemorrhage, similar to those vascular pathologies identified in αv and $\beta 8$ integrin knockout mouse models (110). Consequently, conditional deletion of TGF β RII on Alk1-positive endothelial cells leads to similar brain-specific vascular pathologies (Paul Oh, University of Florida College of

Medicine). Collectively, these models identify the $\alpha v\beta 8$ integrin-TGF β axis as a key regulator of brain angiogenesis in which genetic ablation of any component leads to intracranial-specific vascular pathologies commonly observed in GBM.

Thus, we hypothesized that abnormal $\alpha v\beta 8$ integrin expression and/or function contributes to the angiogenesis pathologies in malignant brain tumors. Herein, a mosaic mouse model of astrocytoma was developed to elucidate the functional roles for $\alpha v\beta 8$ integrin in glioma-induced angiogenesis.

Results

Isolation of Primary Astroglia from Wild Type and $\beta 8^{-/-}$ Mice

Primary astroglial cells were cultured from neonatal (P0-P3) wild type (+/+) and $\beta 8$ integrin homozygous ($\beta 8^{-/-}$) mutant mice from cerebral cortices. Neonatal $\beta 8^{-/-}$ mice exhibited distinctive intracerebral hemorrhage (Figure 7c) as compared to wild type (Figure 7a) mice, thus making them easily distinguishable. In addition, mice were genotyped via PCR utilizing genomic tail DNA as previously described (44). Cells were grown on dishes coated with laminin, a basement membrane protein known to support neural stem and progenitor cell proliferation (111). The majority of wild type and $\beta 8^{-/-}$ astroglia expressed the astrocytic and sometimes neural progenitor marker (112), glial fibrillary acidic protein (GFAP) (Figure B, D upper panel) while nearly 100% of the cells expressed robust levels of Nestin, a marker for neural progenitors within the brain (Figure 7b, d middle panel) (113). Co-localization of GFAP and Nestin reveals nearly 100% overlap (Figure 1b, d lower panel). To verify integrin expression, both wild type and $\beta 8^{-/-}$ primary astroglial cell surfaces were labeled with an amine-reactive derivative of biotin. Immunoprecipitation with integrin-specific antibodies was performed showing robust levels of both $\alpha\beta 5$ and $\alpha\beta 8$ integrins expressed on wild type primary astroglia (Figure 7e, left panel), similar to the integrin profile of primary human astrocytes (49). The $\beta 8^{-/-}$ cells express $\alpha\beta 5$ integrin, but not $\alpha\beta 8$ integrin (Figure 7e, right panel) due to the genetic ablation of the $\beta 8$ integrin gene. Both cell lines also express robust levels of $\alpha\beta 3$ and $\alpha\beta 1$ (data not shown). Wild type and $\beta 8^{-/-}$

primary astroglial proliferation rates were quantified over a 96-hour period identifying no obvious differences.

Figure 7: Wild Type and $\beta 8^{-/-}$ Primary Astroglia

Wild type (A) and $\beta 8^{-/-}$ (C) postnatal day 1 whole brains are distinguishable based on the hemorrhage throughout knockout brain. Wild type (B) and $\beta 8^{-/-}$ (D) neonatal primary astroglia are microdissected from cerebral cortices. Both cell types express similar levels of GFAP (B, D upper panels) and Nestin (B, D middle panels), displaying high co-localization (B, D lower panels). (E) Cell-surface analysis of integrin expression on wild type and $\beta 8^{-/-}$ primary astroglia. Biotinylation and immunoprecipitation reveals the lack of $\alpha \nu \beta 8$ integrin expression in $\beta 8^{-/-}$ primary astroglia. (F) $\alpha \nu \beta 8$ integrin expression status does not alter *in vitro* proliferation rates of primary astroglia (n=3/timepoint) at 24, 48, 72 and 96 hours post-plating.

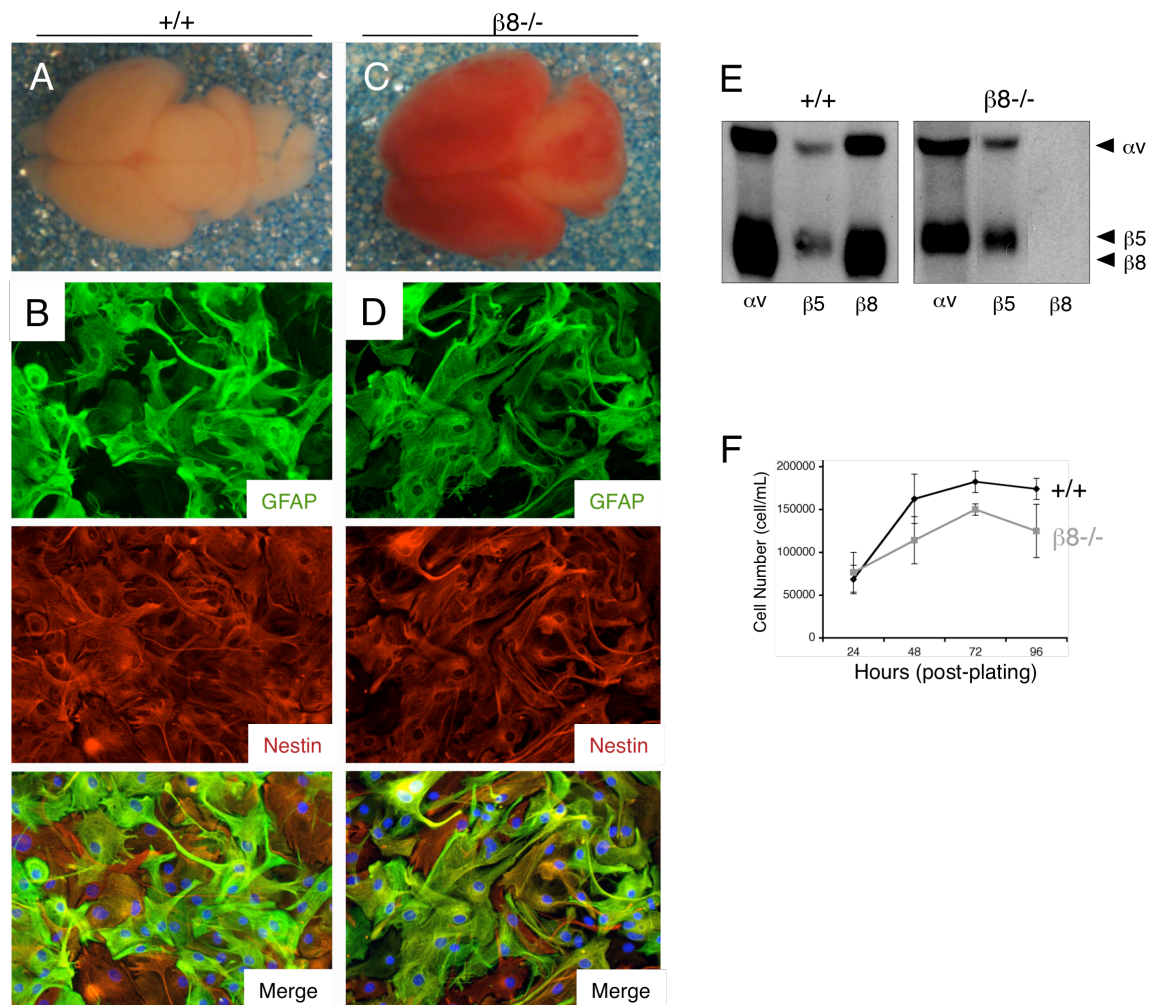


Figure 7

Immortalization and Transformation of Wild Type and β 8-/- Primary Astroglia

Nestin-positive primary wild type (Figure 8a, upper panel) and β 8-/- (Figure 8a, bottom panel) astroglia were transduced with a retrovirus expressing human papilloma virus (HPV) E6 and E7 proteins (80), thus immortalizing them (Figure 8d, middle panel). The E6 oncoprotein ubiquitinates p53, a major tumor suppressor, and sends it to the proteosome for degradation while E7 inhibits the association of pRB with the E2F transcription factor allowing for uncontrolled cell cycle progression (Figure 8c) (114). p53 and pRb functions are often abrogated in human gliomas (108, 115). Next, immortalized astroglia were transformed by a second retroviral transduction producing an oncogenic version of H-Ras (G^{12V} H-Ras) (80) (Figure 8d, upper panel) as Ras function is often elevated in the glioma setting, either via gene mutations or increased expression of other upstream tyrosine kinases (65). While nestin expression did not change among primary and transformed astroglial populations, the transformed morphologies certainly appeared smaller, spindled and elongated as compared to their primary form (Figure 8a,b).

Upon transformation of the wild type and β 8-/- primary astroglia, we observed a substantial gain in CD133/Prominin 1 expression (Figure 9a, lower panel; 9b 2nd panel), a transmembrane protein commonly expressed in embryonic neural stem cells (116), GBM and other solid tumors (57, 117). Any expression of GFAP in the primary astroglia was completely lost post-transformation (Figure 9a, top panel; 9b, 3rd panel), although nestin expression remained ubiquitous among the cell lines (Figure 9a, middle panel; 9b, 1st panel). CD133/Prominin 1's increase in expression coupled with GFAP loss tends to suggest that upon transformation,

these astroglia are becoming 'de-differentiated', commonly observed by others upon oncogenic transformation (115, 118).

Lastly, *in vitro* evaluation of the wild type and $\beta 8^{-/-}$ transformed astroglia was necessary to assess the necessity of $\alpha v\beta 8$ integrin for proliferation and growth anchorage independence. Firstly, proliferation rates were analyzed over a 96-hour time period (n=3/cell line) showing no obvious differences (Figure 10a). Secondly, a classical assay was used to establish the doubly transduced astroglia as being 'transformed,' essentially evaluating the ability of the cells to form colonies in an anchorage independent fashion, as non-malignant cells will not. Again, soft agar colony formation did not differ among the wild type and $\beta 8^{-/-}$ transformed astroglia (Figure 10b).

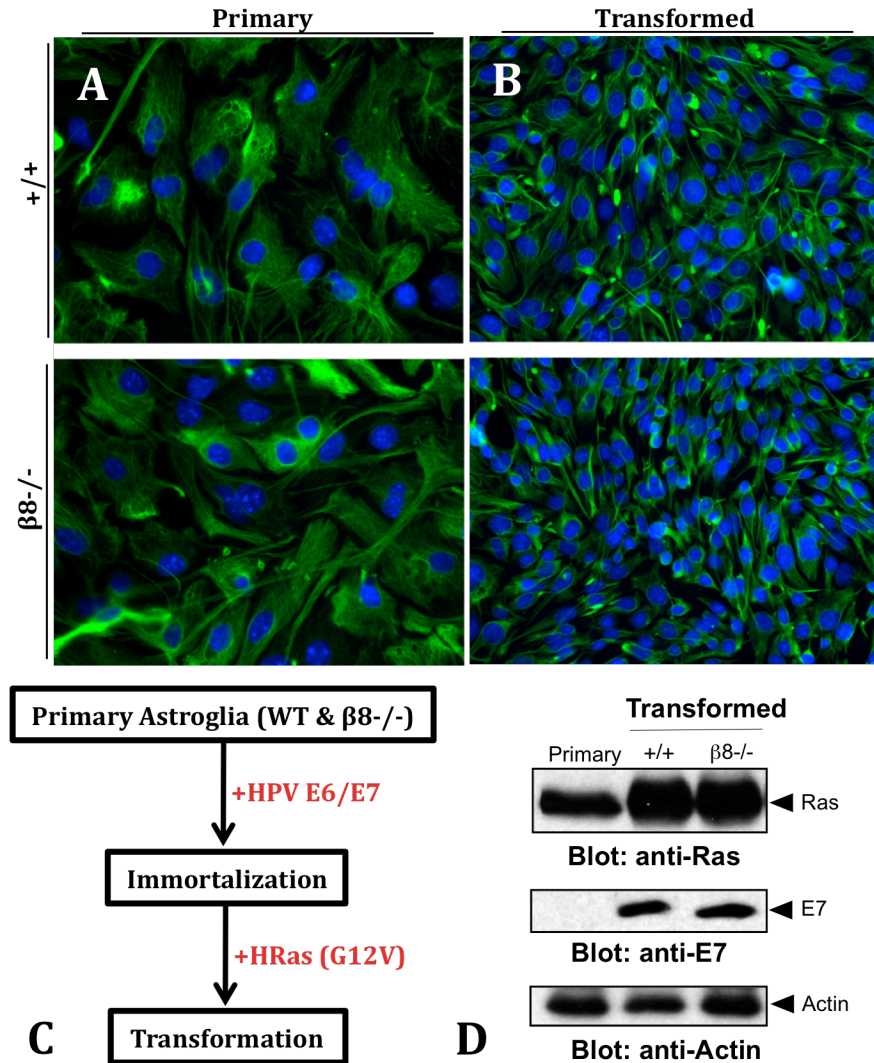


Figure 8: Malignant Transformation of Primary WT and $\beta 8^{-/-}$ 1° Astroglia

Upon immortalization and transformation of wild type and $\beta 8^{-/-}$ astroglia, nestin expression is retained although transformed astroglia display a more spindled morphology (A, B) (C) Scheme for two-step retroviral immortalization and transformation of primary wild type and $\beta 8^{-/-}$ astroglia. (D) Overexpression of mutant HRas (G12V) and E7 oncoprotein whole cell lysates immunoblotted with anti-Ras, E7 and β -actin antibodies.

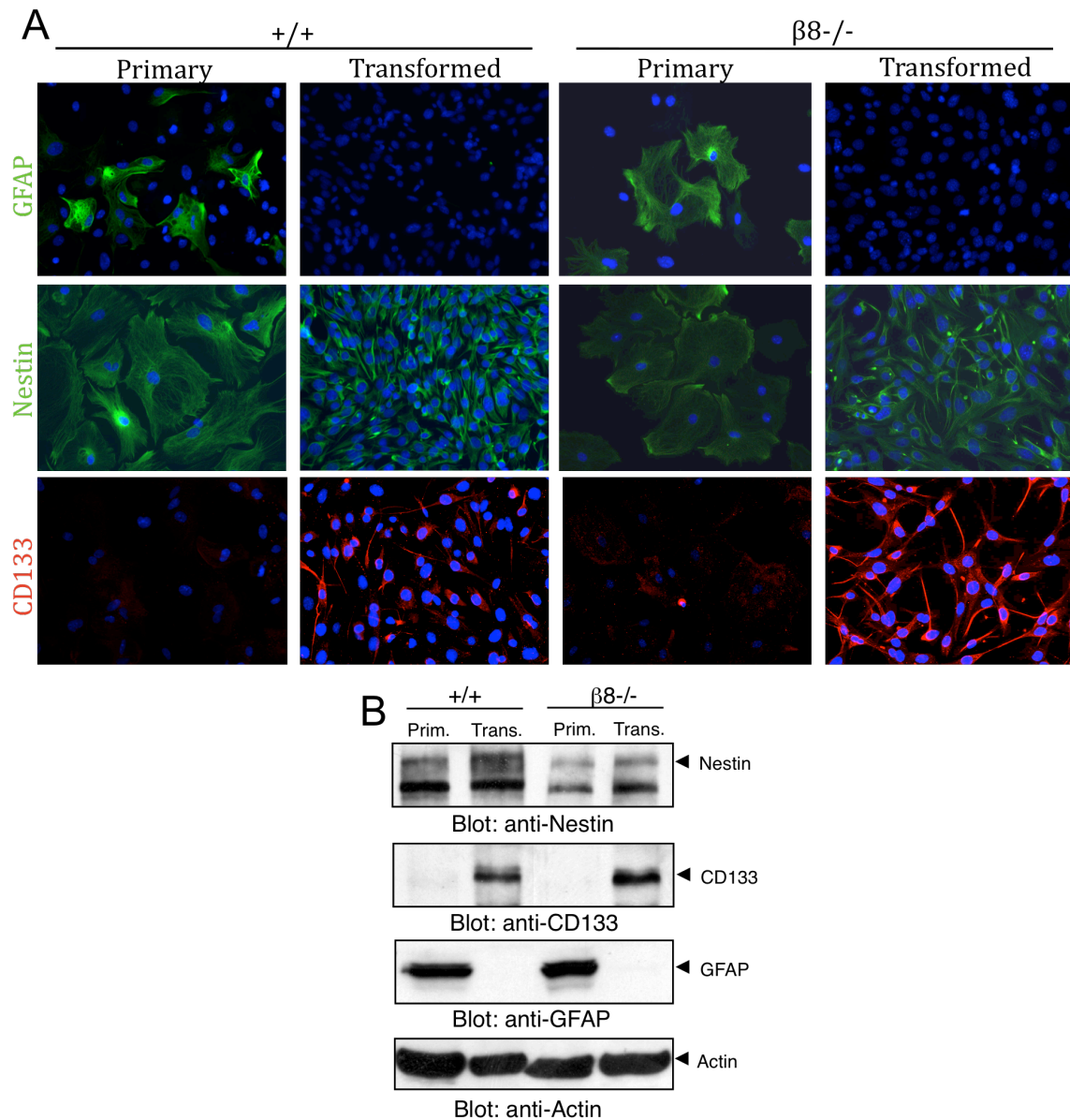


Figure 9: ‘De-differentiation’ upon Transformation of Astroglia

(A/B) Malignant transformation of wild type and $\beta 8^{-/-}$ astroglia induces suspected ‘de-differentiation’ evident by a loss of GFAP expression (A, upper panel IF & B, GFAP immunoblot) and gain of CD133 expression (A, bottom panel IF & B, CD133 immunoblot). Nestin expression (A, middle panel IF & B, Nestin immunoblot) remains ubiquitous among the cells lines. β -actin acts as a loading control for the immunoblot.

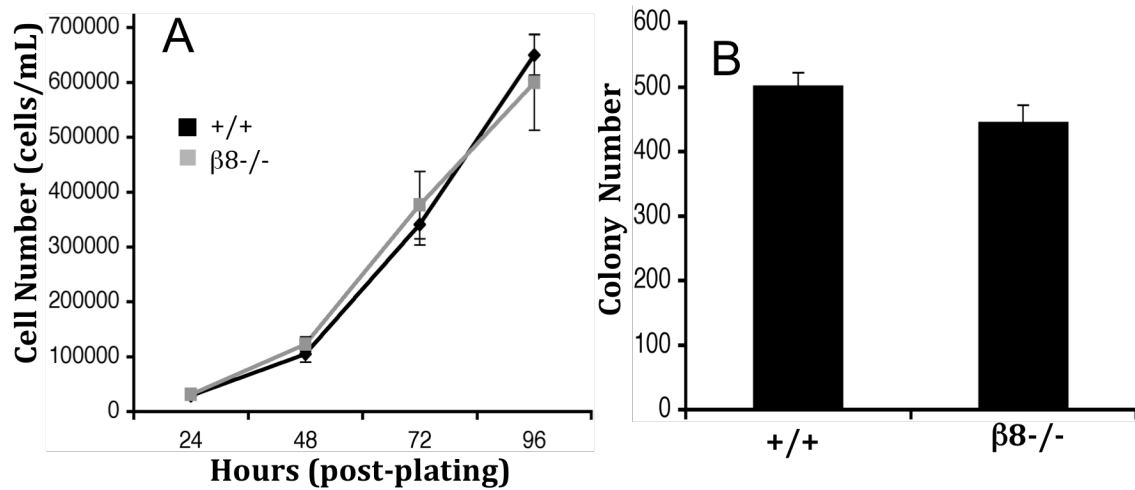


Figure 10: Wild Type and $\beta 8^{-/-}$ Transformed Astroglia *in vitro* Growth Characteristics

(A) $\alpha \beta 8$ integrin expression status does not alter *in vitro* proliferation rates of transformed astroglia (n=3/timepoint) at 24, 48, 72 and 96 hours post-plating. (B) $\alpha \beta 8$ integrin expression status does not alter *in vitro* anchorage independence of transformed astroglia in a soft agar colony formation assay (n=3/cell type).

Oncogenic Transformation Reduces $\alpha\beta 8$ Integrin Expression

Due to the lack of specificity of all commercially available anti- $\beta 8$ antibodies, primary and transformed wild type and $\beta 8^{-/-}$ astroglia were characterized for their $\alpha\upsilon$ integrin cell surface protein expression via fluorescent activated cell sorting (FACS). Among the primary cells, upwards of 90% of them expressed $\alpha\upsilon$ integrin (Figure 11a, upper plots). Upon transformation, a two-fold reduction in cell surface $\alpha\upsilon$ integrin expression was observed (Figure 11a, bottom plots). Corroborating evidence of the FACS data was established upon further analysis of whole cell lysates from primary and transformed astroglia. The wild type cells lost upwards of 90% of their $\beta 8$ integrin expression while also exhibiting a reduction in overall $\alpha\upsilon$ integrin expression (Figure 11b, top two panels). Oncogenic-mediated transformation did not promote an overall reduction in 'global' integrin expression, as $\beta 1$ integrin is ubiquitously expressed among the cell lines, both primary and transformed (Figure 11b, 3rd panel). Interestingly, upon wild type transformed astroglia passaging, $\beta 8$ integrin expression diminishes and was completely lost by p10 (Figure 11c) while $\alpha\upsilon$ integrin expression decreased. This was not a cell culture artifact as primary wild type neurospheres cultured over 6 passages did not lead to the same result (Figure 11d). Additionally, these neurospheres have been passaged out to p10 (data not shown) exhibiting no change in $\alpha\upsilon\beta 8$ integrin expression.

Figure 11: Reduced $\alpha v\beta 8$ Integrin Protein Expression Post-transformation.

(A) Primary cells (top panel) and transformed cells (lower panel) were analyzed by fluorescent-activated cell sorting using an anti- αv integrin phycoerythrin (PE) antibody (% positive in red boxed areas). Sort reveals an approximate 50% reduction in overall αv integrin cell-surface expression. (B) Lysates from primary (prim.) and transformed (trans.) wild type and $\beta 8^{-/-}$ astroglia were immunoblotted with anti- αv , $\beta 8$, and $\beta 1$ integrin. β -actin acts as a loading control (same lysates used in Figure 10). Note the progressive loss of both αv and $\beta 8$ integrin proteins as a result of oncogene transformation, while $\beta 1$ integrin expression remains ubiquitous. The lower band in the αv integrin blot most likely represents a non-glycosylated integrin isotype. (C) Wild type transformed astroglia grown for 12 passages. P2-P12 lysates were immunoblotted with antibodies against αv and $\beta 8$ integrins. β -actin acts as a loading control. Note the progression of $\alpha v\beta 8$ integrin loss as cells are passaged. (D) Primary neurospheres were grown for 6 passages and no changes in αv or $\beta 8$ integrin expression were evident. β -actin is as a loading control.

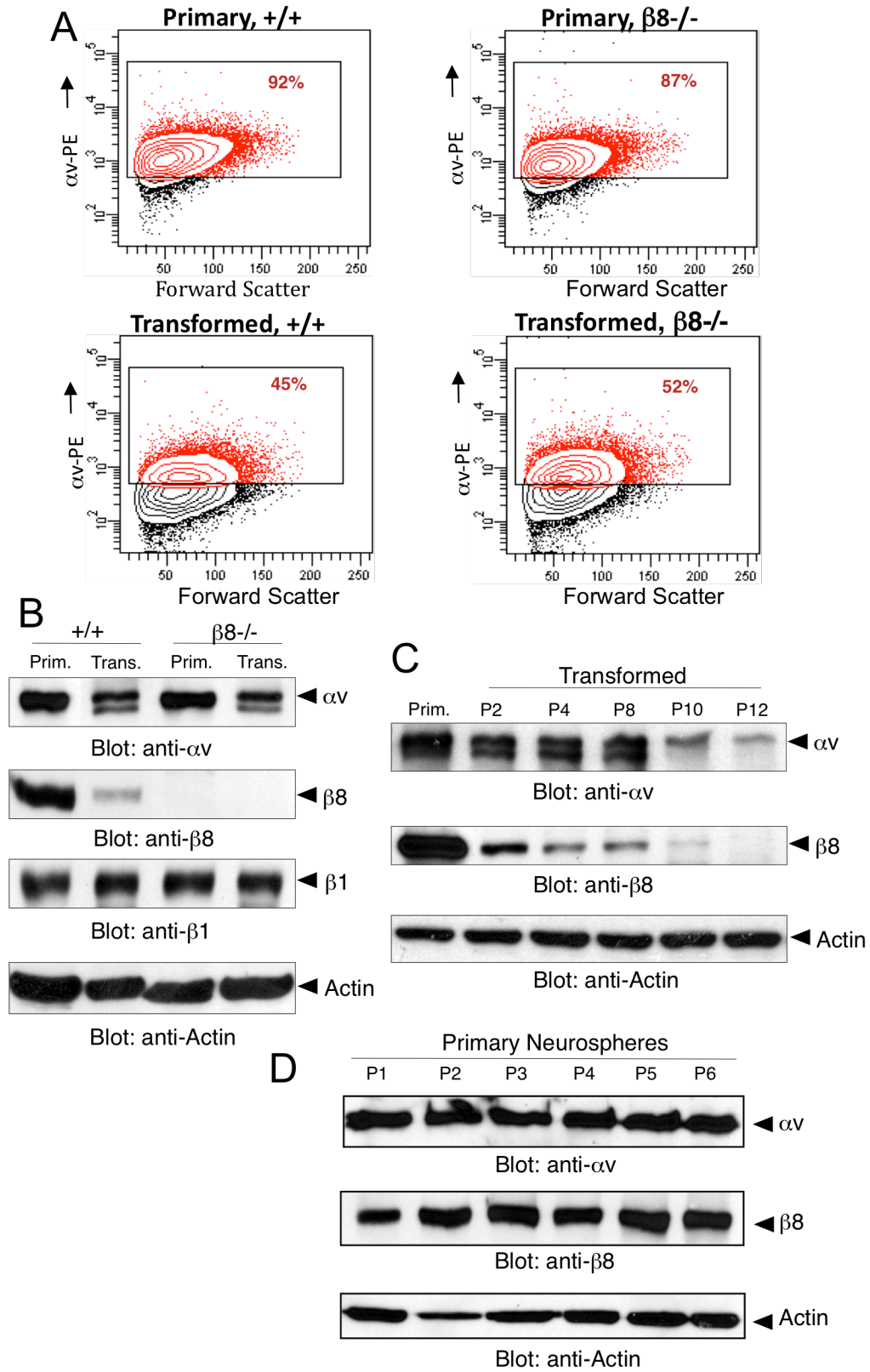


Figure 11

Gross Analysis of $\beta 8$ Integrin Expression in a Mosaic Mouse Model of Astrocytoma

Due to evidence of diminished $\alpha v\beta 8$ integrin expression beyond passage four in wild type transformed astroglia (Figure 11c), we only used early passage cells (p2-p4) in this study. Wild type and $\beta 8^{-/-}$ transformed astroglia were stereotactically injected into the striatum of immunocompromised mice to evaluate their *in vivo* tumorigenicity. In the first set of injections, 500,000 wild type and $\beta 8^{-/-}$ transformed astroglia were implanted and allowed to proliferate for 21 days ($n=20$ /cell line). The tumor bearing mice were anesthetized and cardiac perfused to flush out any of the properly functioning vessels and to attain a better fix of the brain tissue. After a 24-hour post-fix, brains were coronally sliced at 1mm increments. There were clear macroscopic differences among the appearances of the wild type and $\beta 8^{-/-}$ astrocytomas (Figure 12a, b). While all mice injected developed tumor, only two of the 20 wild type astrocytomas developed gross intratumoral hemorrhage while nearly all $\beta 8^{-/-}$ tumor bearing mice (17/20) exhibited it.

A Kaplan-Meier survival study evaluated the overall effect of wild type ($n=20$) and $\beta 8^{-/-}$ ($n=16$) tumor bearing animals where 25,000 cells were injected into the same location. Tumors were allowed to grow until the mice succumbed to tumor burden. $\beta 8^{-/-}$ tumor bearing animals survived significantly less than wild type tumor bearing animals (Figure 12c). At 50% survival, $\beta 8^{-/-}$ tumor bearing mice survived 26 days while wild type tumor bearing mice survived 33 days. The primary reason for premature death of the $\beta 8^{-/-}$ tumor bearing mice is most likely due to the severe

intratumoral hemorrhage leading to cerebrospinal fluid blockage resulting in hydrocephaly thus causing severe neurological defects.

In a separate set of experiments, 500,000 wild type and $\beta 8^{-/-}$ transformed astroglia were intracranially implanted into nude mice and tumor volume was evaluated at 14 and 21 days post-injection (n=9/cell line/time point). Tumor volumes were assessed by measuring the largest cross-section of H&E-stained tumor sections multiplied by the thickness of the coronal sections and how far the tumor spanned the brain parenchyma. Although clear macroscopic pathologies and a significant decrease in overall survival in $\beta 8^{-/-}$ astrocytomas were obvious, tumor volumes did not vary (Figure 12d).

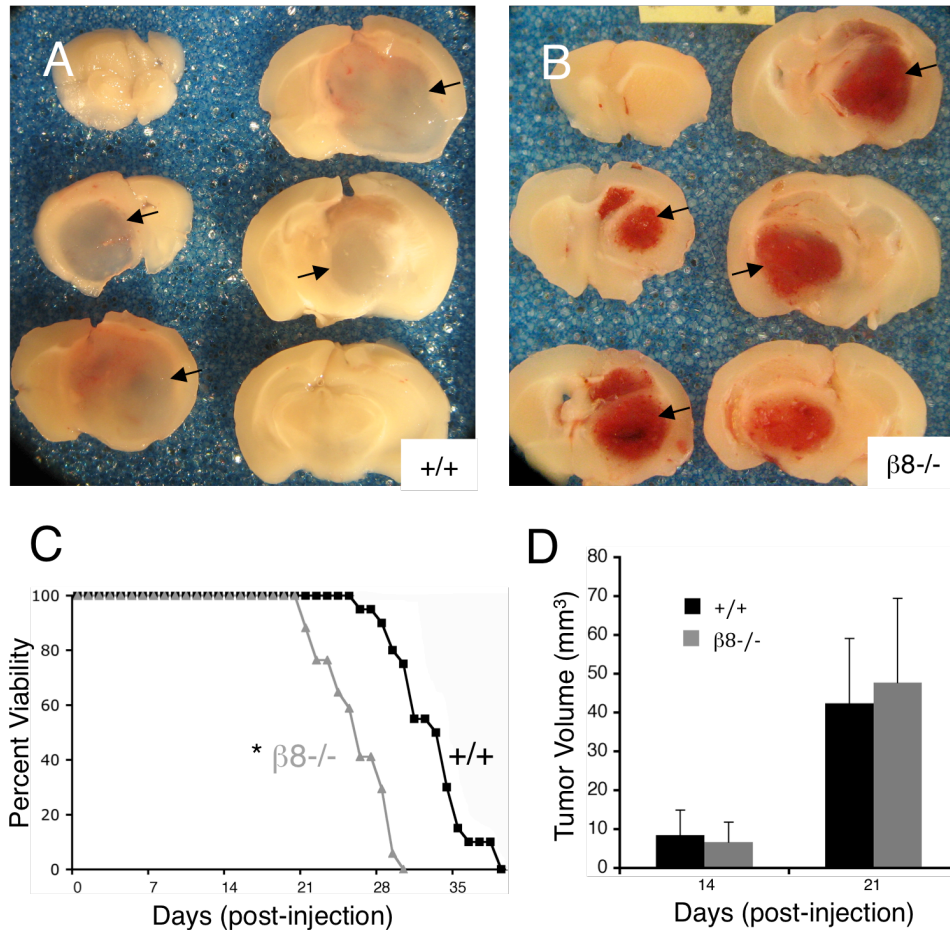


Figure 12: Severe Intratumoral Vascular Pathologies in $\beta 8^{-/-}$ Tumor Bearing Animals Cause Reduced Overall Survival.

(A) Wild type and (B) $\beta 8^{-/-}$ tumor bearing mice were cardiac perfused and sectioned at 1mm increments. Note the gross vascular pathologies in the $\beta 8^{-/-}$ tumors (arrows in B). (C) Kaplan-Meier survival analysis reveals a significant overall reduction in survival in $\beta 8^{-/-}$ tumor bearing mice (n=16) versus wild type tumor bearing mice (n=20) (*p<0.001 at 50% survival). (D) Athymic mice harboring wild type and $\beta 8^{-/-}$ astrocytomas were sacrificed at 14 days (n=9/genotype) and 21 days (n=8/genotype) after injection. No differences in tumor volume were observed among the wild type and $\beta 8^{-/-}$ astrocytomas.

Microscopic Analysis of Wild Type and $\beta 8^{-/-}$ Astrocytomas

Coronal sections of wild type and $\beta 8^{-/-}$ astrocytomas were H&E-stained revealing differences in the vascular make-up of these tumors. Wild type (Figure 13a) tumors were well-vascularized and displayed pathologies consistent with those present in grade III anaplastic astrocytomas (119, 120). However, $\beta 8^{-/-}$ astrocytomas displayed severe vascular pathologies including intratumoral hemorrhage as well as vascular edema and thrombosis (Figure 13b). Pathologies evident in knockout tumors are consistent with those hallmarks of grade IV GBMs (55). Blood vessel immunostaining of wild type and $\beta 8^{-/-}$ coronal astrocytoma samples revealed CD34-positive vascular endothelial cells lining the intratumoral vascular networks. $\beta 8^{-/-}$ tumor-associated vessels (Figure 13d, f) were far more distended and tortuous exhibiting signs of thickening of the vessel walls as compared to those found in wild type tumors (Figure 13c, e). Moreover, $\beta 8^{-/-}$ astrocytomas displayed significantly more microvascular density (MVD) than wild type astrocytomas. There were significantly more blood vessels per 200x field ($n=5$ /tumor type), assessed by tallying number of vessels (Figure 13h) and quantifying CD34+ fluorescence (Figure 13g) in knockout tumors compared to wild type tumors. Pericytes are vascular support cells fundamental for normal vascular support and function (121). Therefore wild type and $\beta 8^{-/-}$ astrocytomas were immunostained for desmin, a marker for pericytes, resulting in nearly all intratumoral vascular networks exhibiting proper pericyte coverage (Figure 13e, f).

Figure 13: Histological Analysis of Wild Type and $\beta 8^{-/-}$ Astrocytomas.

Coronal sections of wild type (A) and $\beta 8^{-/-}$ (B) astrocytomas were stained with hematoxylin and eosin (H&E) and visualized microscopically (200x). Note severe vascular pathologies including intratumoral hemorrhage, edema and thrombosis. Coronal sections of wild type (C) and $\beta 8^{-/-}$ (D) astrocytomas were immunostained with an antibody against vascular endothelial cells (arrows), CD34 (400x). CD34 (green) and desmin (red), a marker for pericytes, merged immunofluorescent images of coronal wild type (E) and $\beta 8^{-/-}$ astrocytomas (200x). Coronal sections of wild type (E) and $\beta 8^{-/-}$ (F) astrocytomas were immunofluorescently double-stained with CD34 (green, vessels) and desmin (red, pericytes) (200x). The areas boxed are magnified at the bottom right of these images to illustrate the pericyte coverage of the CD34+ vessels. (G) CD34 immunofluorescence intensity was quantified for wild type and $\beta 8^{-/-}$ astrocytomas (n=5/cell line). (H) Mean vessels were quantified per 200x field in wild type and $\beta 8^{-/-}$ astrocytomas. Note both evaluations of vessel characteristics exhibited significantly more vessel density and number in $\beta 8^{-/-}$ astrocytomas versus wild type astrocytomas (G, *p<0.001; H, *p<0.05).

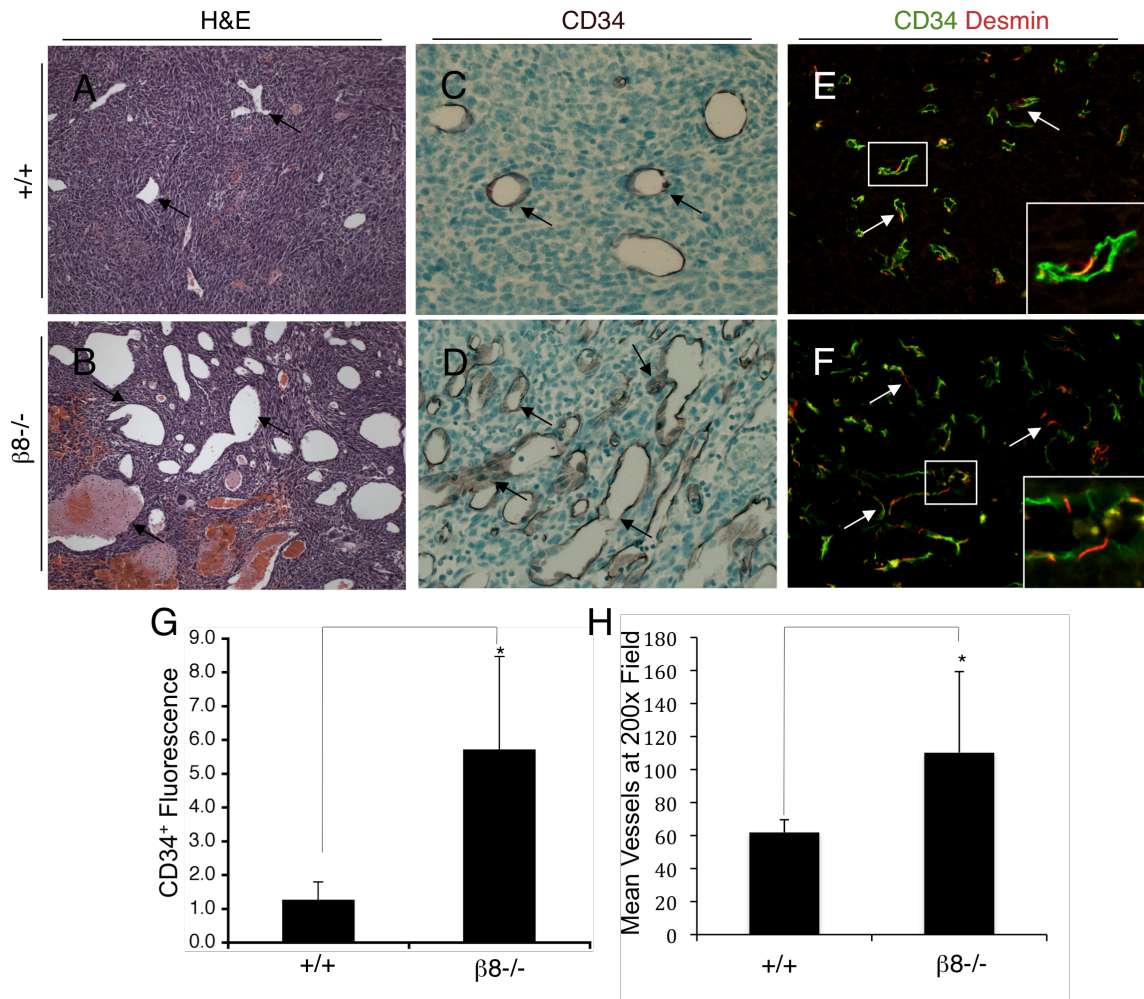


Figure 13

Rescuing $\beta 8$ Integrin Expression in $\beta 8^{-/-}$ Transformed Astroglia

In order to confirm the vascular pathologies found in the $\beta 8^{-/-}$ astrocytomas were due to the genetic ablation of the integrin subunit, $\beta 8$ integrin was overexpressed in the $\beta 8^{-/-}$ transformed astroglia. The cells were stably transfected with a plasmid expressing human $\beta 8$ integrin protein with a C-terminal V5 epitope tag ($\beta 8$ -V5). Expression was verified by western blot with the $\beta 8^{-/-}$ (+ $\beta 8$ -V5) cells displaying robust $\beta 8$ integrin and V5 protein expression (Figure 14A). $\beta 8^{-/-}$ transformed astroglia were stably transfected with empty pcDNA4.0 and intracranially implanted into the striatum of athymic mice (n=5). Resulting tumors recapitulated the overall macro- and microscopic vascular pathologies of the untransfected $\beta 8^{-/-}$ cells (Figure 14b, right panel). Conversely, upon injection of the $\beta 8^{-/-}$ transformed astroglia (n=5) stably restored with $\beta 8$ integrin expression, $\beta 8^{-/-}$ astrocytoma pathologies were largely resolved evident by the loss of gross hemorrhage (Figure 14b, left panel). Vessel pathologies were restored in the 'rescued' tumors (Figure 14c, e) while tumor cells stably transfected with the empty vector exhibited similar microscopic vascular pathologies evident in parental $\beta 8^{-/-}$ tumors (Figure 14d, f). In fact, the severe microvascular density evident in the knockout tumors was significantly reduced in the $\beta 8$ integrin expressing tumors as assessed by CD34 immunofluorescence intensity quantitation (Figure 14g).

Figure 14: Exogenous Expression of $\beta 8$ Integrin Resolves $\beta 8^{-/-}$ Astrocytoma-induced Vascular Pathologies.

(A) $\beta 8^{-/-}$ transformed astroglia were stably transfected with empty vector or vector expressing human $\beta 8$ integrin protein with a V5 C-terminal tag ($\beta 8$ -V5). Cell lysates were immunoblotted against antibodies against $\beta 8$ integrin (top panel) and V5 epitope tag (middle panel). β -actin (bottom panel) acts as a loading control. (B) Athymic mice were intracranially implanted with $\beta 8^{-/-}$ transformed astroglia transfected with vector alone (right panel) or vector plus $\beta 8$ -V5 (left panel). Upon tumor formation, mice cohorts were cardiac perfused and coronally section in 1mm increments. Note the gross hemorrhagic pathology (arrows) in the vector alone $\beta 8^{-/-}$ astrocytomas is largely resolved by exogenous expression of $\beta 8$ integrin. Coronal sections from $\beta 8^{-/-}$ (+ $\beta 8$ -V5) astrocytomas (C) and $\beta 8^{-/-}$ (+vector alone) astrocytomas (D) were H&E-stained (200x). Note the dilated intratumoral blood vessels in $\beta 8^{-/-}$ (+vector alone) astrocytomas are resolved in tumors exogenously expressing $\beta 8$ -V5 integrin protein. Coronal sections from astrocytomas were immunofluorescently stained with CD34 (red) to reveal intratumoral blood vessels, counterstained with a DAPI nuclei stain (blue) (200x). Note the clear differences in vascular patterning in $\beta 8^{-/-}$ (+ $\beta 8$ -V5) tumors (E) compared to $\beta 8^{-/-}$ (+vector) tumors (F). (G) CD34 immunofluorescence intensity was quantified to be significantly less in $\beta 8^{-/-}$ tumors exogenously overexpressing $\beta 8$ integrin protein (* $p < 0.002$).

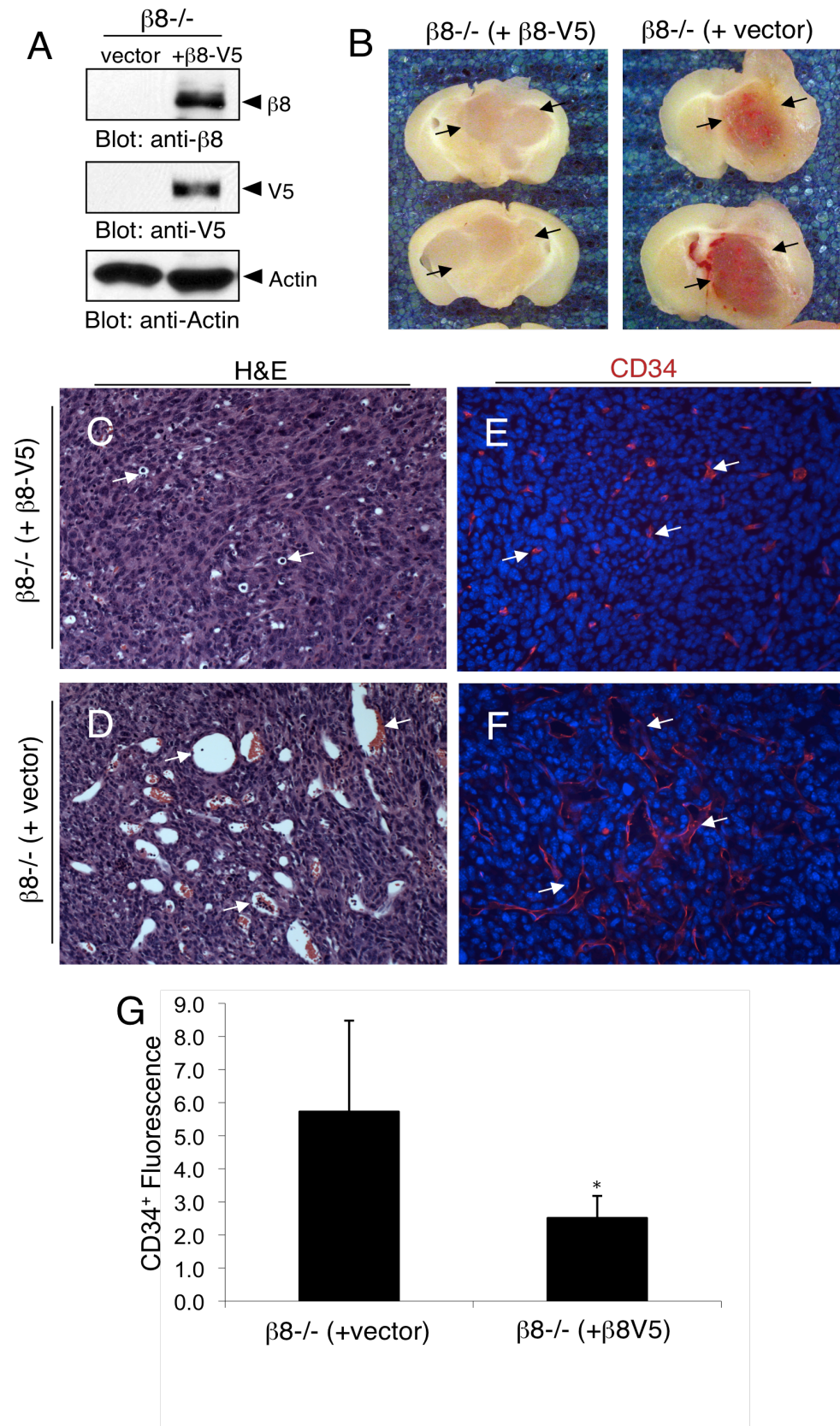


Figure 14

Assessing the Mechanism Behind Severe $\beta 8^{-/-}$ Tumor Vascular Pathologies

Integrin-dependent VEGF expression

Upon initial observation of the knockout tumor obvious vascular pathologies, vascular endothelial growth factor (VEGF), consistent with literature involving the growth factor with pathological hemorrhage and angiogenesis in glioma, was considered to be mechanistically involved (99, 100, 122). Therefore, VEGF levels were assessed at both the mRNA and protein level. Via semi-quantitative RT-PCR, VEGF isoforms -164 and -120 mRNA levels were nearly non-detectable in the $\beta 8^{-/-}$ transformed astroglia as compared to wild type cells (Figure 15a). Furthermore, an ELISA showed $\beta 8^{-/-}$ transformed astroglia conditioned media containing significantly less soluble VEGF as compared to wild type cells (Figure 15b). Wild type and knockout astrocytomas were microdissected from the normal brain parenchyma and lysed (n=2/tumor type). Although *in vitro* analyses would suggest reduced VEGF expression *in vivo*, there was no obvious difference in wild type and knockout tumor lysates (Figure 15c). In addition, *ex vivo* VEGF analysis of both tumor types via immunofluorescence further corroborated what was observed in tumor lysates as no clear distinctions in overall VEGF expression could be elucidated (Figure 15d, e).

Figure 15: VEGF mRNA and Protein Status in WT and $\beta 8$ -/- Astrocytomas.

(A) VEGF mRNA expression analysis of wild type and $\beta 8$ -/- transformed astroglia reveals reduced VEGF120 and VEGF164 isoforms in knockout astrocytomas via semi-quantitative reverse transcription-PCR (RT-PCR). (B) VEGF presence in conditioned media from wild type and $\beta 8$ -/- transformed astroglia was analyzed via a VEGF ELISA (n=3/cell line). Note the significant reduction in VEGF protein levels in $\beta 8$ -/- transformed astroglia conditioned media (*p<0.001). (C) Western blot analysis revealed no difference in intratumoral VEGF protein expression in wild type and $\beta 8$ -/- transformed astrocytomas (n=2/genotype). β -actin (bottom panel) acts as a loading control. Coronal sections of wild type (D) and $\beta 8$ -/- astrocytomas were immunofluorescently stained for CD31 (vessels; arrows, red) and VEGF (green) revealing no obvious differences in VEGF among the tumor types.

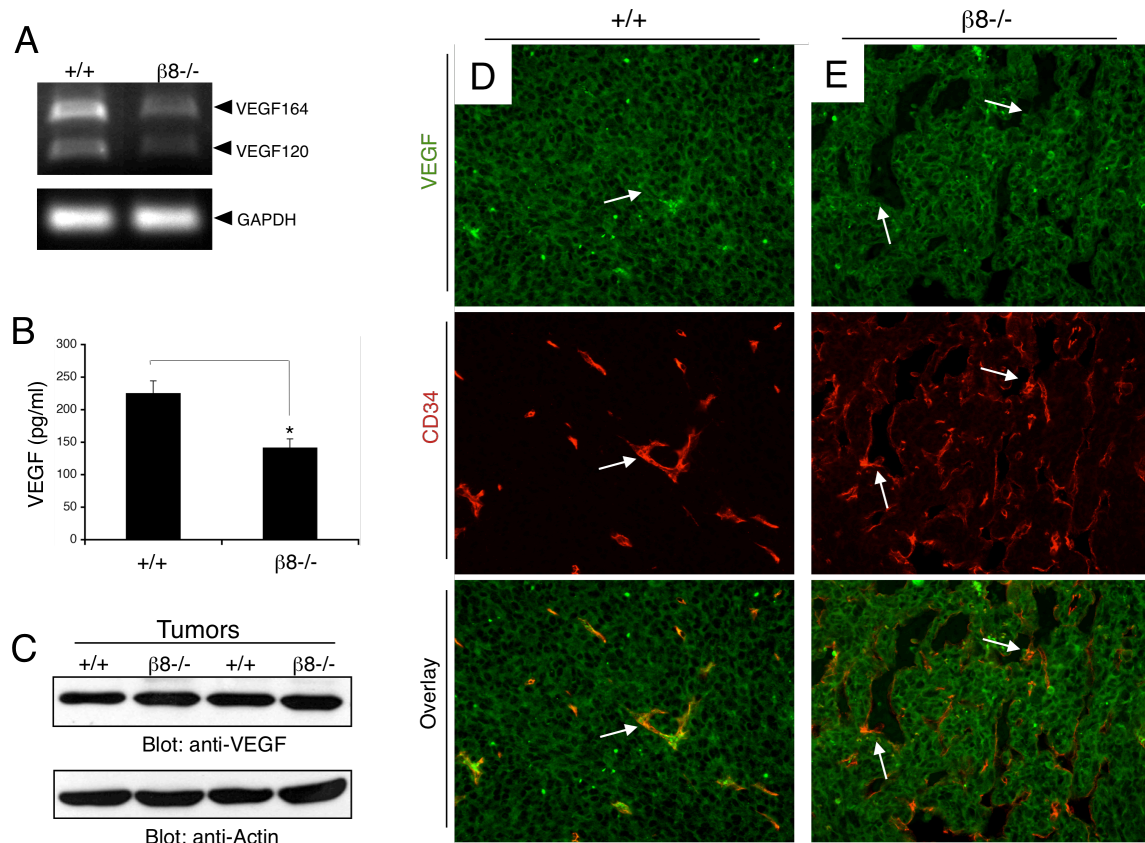


Figure 15

$\alpha v\beta 8$ integrin-mediated activation of TGF β and signaling

$\alpha v\beta 8$ integrin is expressed on normal human astrocytes where it has the ability to bind the RGD tripeptide motif in latent-TGF β s allowing for their bio-activation. Furthermore, integrin-regulated activation of the inactive cytokine plays fundamental roles in blood vessel homeostasis (49). TGF β has been shown to be involved in a wide range of physiologically normal and pathological cellular processes, such as proliferation, apoptosis, and differentiation and more specifically for this dissertation, critical roles in vascular development (112-114). In short, upon TGF β activation, the cytokine homodimerizes and targets its cognate receptor, TGF β RII which then recruits and transphosphorylates TGF β RI leading to intracellular signaling. Downstream of the receptor complex, common receptor Smads (R-Smads) 2 and 3 are phosphorylated and with the help of a co-Smad 4, enter the nucleus and up regulate transcription of target genes (123).

Complete loss of TGF β 1 leads to embryonic lethality; therefore in order to study the integrin-mediated activation of the cytokine, the Munger lab mutated the RGD binding site for $\alpha v\beta 8$ integrin to an RGE tri-peptide motif. Concomitant loss of integrin-activated TGF β 1, via a RGE knockin mouse model, and complete loss of TGF β 3 leads to acute intracranial hemorrhage, commonly observed in the complete αv and $\beta 8$ integrin knockout mice (110, 124) (Figure 3a-d; 16a). Moreover, upon conditional deletion of TGF β RII on endothelial cells via an Alk1-Cre recombinase; similar intracerebral hemorrhage was observed (Paul Oh, University of Florida College of Medicine, unpublished data) (Figure 16c). Our lab conditionally deleted TGF β RII on neural cells via a Nestin-Cre transgene and no phenotype was

observed, therefore giving credence towards a $\alpha\text{v}\beta 8$ integrin-dependent paracrine role for cerebral vessel homeostasis (124).

Cambier and colleagues provided evidence for $\alpha\text{v}\beta 8$ integrin's role in the bioactivation of latent TGF β s (49), therefore, we set forth to verify this phenomenon. 293-T cells were stably transfected with human $\beta 8$ integrin protein or empty pcDNA4.0 vector alone. Then, both stable cell lines were transiently transfected with a TGF β reporter plasmid containing a truncated plasminogen activator inhibitor-1 (PAI-1L) promoter leading to firefly luciferase expression upon R-Smads engagement (106). Endogenous production of latent TGF β s led to a significant bioactivation upon 293T cells stably expressing human $\beta 8$ integrin protein (Figure 16e). Exogenous addition of LAP-TGF $\beta 1$ caused an even more significant increase in cytokine activation confirming the fundamental role of $\alpha\text{v}\beta 8$ integrin-mediated bioactivation of latent TGF β s (Figure 16e).

Next, a similar approach was taken to analyze TGF β 's activation status utilizing an *in vitro* two-cell based firefly luciferase reporter assay. Firstly, mink lung epithelial cells (MLECs) were stably transfected with the same truncated PAI-1L promoter plasmid (106). Wild type and $\beta 8^{-/-}$ transformed astroglia were exposed to 10ng/mL LAP-TGF $\beta 1$ for 18 hours ($n=3/\text{cell line } +/- \text{ LAP-TGF}\beta 1$). Serum-starved MLECs +PAI-1L reported the activation of the exogenously added latent TGF β . Wild type transformed astroglia activated significantly more (~30%) LAP-TGF $\beta 1$ than the $\beta 8^{-/-}$ transformed cells (Figure 17a). In the samples that were not exposed to exogenous latent TGF β , no significant difference among the cell lines was

observed (Figure 17a, gray bars), suggesting other mechanisms for latent TGF β activation.

In vivo analysis was a next logical step to dissect out the 3-D tumor microenvironment and further evaluate integrin-mediated bioactivation of latent TGF β s. Therefore, TGF β signaling was analyzed by inspecting the nuclear localization of endothelial phosphorylated Smad-3 (pSmad3), an intracellular indicator of TGF β RII canonical signaling (125). β 8 integrin tumor-associated CD31+ vessels exhibited robust pSmad3 nuclear localization (Figure 17b) whereas knockout tumors, in large part, did not (Figure 17c). Although wild type intratumoral vessels displayed increased TGF β activity, a more quantitative assay was developed to sort out CD31+ endothelial cells from both tumor types. Endothelial cells isolated from β 8 integrin-expressing tumors displayed significantly more phosphorylated Smad2 (pSmad2) (2-fold) and pSmad3 (3-fold) proteins (Figure 17d; bands were normalized to total-Smad2/3 protein levels).

Collectively, these data suggest that β 8^{-/-} astrocytomas pathologies are due to a defect in α v β 8 integrin-mediated TGF β bioactivation in the tumor-associated endothelium.

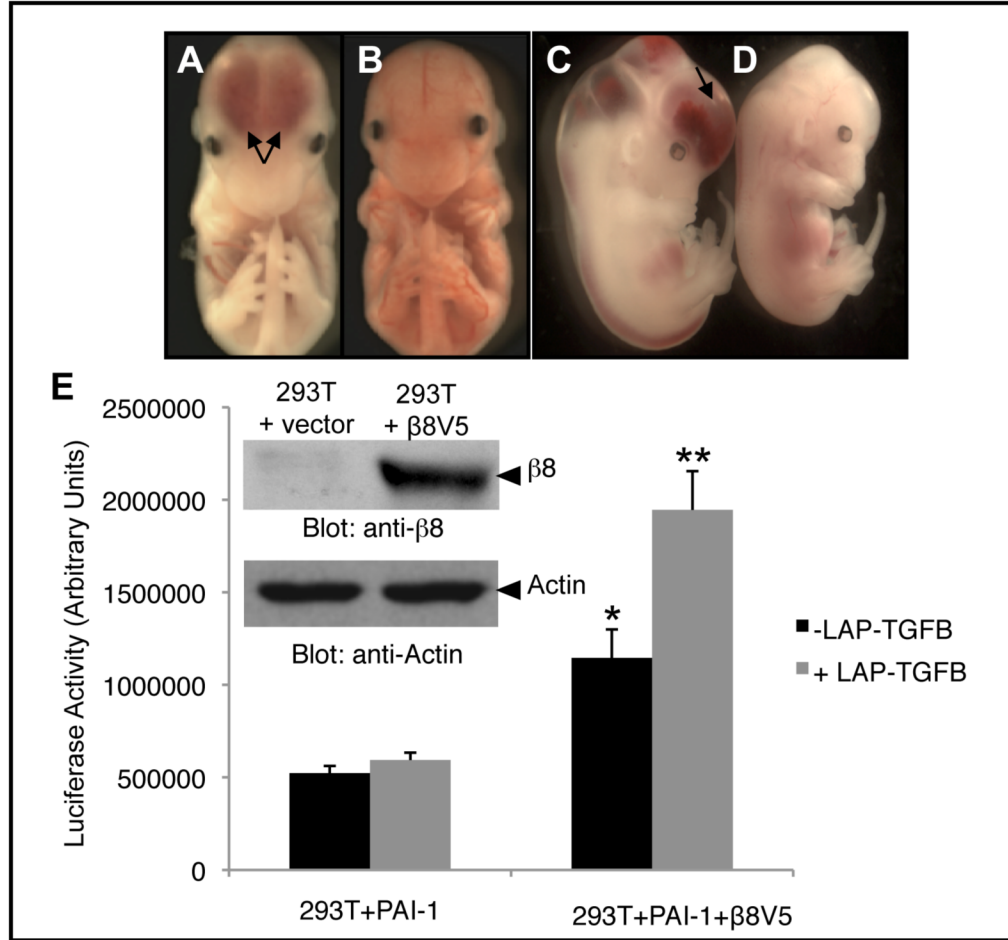


Figure 16: TGFβ-related Models Examining Paracrine Signaling Biology.

(A) Combined loss of TGFβ1 and 3 (TGFβ1^{RGE/RGE};TGFβ3^{-/-}) leads to severe intracerebral hemorrhage (black arrows) absent from wild type littermates (B) (C). Conditional deletion of TGFβRII on Alk-1 Cre⁺ endothelial cells mimics integrin knockout model pathologies, not observed in a control Alk-1 Cre⁺;flox/+ littermate. (E) 293-T cells stably transfected (inlayed immunoblot) with human β8 integrin protein bioactivates latent TGFβs significantly more than non-β8 integrin expressors (*p<0.05; **p<0.0001). Figure (A-D) adapted from Mu et al. 2008 (110).

Figure 17: *In vitro* and *in vivo* Impaired TGF β Activation and Signaling in β 8-/- Astrocytomas.

(A) A PAI-1 luciferase reporter assay shows diminished TGF β activation in β 8-/- transformed astroglia as compared to wild type transformed astroglia. Conditioned media (+/- LAP-TGF β 1) from wild type (n=3) or β 8-/- (n=3) transformed astroglia were transferred onto mink lung epithelial cells (MLEC) stably transfected with PAI-1 luciferase (106) and assayed for luciferase activity shortly thereafter. Conditioned media from wild type cells pre-treated with LAP-TGF β 1 induced significantly more luciferase activity as compared to the β 8-/- cells (**p=0.04). Note the significantly reduced luciferase activity of control MLECs never exposed to TGF β 1 compared to both transformed astroglial cell types - LAP-TGF β 1 (*p<0.0001). Also, note a significant increase of luciferase activity in wild type cells exposed to TGF β 1 versus control MLECs (**p<0.004). (B) Coronal sections of β 8-/- astrocytomas stably expressing β 8V5 integrin protein and (C) empty vector were immunofluorescently stained for CD31 (red, vessels) and nuclear pSMAD3 (green) to monitor canonical TGF β signaling (400x). Note that most of the β 8 expressing astrocytoma vessels display a nuclearly localized pSMAD3 signal (arrows in B) whereas non- β 8 expressing astrocytomas were largely negative for nuclearly localized pSMAD3 (arrows in C). Lower right boxes in B & C are higher magnifications of boxed areas in 200x images. (D) CD31+ tumor associated endothelial cells of β 8 expressing astrocytomas exhibited significantly more pSMAD2 and pSMAD3 protein expression as compared to those non- β 8 expressing astrocytomas (n=3/cell line). β -actin/tSMAD2/3 acted as loading controls.

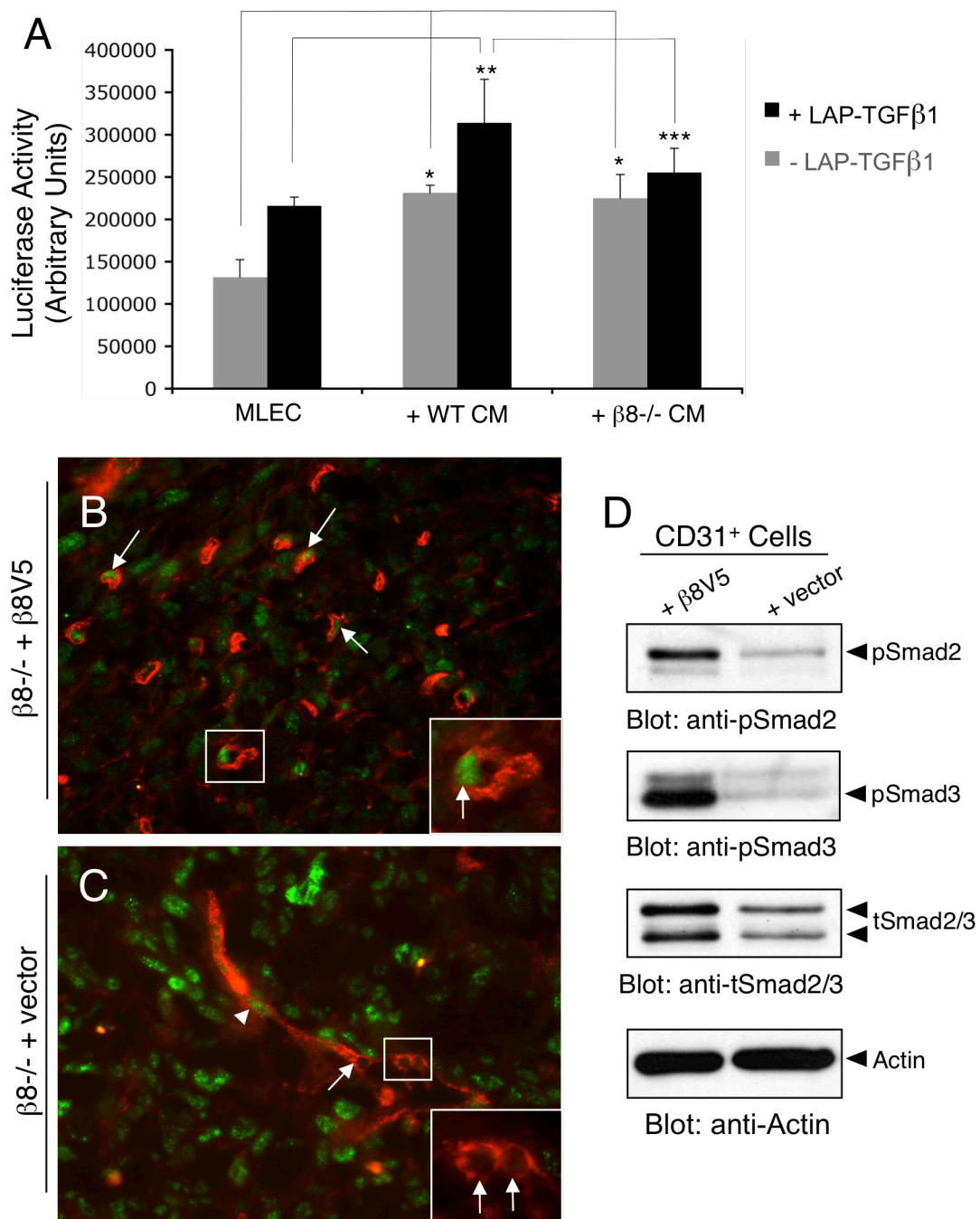


Figure 17

Further Evaluation of Wild Type and $\beta 8^{-/-}$ Astrocytomas

Analysis of adhesion and migration characteristics

Using semi-quantitative RT-PCR, wild type and $\beta 8^{-/-}$ transformed astroglia expressed similar levels of TGF β 1, TGF β 2 and TGF β 3 mRNA (Figure 18a) further corroborating the necessity of $\alpha v\beta 8$ integrin for latent TGF β activation. Indifferent ELISA data measuring transformed astroglial TGF β production into conditioned media allowed us to disregard the possibility that $\alpha v\beta 8$ integrin dictates TGF β expression. Integrins play roles in cellular adhesion and migration, therefore, we investigated the role of $\alpha v\beta 8$ integrin in these processes (15). Furthermore, $\alpha v\beta 3$ integrin has been implicated in glioma growth and invasion (99), where it's often expressed in GBM tumor cells (87). $\alpha v\beta 3$ and $\alpha v\beta 5$ integrins are commonly overexpressed along the tumor periphery allowing for increased invasion into the brain parenchyma (97). Therefore, the inherent adhesive nature of wild type and $\beta 8^{-/-}$ transformed astroglia was evaluated. Both cell lines displayed no obvious differences in their adhesion or morphological properties (Figure 18b). Next, cells were plated onto laminin-coated coverslips, and upon reaching confluence, were scratched and cell invasion was analyzed over 72 hours. Again, no distinct differences were observed in their ability to fill in the scratch, suggesting a minimal *in vitro* role for $\alpha v\beta 8$ integrin during migration (Figure 18c).

Upon evaluation of *in vivo* characteristics, wild type and $\beta 8^{-/-}$ transformed cells continued to express robust levels of nestin (Figure 19b) and diminished amounts of GFAP (Figure 19c). The GFAP signal, observed along the periphery of the tumors, represents the host's reactive astrocytes forming a glial scar to

sequester the tumor from the normal brain parenchyma. A closer look at the tumor periphery on a representative coronal H&E-stained section of a wild type and $\beta 8^{-/-}$ astrocytomas reveals similar patterns of invasion, especially perivascularly (Figure 19a). Taken together, these data do not suggest a role for $\alpha v\beta 8$ integrin during glioma invasion in this orthotopic mouse model of astrocytoma.

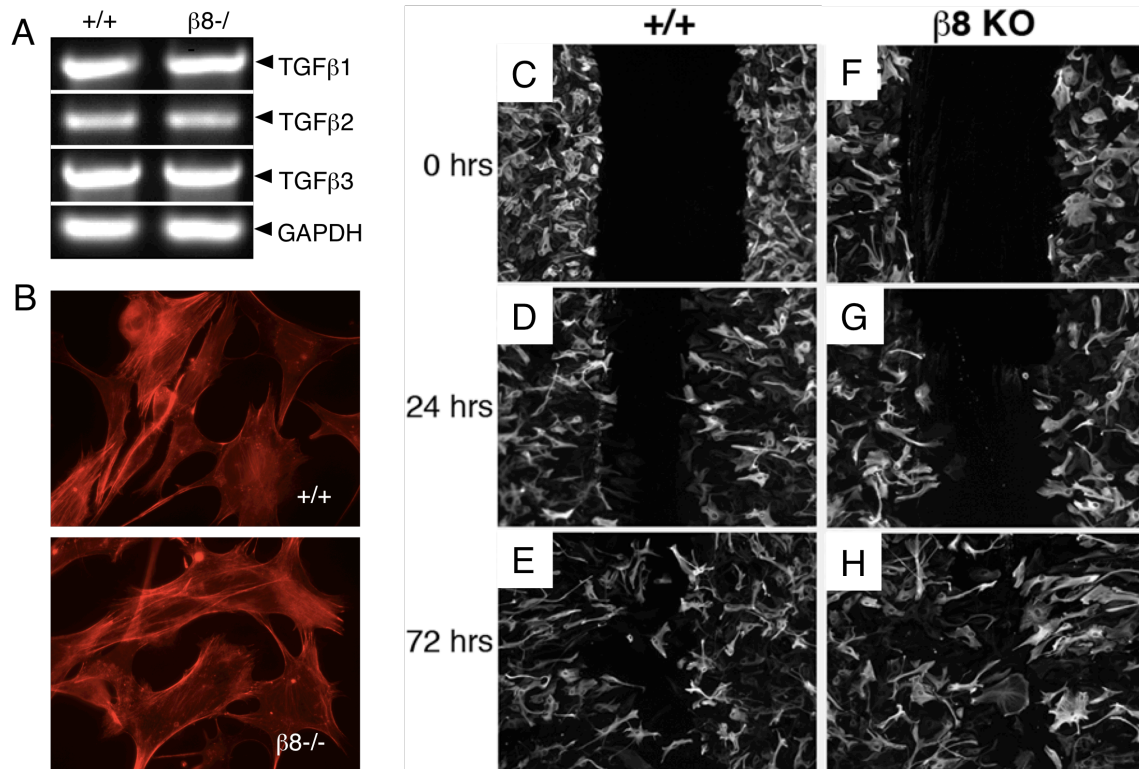


Figure 18: Wild Type and $\beta 8^{-/-}$ Transformed Astroglia Display Similar Adhesion and Migration Characteristics.

(A) Expression analysis of TGF β 1, TGF β 2 and TGF β 3 mRNAs in wild type and $\beta 8^{-/-}$ transformed astroglia was determined by semi-quantitative RT-PCR. (B) Transformed wild type (upper) and $\beta 8^{-/-}$ (lower) astroglia were plated on truncated LAP peptide-coated coverslips and allowed to adhere for 4 hours. Cells were immunofluorescently labeled with phalloidin-Texas Red to visualize the intracellular actin cytoskeleton. Note no differences in morphological or adhesive properties. Wild type (C-E) and $\beta 8^{-/-}$ (F-H) transformed astroglia migrated similarly over a 72-hour period on laminin coated coverslips.

Figure 19: Wild Type and $\beta 8^{-/-}$ Astrocytomas Display No Obvious Differences in Invasiveness *in vivo*.

(A) Coronal sections from wild type (left panel) and $\beta 8^{-/-}$ (right panel) astrocytomas were H&E-stained exhibiting the tumor (T) peripheries. Both astrocytomas invade into the brain parenchyma similarly. (B) Coronal sections from wild type (left panel) and $\beta 8^{-/-}$ (right panel) were immunofluorescently stained with an anti-Nestin antibody exhibiting tangential tumor cell invasion (arrows). (C) Coronal sections from wild type (left panel) and $\beta 8^{-/-}$ (right panel) were immunofluorescently stained with an anti-GFAP antibody revealing non-malignant reactive astrocytes forming a glial scar along the tumor periphery (arrows). Conversely, tumors (T) did not express GFAP. (All images=200x)

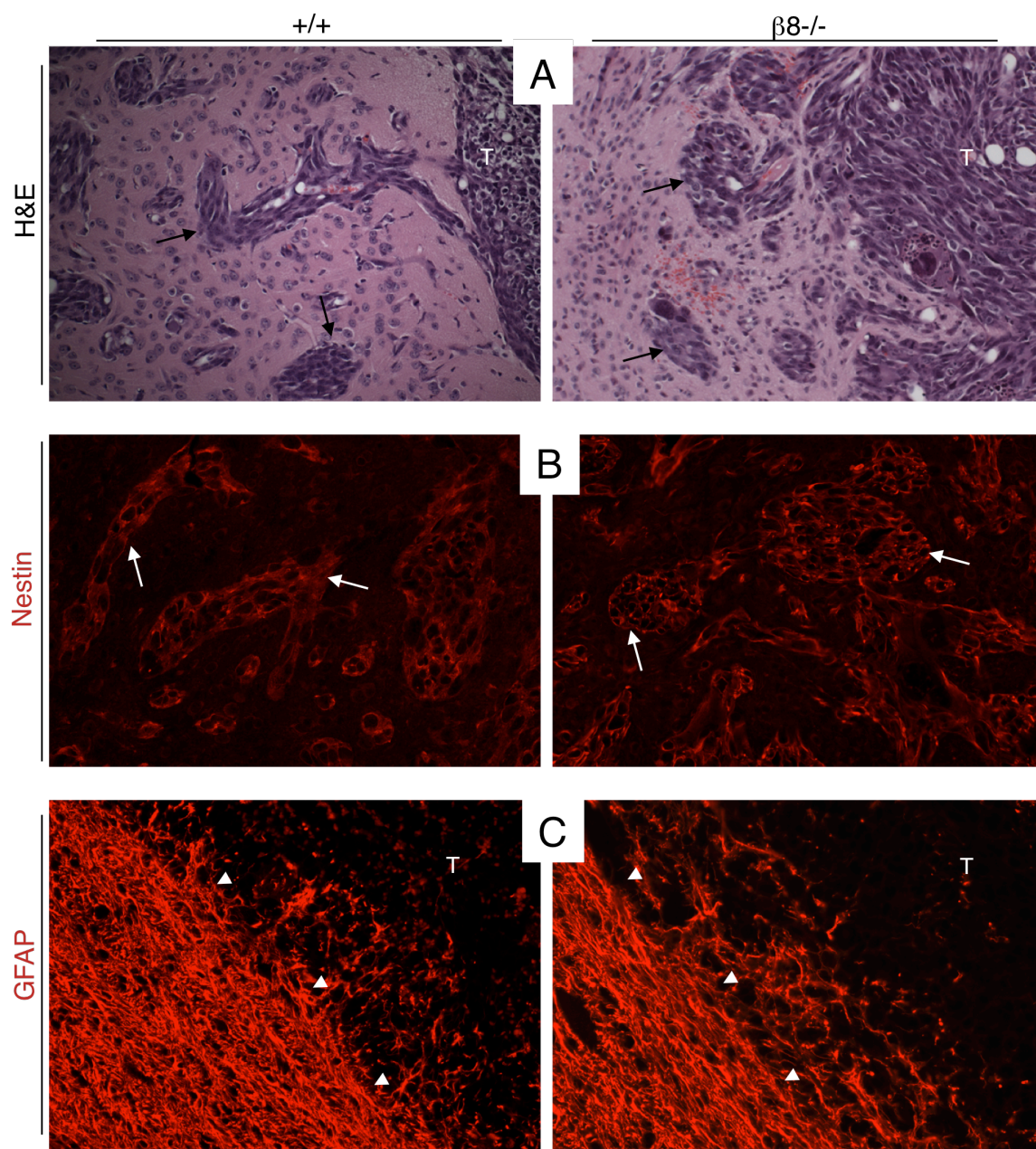


Figure 19

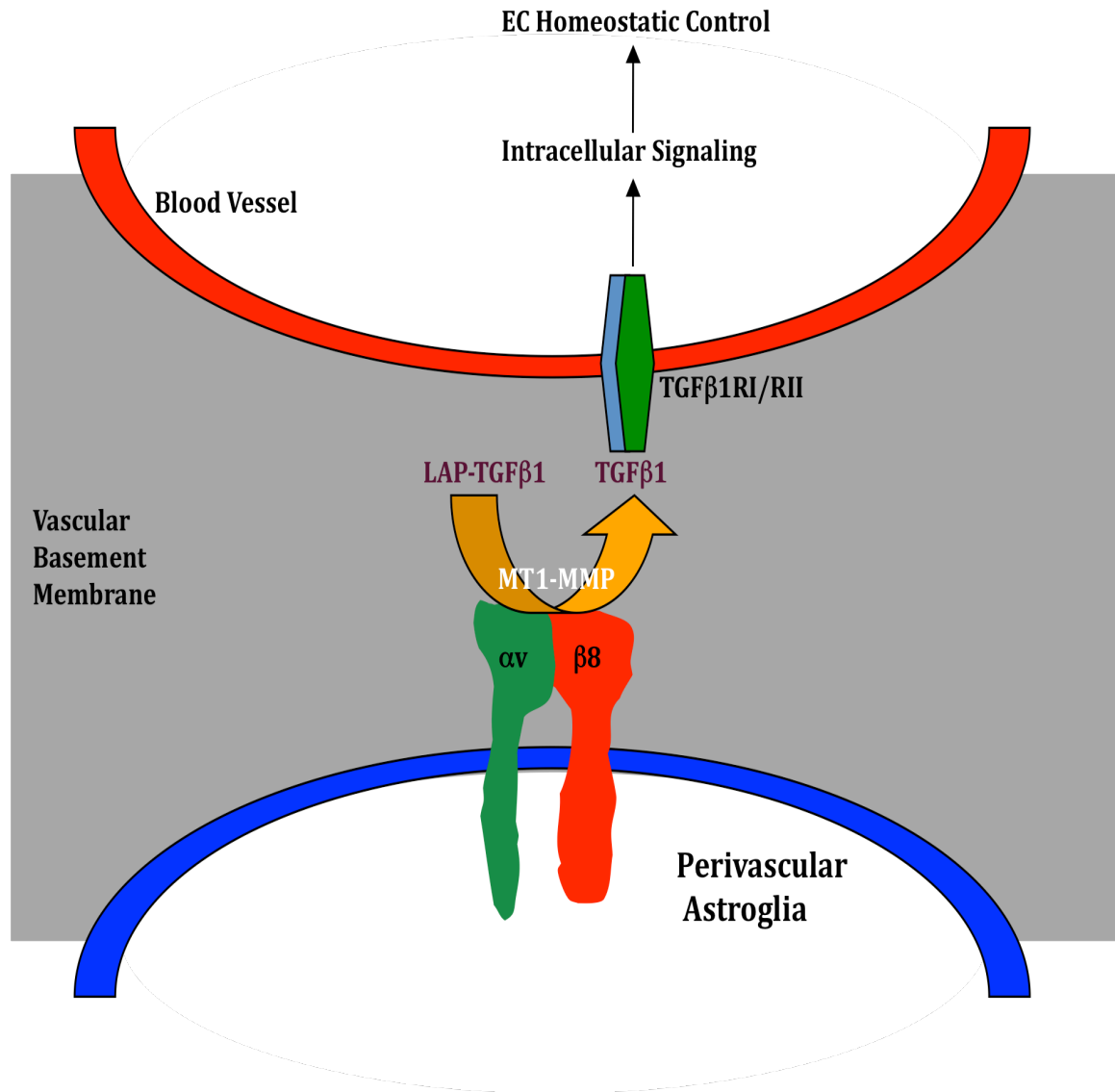


Figure 20: A Model for β_8 Integrin-mediated Homeostatic Control of Blood Vessels in the Normal Brain.

In the normal brain, $\alpha_v\beta_8$ integrin is expressed on the perivascular astroglia (blue) allowing for the bio-activation of LAP-TGF β 1 into its bioactive form with the help of MT1-MMP (49). Bioactive TGF β 1 targets TGF β RII, which then recruits TGF β RI leading to intracellular signaling, involved in blood vessel (red) homeostasis.

Discussion

Previously, our lab and others have shown that $\beta 8$ integrin knockout mice develop severe intracerebral hemorrhage. Although these pathologies have been well documented (44), little was known about the integrin's role in brain tumorigenesis. The data within this chapter is the first to connect the dysregulation of $\alpha v\beta 8$ integrin function to vascular pathologies in high-grade glioma.

Cultured wild type and $\beta 8^{-/-}$ primary astroglia express robust levels of nestin and GFAP, both markers of putative cells of origin for high-grade gliomas (55). Oncogenic transformation resulted in a substantial loss of αv and $\beta 8$ integrin expression, further supporting a role for $\alpha v\beta 8$ integrin in glioma progression. Although wild type transformed cells were just as tumorigenic as the $\beta 8^{-/-}$ cells *in vivo*, the glioma-induced pathologies were far from similar. Knockout tumors displayed pathological hallmarks commonly described in grade IV GBMs, namely intratumoral vascular pathologies including severe hemorrhage inducing significantly early lethality. Conversely, wild type cells injected into the striatum of nude mice produced tumors with pathological features consistent with those observed in grade III anaplastic astrocytomas. Upon forced expression of human $\beta 8$ integrin protein in $\beta 8^{-/-}$ transformed astroglia, the majority of vascular pathologies were largely resolved *in vivo*. Upon further mechanistic evaluation of the observed pathologies, impaired TGF β signaling led to diminished intratumoral endothelial homeostasis due to absence of $\alpha v\beta 8$ integrin on tumor cells. In the normal resting brain, the perivascular astrocyte expresses robust levels of $\alpha v\beta 8$ on its cell surface. αv integrin subunit binding to the RGD tri-peptide domain in the

LAP portion of latent TGF β s leads to the recruitment of MT1-MMP metalloproteinase by the β 8 integrin subunit (49). MT1-MMP is believed to aid in the physical cleavage of the latent peptide from the inactive cytokine. Upon TGF β activation, TGF β receptors are engaged and intracellular signaling cascades ensue, functionally contributing to endothelial cell homeostasis (Figure 20). In the disease state, perivascular α β 8 integrin expression is diminished, thus deregulating vessel homeostasis, leading to higher-grade gliomas, as observed in this orthotopic model.

Astrocytes (Figure 7e) and neural progenitor cells (Figure 11d) express robust levels of α β 8 integrin, which has recently been established to regulate neurovascular homeostasis in the adult mouse brain (14). Furthermore, homozygous β 8 integrin knockout mice display marked increase in intracerebral blood vessel coverage, suggesting α β 8 integrin acts as an angiogenic control switch (49). Indeed, GBM cells play fundamental roles in creating an environment for increased tumor progression often supported by pathological angiogenesis (104). With the evidence collected in this first chapter, it is strongly believed that high-grade brain tumor cells downregulate α β 8 integrin expression and ensuing function. As observed in the wild type astroglia, transition from primary to transformed resulted in a significant reduction in overall α and β 8 integrin expression (Figure 11b). Interestingly, significantly higher VEGF-A protein expression did not lead to increased pathological angiogenesis, as others have reported (126). Moreover, TGF β has been characterized as a potent inhibitor of VEGF and basic fibroblast growth factor (bFGF), both keen contributors to sustained angiogenesis (127). Data presented here further corroborate this

phenomena whereby integrin-mediated activation of latent TGF β s functionally inhibit the pro-angiogenic functions of VEGF highly expressed in the wild type transformed astroglia as compared to mRNA and protein levels detected in $\beta 8^{-/-}$ tumor cells (Figure 15a, b). In addition, TGF β canonical signaling results in the phosphorylation of R-Smad3, which has been attributed to enhancing VEGF expression (128). VEGF production in the $\beta 8^{-/-}$ tumor cells, albeit low, coupled with impaired TGF β endothelial cell homeostasis, creates a tumor environment that promotes pathological angiogenesis resulting in human grade IV GBM-like lesions.

Oncogene-mediated reduction in overall $\beta 8$ integrin protein expression in wild type astroglia suggests $\alpha v\beta 8$ integrin as a possible tumor suppressor as the majority of $\beta 8^{-/-}$ astrocytomas resembled pathological hallmarks of human GBM. On a related note, diminished $\alpha v\beta 8$ integrin status alone was not sufficient to induce spontaneous tumorigenesis, consistent with reports in complete $\beta 8$ integrin knockout adult mice (14). Therefore, potential activation of specific oncogenes (i.e. HRas^{G12V}) coincident with loss of tumor suppressor functions (i.e. pRb/p53) and $\beta 8$ integrin loss, may lead to spontaneous astrocytomas. Our lab has recently reported that GFAP-cre conditional knockout of αv integrin in epithelial cells of the eyelid skin and conjunctiva commonly lead to squamous cell cancer development 12-18 months, post-natally (129). Taken together, loss of integrin expression coupled with other potent genetic alterations, can lead to tumor formation and progression. Furthermore, our data revealing loss of $\beta 8$ integrin expression by passage 8 could coincide well with p53 loss, a common genetic alteration that occurs early-on during gliomagenesis, especially in newly forming astrocytomas (130). Indeed, these

speculations need to be further investigated to truly understand the dynamic between $\alpha\text{v}\beta 8$ integrin function and tumor suppressor/oncogene activities during gliomagenesis.

The novel concept that $\alpha\text{v}\beta 8$ integrin is lost during gliomagenesis has sparked many different avenues of investigation. The vascular pathologies observed in the $\beta 8^{-/-}$ astrocytomas were so striking that many of the other integrin-related functions that could contribute to tumorigenesis were not pursued. Further analysis of migration and adhesion functions based on $\alpha\text{v}\beta 8$ integrin expression status was further elucidated. αv integrins have been identified as being involved in tumor cell adhesion and migration along white matter tracts and blood vessels (131). More specifically, αv integrins have been correlated to promoting colon cancer liver metastasis. Small molecule inhibitors directed against $\alpha\text{v}\beta 3$ and $\alpha\text{v}\beta 5$ integrins reduced overall cell proliferation and adhesion in highly metastatic colon cancer cells (132). In addition, $\alpha\text{v}\beta 3$ and $\alpha\text{v}\beta 5$ integrins are known to play roles in glioma neo-angiogenesis, but have also been linked to increased expression along glioma tumor periphery aiding in their migratory capacity into the normal brain parenchyma (97). Unfortunately for $\alpha\text{v}\beta 8$ integrin, with regard to this mouse model, its absence showed no obvious differences in *in vitro* adhesion and migration assays (Figure 18b-h), for *in vivo* peripheral tumor perivascular invasion (Figure 19a, b). Although these data have identified novel roles for $\alpha\text{v}\beta 8$ integrin in pathological angiogenesis in glioma, further focus will be placed upon the role of the integrin during the human disease setting in the hopes of identifying a new

therapeutic target to contribute to possible increased prevention and early diagnosis of GBM.

CHAPTER 4: Specific Aim 2

Elucidate the Functional Roles for $\alpha\beta 8$ Integrin in Glioma-Induced Angiogenesis During the Pathogenesis of Human Gliomas

Introduction

In the previous chapter, we utilized a genetically tractable mouse model whereby $\beta 8$ integrin was transgenically knocked out, which led to severe intratumoral hemorrhage (44). Inhibition of p53 and Rb tumor suppressors and stable incorporation of an oncogenic H-Ras (G12V) into wild type and $\beta 8^{-/-}$ primary astroglia promoted tumor formation in the striatum of nude mice. Overall, $\beta 8^{-/-}$ tumors exhibited significantly increased CD34+ fluorescence intensity partially attributed to a significant decrease in activation of latent TGF β s. Moreover, mice harboring knockout transformed astroglia survived significantly less than mice harboring wild type transformed astroglia. While this orthotopic mouse model of astrocytoma has revealed a significant role for $\alpha\beta 8$ integrin during gliomagenesis, further inquiry is necessary to elucidate the functional contributions in human GBM.

Human glioma cell lines harvested from patients have long been commercially available in order to determine the functional roles of specific genes and proteins in the disease (133). Furthermore, freshly resected tumors are a potential avenue to culture cells and analyze protein expression profiles in different grades of human glioma. However, one caveat to analyzing bulk tumor masses is

that they are often infiltrated by stromal reactive astrocytes that have the potential of skewing expression profiles (134).

In recent years, there has been compelling evidence supporting the presence of 'cancer stem cells' (CSCs) within hematopoietic, breast, colon and brain cancers (135-138). GBM CSCs are considered to be the primary reason for GBM tumor recurrence post-therapy due to their ability to remain quiescent while target therapies target rapidly dividing cells (139). Within the adult human brain, neural stem cells (NSCs) reside in two specific locations, the subventricular zone of the lateral ventricle and the subgranular zone of the dentate gyrus of the hippocampus. NSCs are defined as multipotent cells with the ability to proliferate and self-renew (140). Upon transformation, primary GBM progenitor cells are identified as a small subset population (<5%) of the tumor bulk that retain the ability to establish tumors (141). Recently, our lab and others have begun to culture these CSCs from freshly resected GBMs. A caveat to this model is that lower grade anaplastic astrocytomas rarely, if ever, produce CSCs that can be compared to those harvested from GBMs. Nonetheless, expression and function of $\alpha\beta 8$ integrin will be evaluated. Next, primary GBM cell lines will be transduced with lentiviral-based small hairpin RNAs (shRNAs) to stably silence gene targets including both αv and $\beta 8$ integrin.

Lastly, a similar genetically tractable mouse model used in the previous chapter will employ transformed human astrocytes to produce astrocytomas. Transformed cells were acquired from Dr. Russel Pieper laboratory (80) and lentiviral-based RNAi technology will ablate $\beta 8$ integrin expression. Resulting intracranial tumors will be characterized based upon their *in vivo* pathologies in

order to corroborate the strong body of evidence discussed in the previous chapter. Collectively, the main objective of this chapter is to elucidate a functional role for $\alpha\text{v}\beta 8$ integrin in human gliomas.

Results

Characterization of $\alpha v\beta 8$ Integrin Expression in Human Glioma Cell Lines

A panel of commercially available human GBM cell lines were purchased (ATCC) or acquired from the Brain Tumor Center at M.D. Anderson and characterized for αv and $\beta 8$ integrin expression. Transformed human astrocytes (THAs) were acquired from Dr. Russel Pieper. Although five of the seven cell lines evaluated expressed robust levels of $\alpha v\beta 8$ integrin, there were two, U87 and LN18, which expressed little, if any $\beta 8$ integrin (Figure 21a). Transformed human astrocytes lost approximately 90% of $\beta 8$ integrin expression while also exhibiting a 50% decrease in αv integrin expression (Figure 21a) (142).

To establish a link between $\beta 8$ integrin expression and *in vivo* tumor-induced angiogenesis, U87 and SNB-19 GBM cells were stereotactically injected into the striatum of immunocompromised mice to evaluate their *in vivo* tumorigenicity. 500,000 cells were implanted and allowed to form tumors for 6 weeks (n=5 mice/cell line). The tumor bearing mice were anesthetized and cardiac perfused with 4% paraformaldehyde. Macroscopic coronal U87 tumors revealed a hemorrhagic pathology with tumors forming in nearly the entire injected brain hemisphere (Figure 21b). H&E-stained tumors contained large, distended vessels that displayed sinusoidal-like morphologies further confirmed by anti-CD34 immunohistochemistry (Figure 21d, e). Macroscopic analysis of brains injected with SNB-19 cells did not exhibit obvious tumor formation (Figure 21c) although microscopic analysis of H&E-stained brain sections revealed focal, invasive lesions that preferred growth in a perivascular manner (Figure 21f). Furthermore, anti-CD34 immunohistochemistry

showed limited vascular networks with vessels uniform in diameter lacking hemorrhage, making their vascular patterns distinct from those observed in the U87 tumors (Figure 21g).

In an effort to influence the blood vessel properties in the U87 tumors, a plasmid expressing human $\beta 8$ integrin protein was stably transfected into this cell line. U87 cells were also stably transfected with empty vector pcDNA4.0. Expression of $\beta 8$ integrin was confirmed by western blot analysis (Figure 22a). $\beta 8$ integrin expressing or empty vector U87 cells were stereotactically injected into the striatum of immunocompromised mice (n=5 mice/cell line). U87 tumors expressing $\beta 8$ integrin lacked the macroscopic hemorrhage (Figure 22b) evident in the U87 empty vector tumors (Figure 22c). Furthermore, a panel of tumors (n=5/tumor) from both cohorts was immunofluorescently stained with CD34 to label vascular endothelial cells. U87 vector control tumors exhibited robust microvascular density (MVD) (Figure 22d) as compared to $\beta 8$ integrin-expressing U87 tumors (Figure 22e). Upon analysis of CD34 fluorescence, the U87 empty vector fluorescence intensity was significantly reduced compared to U87 tumors forcibly expressing $\beta 8$ integrin (Figure 22f).

To assess TGF β activation and signaling, the two-cell approach was employed comparing $\beta 8$ integrin low expressing GBM cells versus those that express high levels. In addition to the U87 and SNB-19 cell lines, LN18 and LN229 lines were also analyzed as these express low and high levels of $\alpha v\beta 8$ integrin, respectively. As depicted in Figure 23, those cell lines (LN229 and SNB-19) that express high levels of $\alpha v\beta 8$ integrin activated significantly more latent TGF $\beta 1$

compared to those low expressers (LN18 and U87) (Figure 23, black bars). Moreover, endogenously produced latent TGF β s are also significantly activated more in high expressing cell lines versus U87 cells (Figure 23, gray bars).

Collectively, these data suggested that the gross hemorrhagic and microscopic vessel pathologies observed in the U87 tumors are, in part, due to a defect in integrin-mediated activation of latent TGF β s upon the tumor-associated vasculature. Indeed, forced expression of β 8 integrin in tumor cells diminished these pathologies, therefore providing further evidence that α v β 8 integrin plays significant roles in regulating intratumoral angiogenesis.

Figure 21: $\alpha v\beta 8$ integrin Expression in Human Glioma Cell Lines

(A) Normal and transformed human astrocytes (NHA/THA) and seven human glioma cell lines were immunoblotted with antibodies directed against αv integrin, $\beta 8$ integrin and actin proteins. Note the diminished loss of $\beta 8$ integrin expression in THAs upon transformation, similar to wild type mouse transformed astroglia. Also, notice that some cell lines express differential levels of $\beta 8$ integrin. U87 glioma cells were intracranially injected into the striatum of nude mice (n=5) and cardiac perfused upon tumor formation. Gross coronal sections (B) were stained with H&E (D, 100x) and an anti-CD34 antibody (E, boxed area, 400x). Notice that U87 cells form large intracranial tumors with evidence of vascular hemorrhage and sinusoidal-like vessels (red arrows). SNB-19 glioma cells were intracranially injected into the striatum of nude mice (n=5) and cardiac perfused upon tumor formation. Gross coronal sections (C) were stained with H&E (F, 100x) and an anti-CD34 antibody (G, boxed area, 400x). Note the relatively low vascularity of the tumors (red arrows) compared to U87 tumors and their desire to proliferate periventricularly.

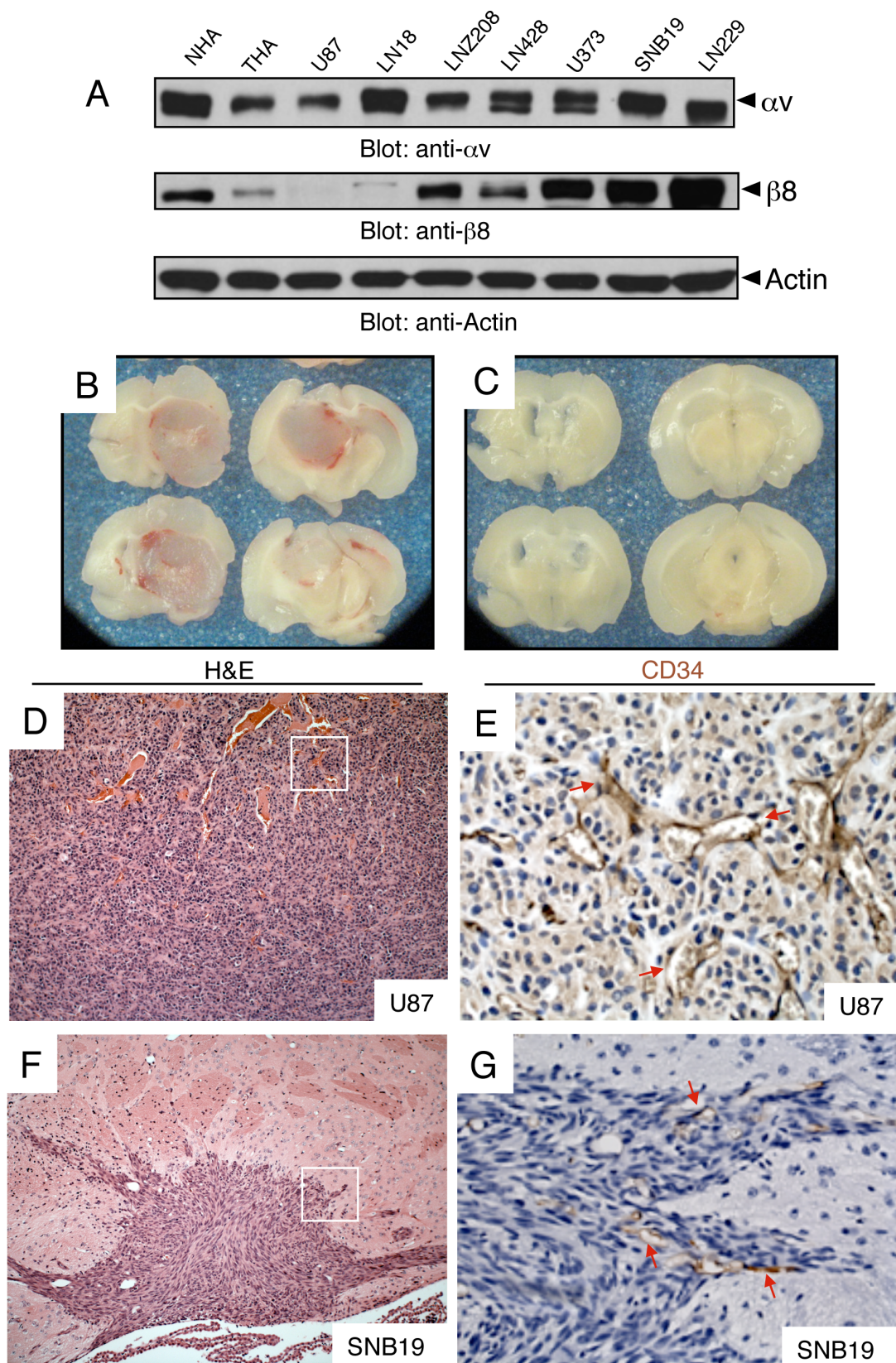


Figure 21

Figure 22: Forced Expression of $\beta 8$ Integrin in U87 Glioma Cells Largely Resolves Macroscopic Vascular Pathologies.

(A) Stably transfected U87 cells (empty vector and vector+ $\beta 8$ -V5) were lysed and immunoblotted with antibodies against $\beta 8$ integrin and actin. Note the substantial increase in $\beta 8$ integrin expression. (B) Both cell lines were stereotactically injected into the striatum of immunocompromised mice (n=5/ cell line). The brains were coronally sectioned; notice the intratumoral hemorrhage evident in the empty vector tumors (pcDNA4.0) (C) is completely resolved upon forced expression of $\beta 8$ integrin protein. (D) U87 glioma tumors stably transfected with an empty (D) or a human $\beta 8$ integrin-expressing vector (E) were immunostained with an anti-CD34 antibody to visualize vascular endothelial cells (Images: 200x). Note the (arrows in D) higher microvascular density in the empty vector expressing tumors versus the relatively minimal vascularity observed in the rescue U87 tumors (arrows in E). (F) Fluorescence was imaged and quantified to exhibit a significant rescue of microvascular density in the U87 tumors forcibly expressing $\beta 8$ integrin protein (*p<0.0001).

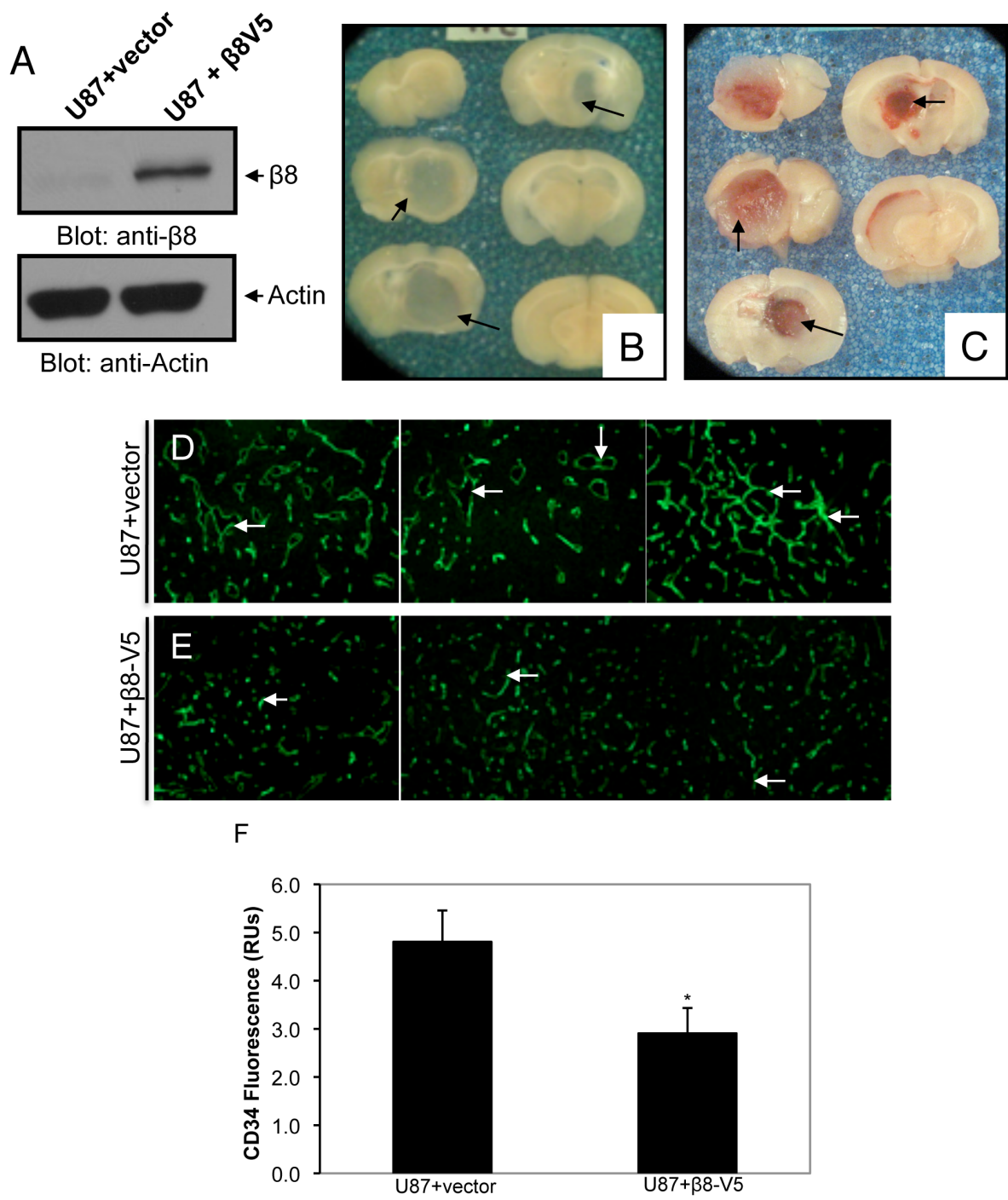


Figure 22

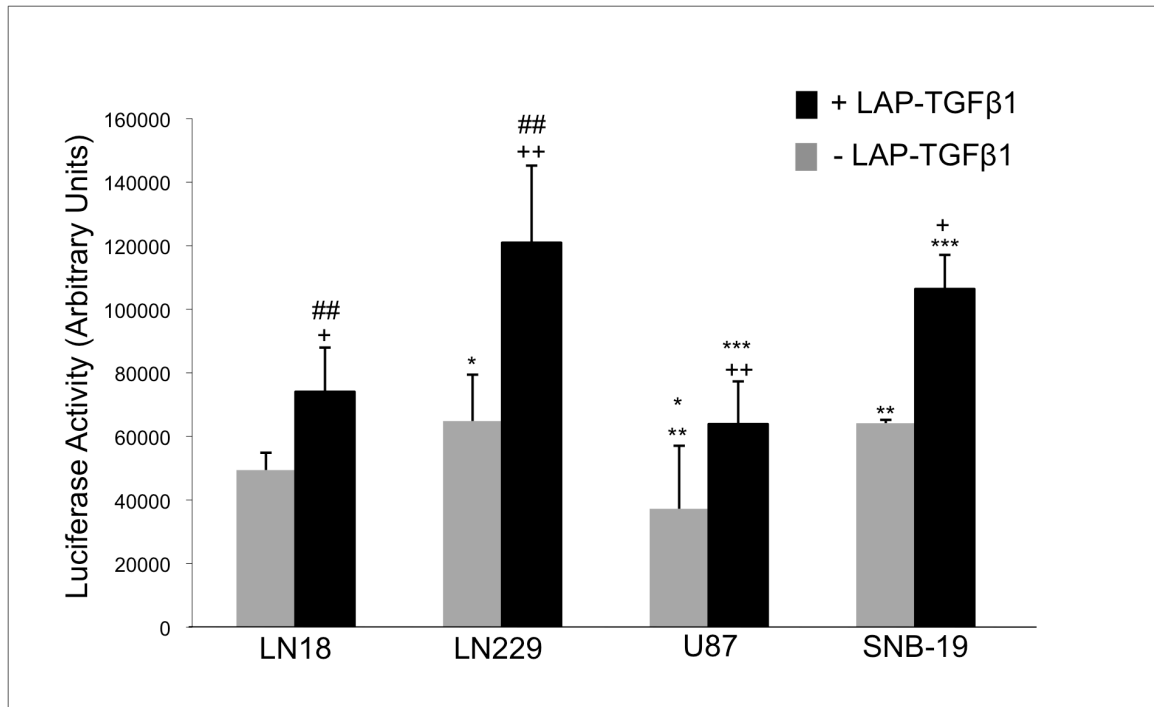


Figure 23: Impaired TGFβ Activation in Human Glioma Cell Lines

A PAI-1 luciferase reporter assay shows substantial reduction of TGFβ activation in glioma cell lines that express minimal β8 integrin expression versus those that expressed elevated levels. Conditioned media (+/- LAP-TGFβ1) from LN18 (n=3), LN229 (n=3), U87 (n=3), or SNB-19 (n=3) were transferred onto MLECs stably transfected with PAI-1 luciferase and assayed for luciferase activity shortly thereafter. First, endogenous latent TGFβs (gray bars) activated by U87 cells were significantly less activated than LN229 and SNB-19 cells (*p<0.02 (U87 v. LN229); **p<0.001 (U87 v. SNB-19)). Second, exogenously added latent TGFβs to LN229 cells led to significantly higher luciferase activity as compared to U87 cells (++p<0.0001) and LN18 cells (##p<0.01). Lastly, exogenously added latent TGFβs to SNB-19 cells led to significantly higher TGFβ activity as compared to U87 cells (***p<0.0001) and LN18 cells (+p<0.03).

Characterization of $\alpha\beta 8$ Integrin Expression in Human Glioma Samples and Primary GBM Cell Lines

Dr. Frederick Lang of MD Anderson Cancer Center kindly supplied us with freshly resected human glioma samples. Lysates made from 8 GBM samples, 3 anaplastic astrocytomas, 1 ependymoma and 1 oligodendroglioma were immunoblotted to characterize their respective $\alpha\beta 8$ integrin expression (Figure 24a). Upon normalization to actin loading control bands, there seemed to be a slight trend towards decreased expression in the GBM samples as compared to the anaplastic astrocytomas, although this difference was not statistically significant. Consistent with reports showing infiltrative reactive astrocytes along the tumor periphery and intratumorally (134), these $\alpha\beta 8$ integrin expressing stromal cells may have skewed our expression profiling. Furthermore, upon effective tumor resection, a surgeon will always have margins that contain normal, non-neoplastic tissue that again could affect expression analysis. Indeed, expression may be present within these tumors, although there may exist a more spatial expression pattern such as perivascularly.

Our lab and others have cultured primary GBM cell lines, which grow as neurospheres in a serum-free, growth factor-supplemented media (Figure 24b, top). These spheroids express robust levels of nestin (Figure 24b, bottom), an intermediate filament protein and an established marker for neural stem cells (138). Within a population of primary GBM cell lines, there are distinct expression patterns evident by FACS analysis. CD133, a marker for cancer stem cells, including those in GBMs (143), is differentially expressed among the primary GBM cell lines.

Approximately 50% of the single cells that make up the neurosphere express high levels of CD133. In another primary GBM cell line analyzed, only 8% of the cells expressed the cell surface marker, consistent with reports of varying expression within these primary brain tumor cells (144), as well as in melanoma and pancreatic cancer (145). Unfortunately, CD133 expression does not correlate with tumorigenesis as CD133⁺ populations produce intracranial tumors, making necessary the discovery of additional biomarkers (146). Several labs have further characterized these primary cells for different markers under normoxic and hypoxic conditions. During times of oxygen deprivation, HIF1 α is upregulated to initiate a significant spike in IL-8 secretion, a powerful angiogenic chemokine (147). Moreover, concomitant activation of Akt and Ras proteins in neural progenitors has produced intracranial lesions, similar to grade IV GBMs (65).

Due to the lack of specific anti- β 8 integrin antibodies for FACS, we used an anti- α v antibody to elucidate the expression profile of the CD133⁺ spheroids. Of this population, 27% of the cells expressed high levels of α v integrin and 20% expressed low levels (Figure 24c). Next, a panel of four primary GBM cell lines, NSC-2, -11, -23 and HT18, were biotinylated and exhibited robust expression levels of α v β 8 integrin (Figure 24d). Although previous data would suggest that these GBM cells would express low levels of the integrin, these cells are progenitor-like compared to those examined in the orthotopic mouse and xenograft (human glioma cell lines) models and therefore may have different integrin expression patterns.

Figure 24: Human Glioma and Primary GBM Cells $\alpha\text{v}\beta 8$ Integrin Characterization

(A) Freshly resected human glioma tumor samples were lysed and immunoblotted with antibodies against $\beta 8$ integrin (upper panel), αv integrin (middle panel) and actin (lower panel) proteins. (Key: CB=Normal cerebellum; O=Oligodendroglioma; E=Ependymoma; AA=Anaplastic Astrocytoma; GS=Gliosarcoma; GBM=Glioblastoma multiforme). Primary GBM cells grew in a manner similar to neurospheres, in suspension (B, top image). A GBM neurosphere was immunostained with anti-Nestin and anti-DAPI (nuclear stain) antibodies (B, bottom panel) (Images: 200x). (C) FACS analysis of NSC11 displays four different populations of cells: Q1: $\text{CD133}^{+}/\alpha\text{v}^{\text{LO}}$; Q2: $\text{CD133}^{+}/\alpha\text{v}^{\text{HI}}$; Q3: $\text{CD133}^{-}/\alpha\text{v}^{\text{LO}}$; Q4: $\text{CD133}^{-}/\alpha\text{v}^{\text{HI}}$. 27% of the NSC11s expressed high levels of CD133 and αv integrin while 20% expressed low levels of αv integrin (CD133^{+}). This data reveals distinct populations within the primary GBM cell lines. (D) Primary GBM cell lines cultured from tumor resections were grown in specialized media. Cell-surface analysis of integrin expression on NSC2, 11, 23 and HT18 revealed similar levels of $\alpha\text{v}\beta 8$ integrin.

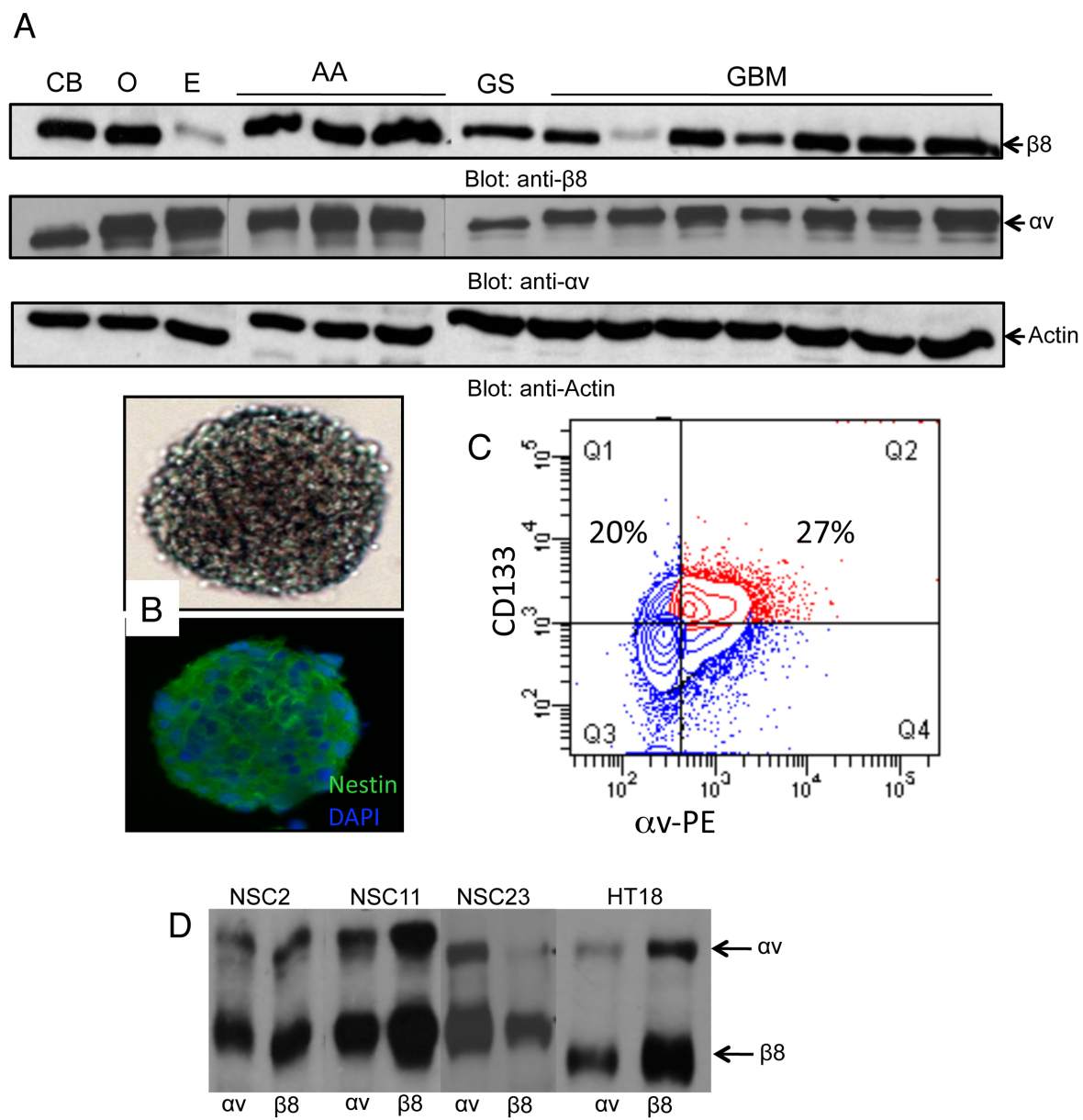


Figure 24

shRNA-mediated silencing β 8 Integrin Expression in Primary GBM Cells

Next, β 8 integrin gene expression was stably silenced via an shRNA lentiviral-based system whereby primary GBM cells were transduced with β 8shRNA or non-targeting (NT) shRNA coupled to green fluorescent protein (GFP) expression (107). NTshRNAs were used to identify incorporation of the lentiviral construct via GFP fluorescence, although the sequence was completely non-specific. Upon successful transduction, retroviral-positive cells were marked green and sorted via live-cell flow cytometry (Figure 25b). After allowing 24 hours for the cells to recover after sorting, lysates were prepared to evaluate β 8 integrin expression. In three of the four primary GBM cell lines transduced with β 8shRNA, substantial knockdown was achieved, most potently in the NSC-2 and NSC-11 populations (Figure 25a). 500,000 cells (NSC-2, -11, HT18) were stereotactically injected into the striatum of immunocompromised mice. Indications of tumor burden were evident by 5 weeks for NSC-2 and NSC-11 lines versus 8 weeks for the HT18 line (n=8/cell line). Upon macro- and microscopic analyses of these tumors, limited phenotypic differences were observed (Figure 26). There are various reasons for the lack of differences in tumor growth and angiogenesis. First, β 8 integrin knockdown was substantial, although, similar levels of β 8 integrin expression were observed in wild type transformed astroglia, which produced tumors that were pathologically less severe than β 8^{-/-} tumors. Thus residual β 8 integrin expression in primary GBM cell lines may be sufficient to negate the formation of tumors exhibiting previously described severe intratumoral pathologies. Second, increased expression of other α v integrins

could be compensating for the loss of the $\beta 8$ subunit, thereby reducing the anticipated presence of pathological differences.

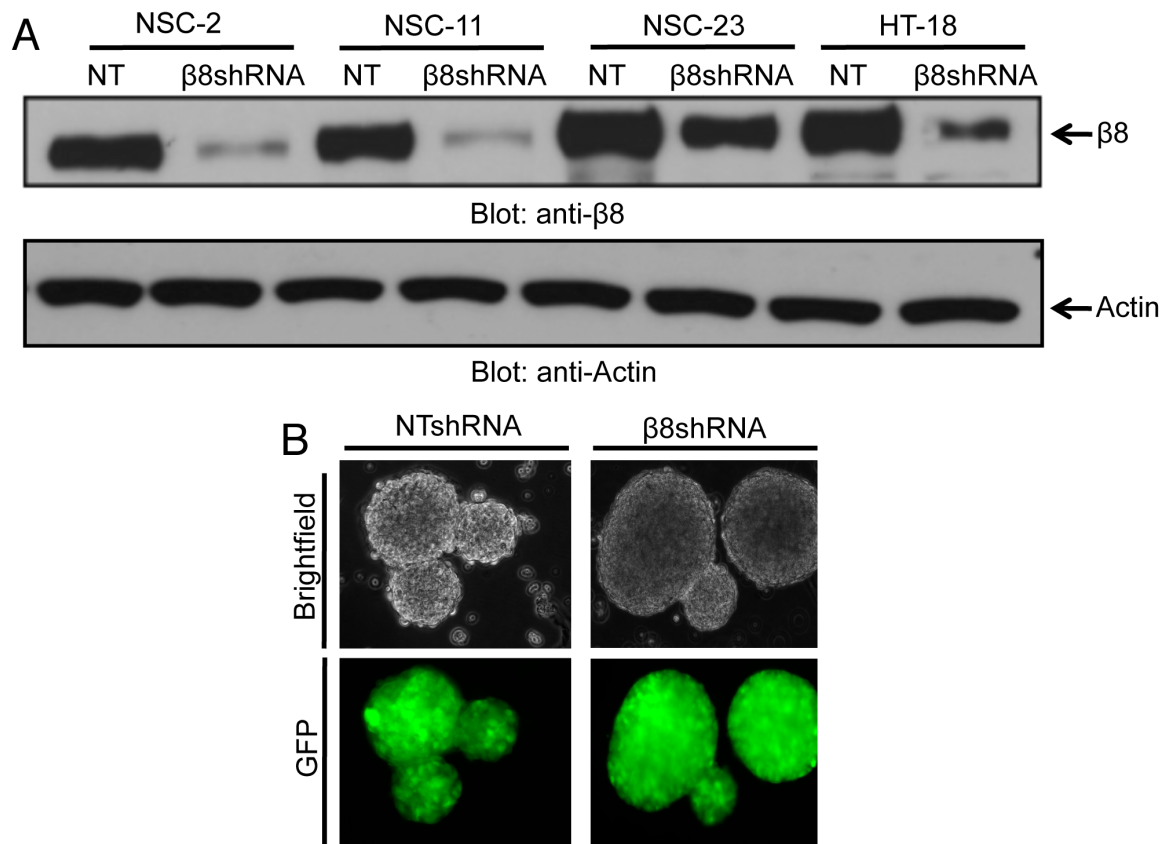


Figure 25: shRNA-mediated Stable Silencing of $\beta 8$ Integrin

(A) Four primary GBM cell lines were stably transduced with non-targeting (NT)-shRNA or $\beta 8$ shRNA. Lysates were immunoblotted with antibodies against $\beta 8$ integrin and actin. Note the substantial knockdown of $\beta 8$ integrin in 3 of the 4 primary GBM cell lines. (B) Brightfield and GFP images of representative NTshRNA and $\beta 8$ shRNA primary GBM cell lines (NSC-11, images: 100x). Note the intense GFP signal in both cohorts.

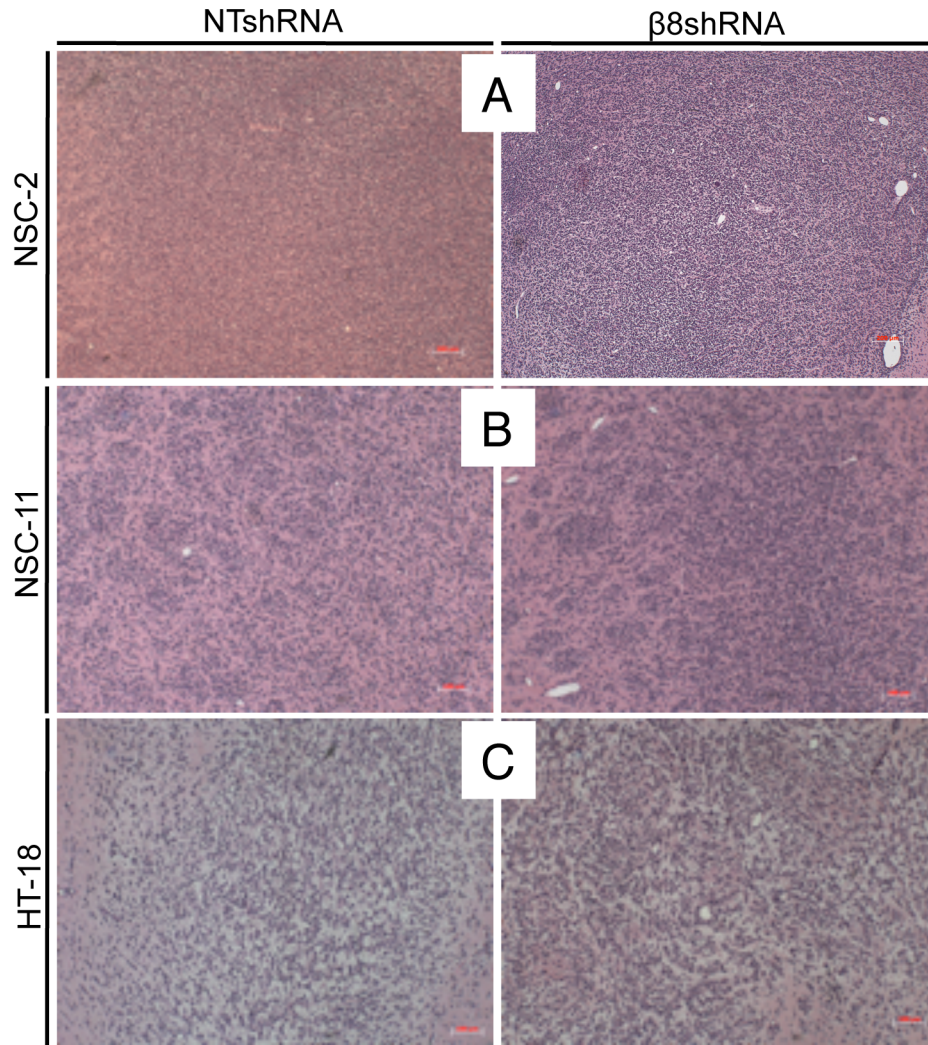


Figure 26: Microscopic Views of NT- and β 8shRNA Intracranial Tumors

Three different primary GBM cell lines stably transduced with NTshRNA or β 8shRNA lentiviruses were stereotactically implanted into the striatum of immunocompromised mice (n=8 mice/cell line). (A) NSC-2, (B) NSC-11 and (C) HT-18 coronal sections were stained with H&E (images 100x). Note the minimal differences in tumor phenotype upon knockdown of β 8 integrin protein.

shRNA-mediated silencing α v Integrin Expression in Primary GBM Cells

A lentiviral shRNA was developed to silence α v integrin expression to address the possibility of compensation or functional redundancy by other integrins in the β 8 integrin knockdown tumors. NTshRNA and α vshRNA lentiviruses were transduced into NSC-2, -11, -23 and HT18 primary GBM cell lines (Figure 27a). Upon transduction, GFP-positive cells were sorted and allowed to recover for several days post-sort (Figure 27b). The primary GBM cell lines were lysed and immunoblotted with an anti- α v integrin antibody. Substantial knockdown of 80% or more was established in all four primary GBM cell lines (Figure 27a), although β 8 integrin expression did not change (data not shown). 500,000 cells (NSC-2 and NSC-11) were stereotactically injected into the striatum of immunocompromised mice and signs of tumor burden were obvious after 5 weeks (n=6 mice/cell line). Similar to β 8shRNA tumors, macro- and microscopic evaluation of NSC-2 NTshRNA and α vshRNA tumors revealed limited phenotypic differences (Figure 28a-d). Furthermore, pathological differences among NSC-11 NTshRNA and α vshRNA tumors were not obvious (Figure 28e-h), although there was evidence of macroscopic hemorrhage in three of the eight animals injected (Figure 28f).

These data suggest that compensation or functional redundancy may not be the reason for a lack of pathologies in the β 8shRNA tumors. There are other possible reasons as to why differences are not observed. Within the population of the knockdown cells, there are most likely subpopulations that may express high levels of α v β 8 integrin. This subpopulation may dominate *in vivo* and the subpopulation with diminished integrin expression may proliferate at a slower rate.

Secondly, existing mutations may also prove $\alpha v\beta 8$ integrin expression status negligible as more potent oncogenes may overshadow the integrin's role *in vivo*. Lastly, the integrin may be mutated as well.

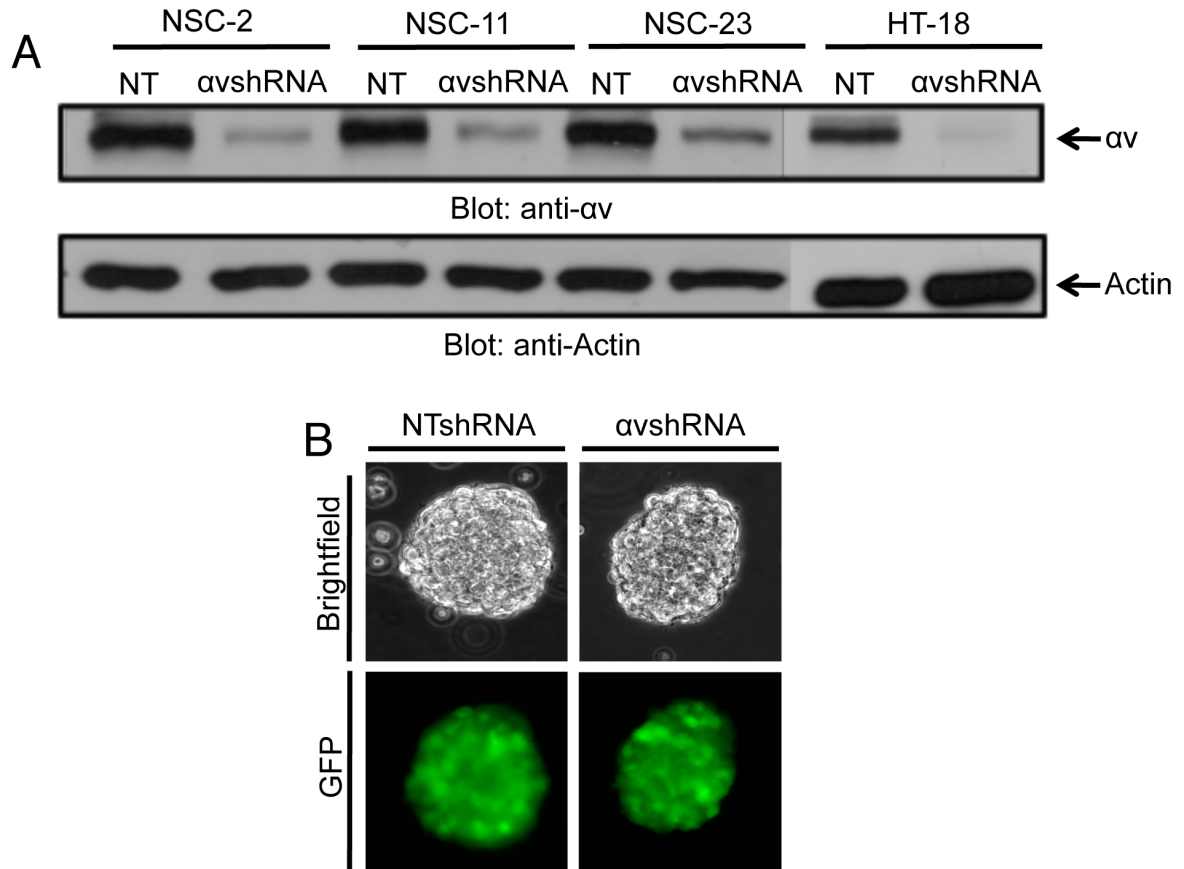


Figure 27: shRNA-mediated Stable Silencing of α v Integrin

(A) Four primary GBM cell lines were stably transduced with non-targeting (NT)-shRNA or α vshRNA. Lysates were immunoblotted with antibodies against α v integrin and actin. Note the substantial knockdown of α v integrin in all 4 primary GBM cell lines. (B) Brightfield and GFP images for a representative NTshRNA and α vshRNA primary GBM cell lines (NSC-11, images: 100x). Note the intense GFP signal in both cohorts.

Figure 28: Micro- and Macroscopic Images of non-targeting (NT)- and α vshRNA Intracranial Tumors

Two of the four different primary GBM cell lines that were stably transduced with NTshRNA or α vshRNA lentiviruses were stereotactically implanted into the striatum of immunocompromised mice (n=8 mice/cell line). (A) NSC-2 NTshRNA and (C) α vshRNA tumors were coronally sectioned. No obvious macroscopic and microscopic differences in tumor phenotypes (images: 200x) were detected via H&E staining (B, D). (E) NSC-11 NTshRNA and (F) α vshRNA tumors were coronally sectioned. Note the hemorrhagic phenotype (3 of 8 mice injected) in the α v integrin knockdown tumors from a macroscopic standpoint (F). Punctate patterns of hemorrhage were detected in NTshRNA tumors. H&E-stained coronal sections showed minimal microscopic differences with the tumors (200x).

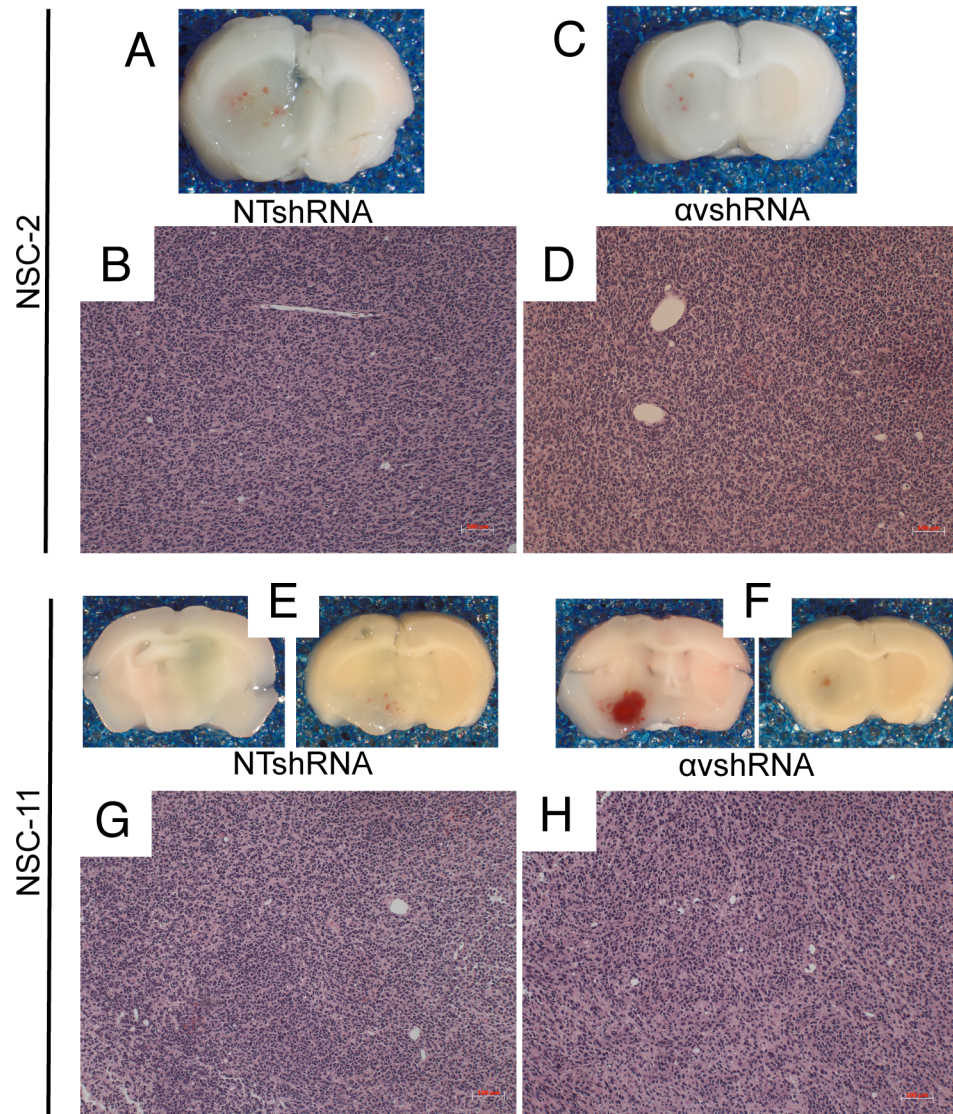


Figure 28

Sorting α^{HI} and α^{LO} NSC-2 and NSC-11 Primary GBM Cells

To evaluate the role of $\alpha\beta 8$ integrin expression utilizing primary GBM cells, NSC-2 and NSC-11 cells were stained with an anti- α integrin antibody. The top and bottom 15% of these populations, in terms of α integrin expression, were isolated and termed α^{HI} and α^{LO} (Figure 29a, b). Sorting efficiency was verified via immunoblotting the populations for α integrin protein (Figure 29c). Surprisingly, $\beta 8$ integrin expression did not change among the sub-populations. Next, 200,000 freshly sorted NSC-2 and -11 α^{HI} and α^{LO} primary GBM cell lines were injected into the striatum of immunocompromised mice (n=5 mice/sorted population) and neurological signs of tumor formation were evident with 5 weeks. Macroscopically, NSC-2 and NSC-11 α^{LO} tumors displayed only minimal evidence of hemorrhage, at best, although overall tumor size was strikingly different from NSC-2 and NSC-11 α^{HI} tumors (Figure 30a-d, left panel). H&E staining of tumors revealed no differences in microscopic phenotype, although differences in tumor volumes were quite obvious (Figure 30a-d, right panel). Resulting α^{LO} tumors were significantly larger than α^{HI} tumors in both primary GBM cell lines (Figure 30e). Therefore, sorting of 'true' $\alpha\beta 8$ high and low expressing populations could prove beneficial in divulging the role of the integrin in the human disease using the primary GBM cell model.

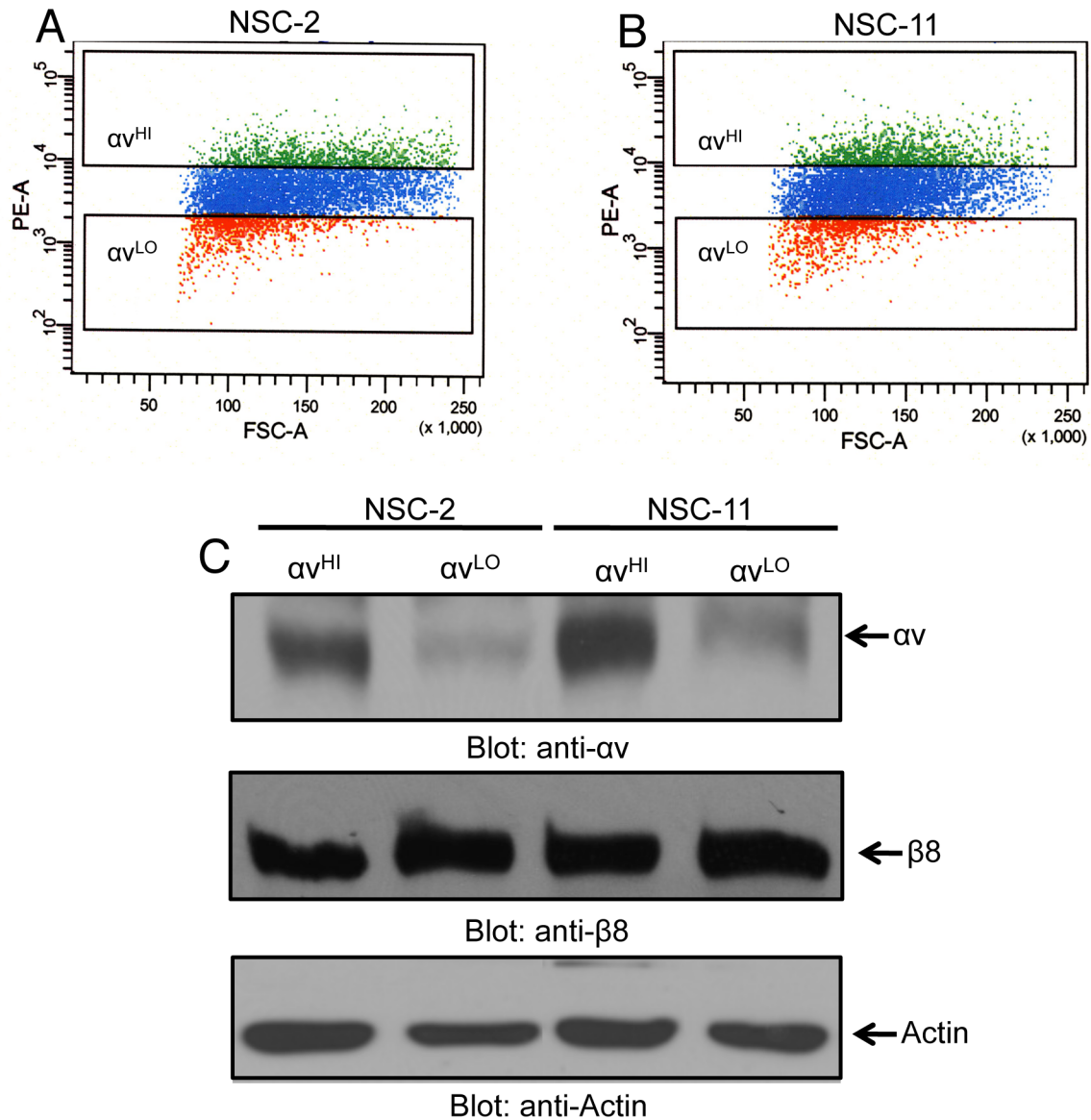


Figure 29: FACS of αv^{HI} - and αv^{LO} -expressing Populations

(A) NSC-2 and (B) NSC-11 primary GBM cells were sorted for αv integrin high and low expressing populations. Top and bottom 15% of each population was isolated and stereotactically injected directly into the striatum of immunocompromised mice (n=5/population). (C) All four populations were lysed to verify high and low expression profiles anti- αv and $\beta 8$ integrin and actin antibodies. Note the substantial decrease in αv integrin expression in the αv^{LO} lanes.

Figure 30: Intracranial Injection of NSC-2 and NSC-11 αv^{HI} and αv^{LO} Populations

Sorted populations (αv^{LO} and αv^{HI}) for NSC-2 (A, B) and NSC-11 (C, D) were stereotactically injected into the striatum of immunocompromised mice. Animals were cardiac perfused and coronally sectioned. H&E-stained sections reveal substantial tumor size differences. (E) Macroscopically, αv^{LO} tumors were significantly larger than αv^{HI} tumors in both NSC-2 (* $p < 0.01$) and NSC-11 (** $p < 0.02$) tumor bearing animals as assessed by quantitating tumor volumes ($n=5$).

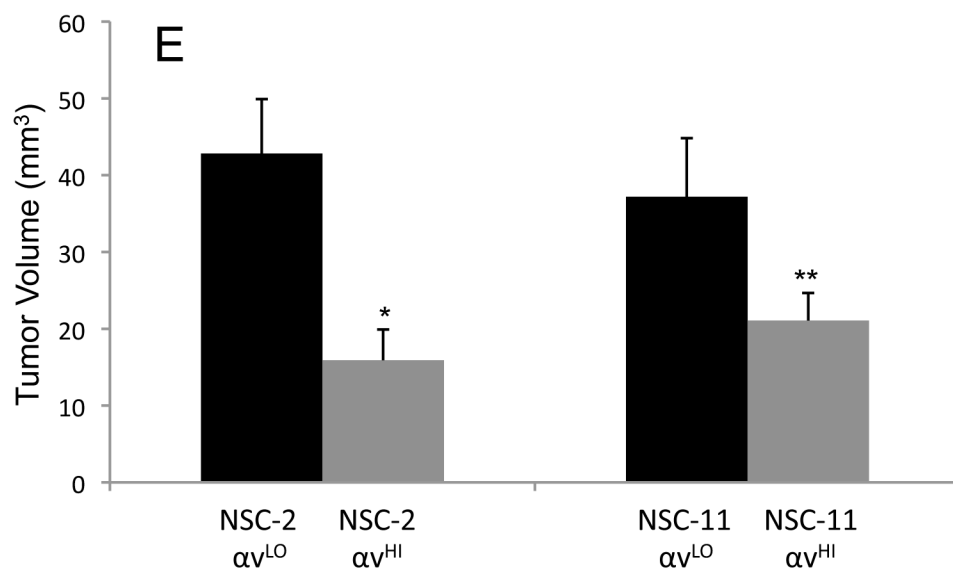
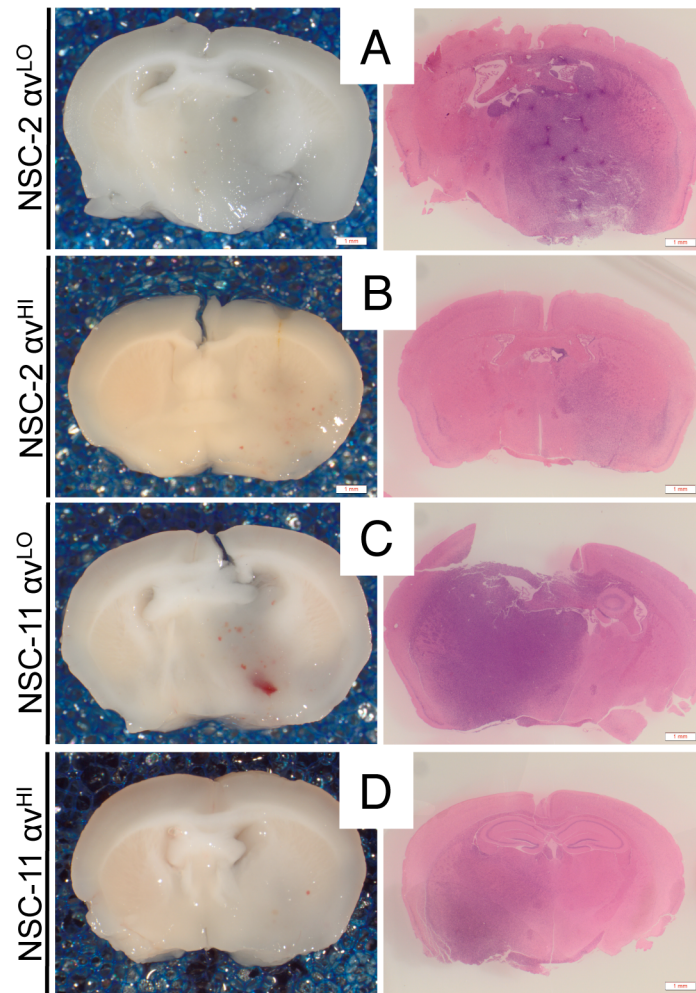


Figure 30

Evaluation of $\alpha\text{v}\beta 8$ Integrin Functions in Transformed Human Astrocytes

Pieper and colleagues developed a model to analyze the roles of astrocyte-derived gliomas by genetically modifying normal human astrocytes (NHAs) (148). First, they showed that retroviral transduction of NHAs with human telomerase catalytic component (hTERT) and E6/E7 oncoproteins allowed the cells to surpass cellular senescence but did not induce transformation. Only upon transduction with mutant H-Ras (G12V), enhancing MAPK signaling cascades and mimicking EGF receptor hyperactivation, did transformation occur (80). Pieper and colleagues concluded that the triple retroviral transduction of normal human astrocytes leads to the formation of grade III anaplastic astrocytomas upon implantation into the cerebral cortex of immunocompromised mice (80). Our lab confirmed this result with immortalized primary mouse astroglia, which were unable to form intracranial tumors (data not shown). However, upon delivering mutant H-Ras (G12V), transformed mouse astroglia were able to proliferate in a growth anchorage independent manner as well as form robust intracranial lesions.

This human cell system was used to model astrocytomas to evaluate the role of $\alpha\text{v}\beta 8$ integrin and determine if lentiviral knockdown of $\beta 8$ integrin increases tumor severity, similarly observed in the mouse model data in chapter 3. Similar to wild type mouse astroglia, transformation of NHAs reduced $\beta 8$ integrin expression by nearly 90% (Figures 11b/21a). Transformed human astrocytes (THAs) were stably transduced with NTshRNA and $\beta 8$ shRNA lentiviruses. Transduced cell populations show robust levels of GFP indicating a high level of transduction efficiency (Figure 31a, bottom panel). GFP positive populations were sorted and knockdown was

verified via immunoblotting with anti- α v and - β 8 integrin antibodies. Gene silencing was nearly 100% complete whereby limited expression was seen in the THAs + β 8shRNA (Figure 31b).

A variety of *in vitro* studies were performed on these manipulated cell populations analyzing cell proliferation, colony formation and migration via wound healing and matrigel invasion assays. 25,000 NTshRNA and β 8shRNA THAs were plated (n=3/cell line/timepoint) and cells were counted every 24 hours thereafter for 4 days. NTshRNA THAs proliferated significantly faster at 48, 72 and 96 hours after plating (Figure 31c). Conversely, β 8shRNA THAs produced significantly more colonies in a soft agar colony formation assay compared to NTshRNA THAs (n=3/cell line) (Figure 31d). NTshRNA and β 8shRNA THAs were plated on glass coverslips and allowed to grow to confluence (n=3/cell line). Cell-free regions were generated using a P-10 pipette tip and imaged over 36 hours via a live-cell imager. β 8shRNA THAs took significantly longer to close the wound than NTshRNA THAs (Figure 31e). Furthermore, a matrigel invasion assay further supported this evidence. 50,000 NTshRNA and β 8shRNA THAs were plated on the upper side of the matrigel invasion insert while using 10% FBS as a chemoattractant to initiate cell migration. Invasion was quantified by measuring crystal violet absorbance of contralaterally migrated cells. β 8shRNA THAs invaded significantly less than NTshRNA THAs (Figure 31f).

Figure 31: $\beta 8$ Integrin Stable Knockdown of Transformed Human Astrocytes

Transformed human astrocytes (THAs) were stably transduced with NTshRNA (A, left panel) and $\beta 8$ shRNA (A, right panel) lentiviruses and GFP+ cells were sorted. (Images=100x) (B) Lysates were immunoblotted with rabbit polyclonal antibodies directed against $\beta 8$ integrin, αv integrin and actin. Note the substantial knockdown of $\beta 8$ integrin protein (left lane). (C) Transformed human astrocytes (THAs) transduced with $\beta 8$ shRNA showed significantly reduced cell proliferation as compared to the NTshRNA cells (n=3/timepoint) (48h.*p<0.001; 72h.*p<0.001; 96h.*p<0.002). (D) $\beta 8$ shRNA THAs formed significantly more colonies in a soft agar assay compared to NTshRNA THAs (n=3/cell line) (*p<0.04). (E) In time-lapse videos, $\beta 8$ shRNA THAs required significantly more time to close the wound as compared to NTshRNA THAs (n=3/cell line) (*p<0.04). (F) In a matrigel invasion assay, $\beta 8$ shRNA THAs migrated at a significantly reduced rate as compared to NTshRNA THAs (n=3/cell line) (*p<0.01).

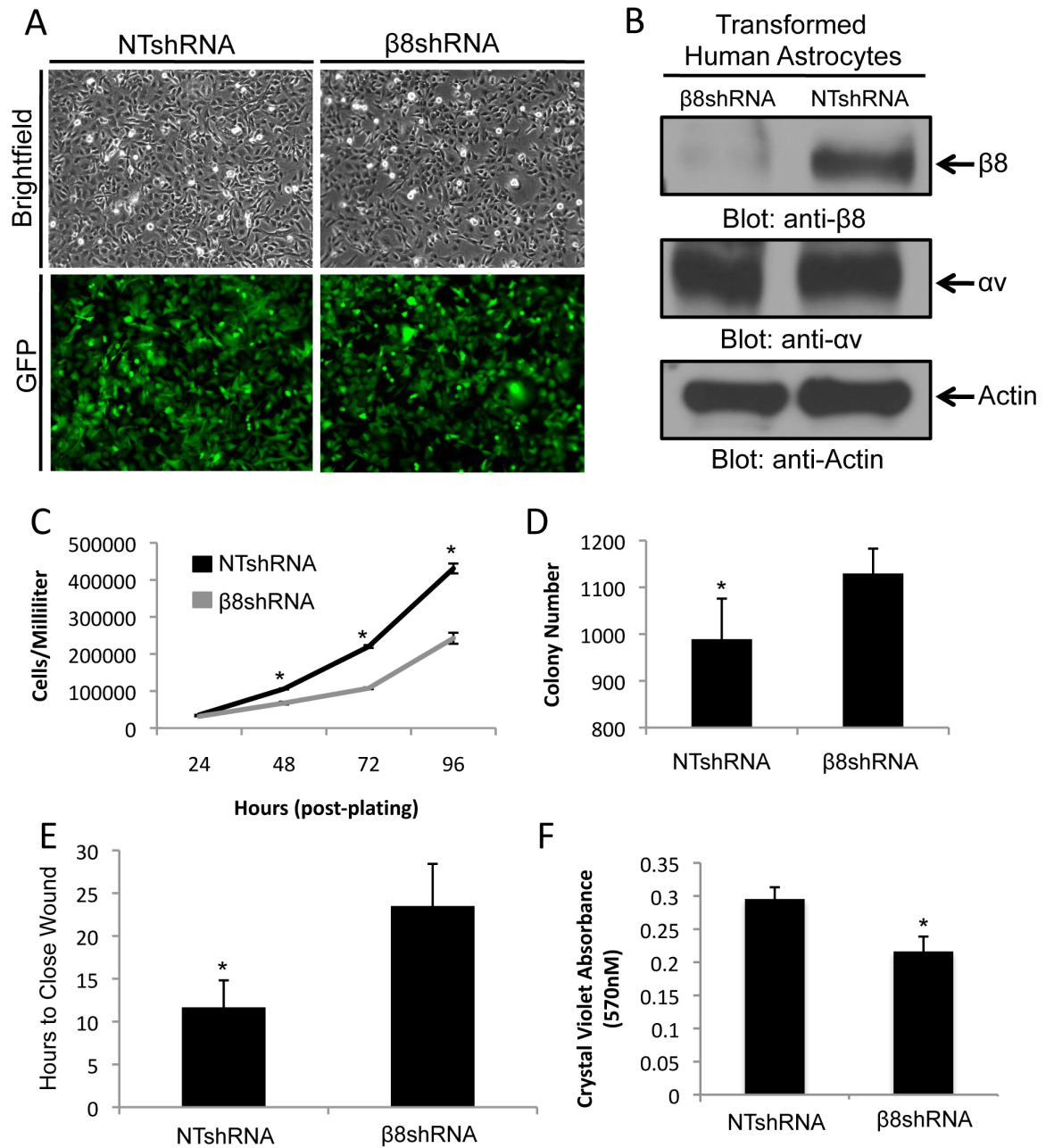


Figure 31

250,000 NTshRNA and β 8shRNA THAs were stereotactically injected in the striatum of immunocompromised mice (n=5/cell line). Five weeks after injection, mice developed clear signs of tumor burden including severe weight loss, hunched posture and in nearly all β 8shRNA tumor bearing mice, severe hydrocephaly. Macroscopically, β 8shRNA coronally sectioned tumors exhibited extremely large, hemorrhagic, non-invasive tumors on the ipsilateral side of injection (Figure 32b) whereas NTshRNA tumors were considerably smaller although they showed evidence of punctate hemorrhage (Figure 32a). After H&E staining, tumor volumes were quantified. β 8shRNA tumors were significantly larger than NTshRNA tumors (Figure 32c), consistent with the higher colony formation rate of β 8shRNA THAs *in vitro*. Representative coronal tumor sections were also H&E-stained to reveal a well-vascularized NTshRNA tumor. In addition, intratumoral vessels were lined with laminin and expressed CD31, an endothelial cell marker (Figure 33a). β 8shRNA coronal H&E-stained tumors revealed an increase in vessel size and overall density with areas of obvious hemorrhage. Further analysis of intratumoral vessels revealed substantial differences in vessel architecture within tumors (Figure 33b). For example, β 8shRNA tumors revealed significantly more microvascular density compared the NTshRNA tumors (Figure 33c). Although knockdown tumors were much larger and vascularized than control tumors, their tumor peripheries were non-invasive, as evidenced by GFP tumor cell fluorescence (Figure 33b, lower panel). NTshRNA tumors had clear areas of invasive fronts at the tumor periphery (Figure 33a, lower panel). Moreover, GFP⁺ tumor cells were detected several microns away from the tumor bulk (data not shown).

Figure 32: Intracranial Injections of NTshRNA and β 8shRNA Transformed Human Astrocytes

Immunocompromised mice were stereotactically injected with NTshRNA (n=8) and β 8shRNA (n=8) transformed human astrocytes. Gross macroscopic coronal sections of NTshRNA (A) and β 8shRNA (B) tumors reveal a robust difference in both tumor size and hemorrhagic phenotypes (arrows). (C) Tumor volume was quantified exhibiting β 8shRNA tumors were significantly larger than NTshRNA tumors (n=5) (*p<0.001).

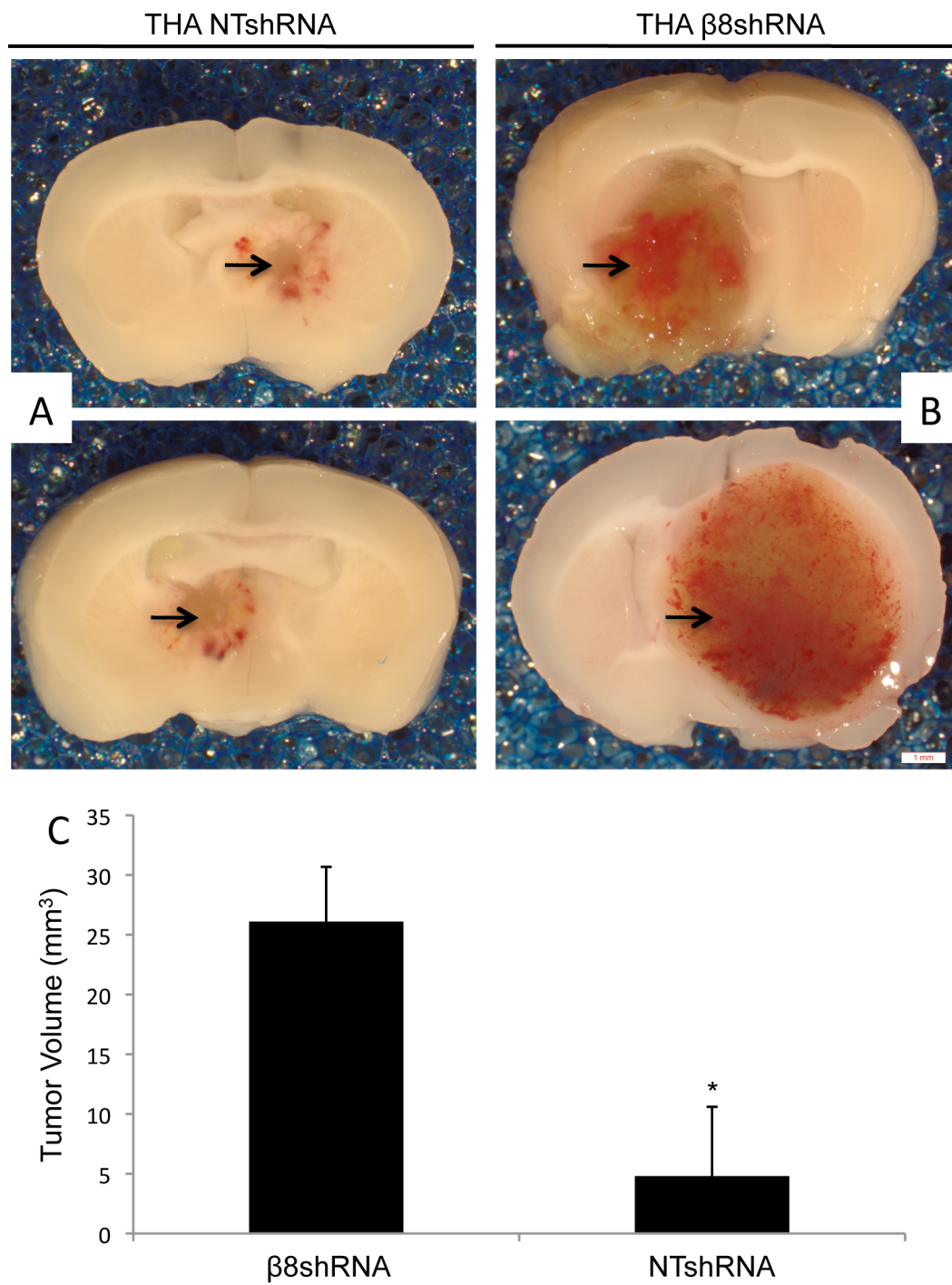


Figure 32

Figure 33: Histological Analysis of NTshRNA and β 8shRNA THA tumors

Coronal sections of NTshRNA (A, top panel) and β 8shRNA (B, top panel) tumors were stained with hematoxylin and eosin (H&E) and visualized microscopically (200x). Note the increase in vessel size in knockdown tumors. Coronal sections of NTshRNA (A, middle panel) and β 8shRNA (B, middle panel) tumors were doubly immunostained with an antibody against the vascular basement membrane (arrows), laminin (red) and an anti-nuclear stain, DAPI (blue) (400x). Note the significant increase in vessel size and volume in the knockdown tumors. Confocal microscopy on coronal frozen sections of NTshRNA (A, bottom panel) and β 8shRNA (B, bottom panel) tumors were stained with an antibody against the green fluorescent protein (GFP; green) expressed on tumor cells and against vascular endothelial cells (CD31; red) (400x). Note the well-defined and non-invasive β 8shRNA tumor periphery (arrow) as compared to the migratory cells at the NTshRNA tumor margins (arrows). (C) CD34 fluorescence, another marker of vascular endothelial cells, was measured to exhibit the significant increase in microvascular density in β 8shRNA tumors versus NTshRNA tumors (n=5/tumor) (*p<0.001).

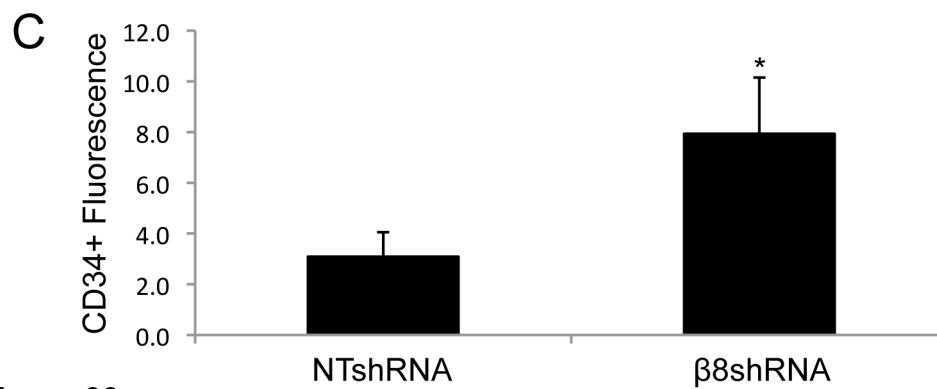
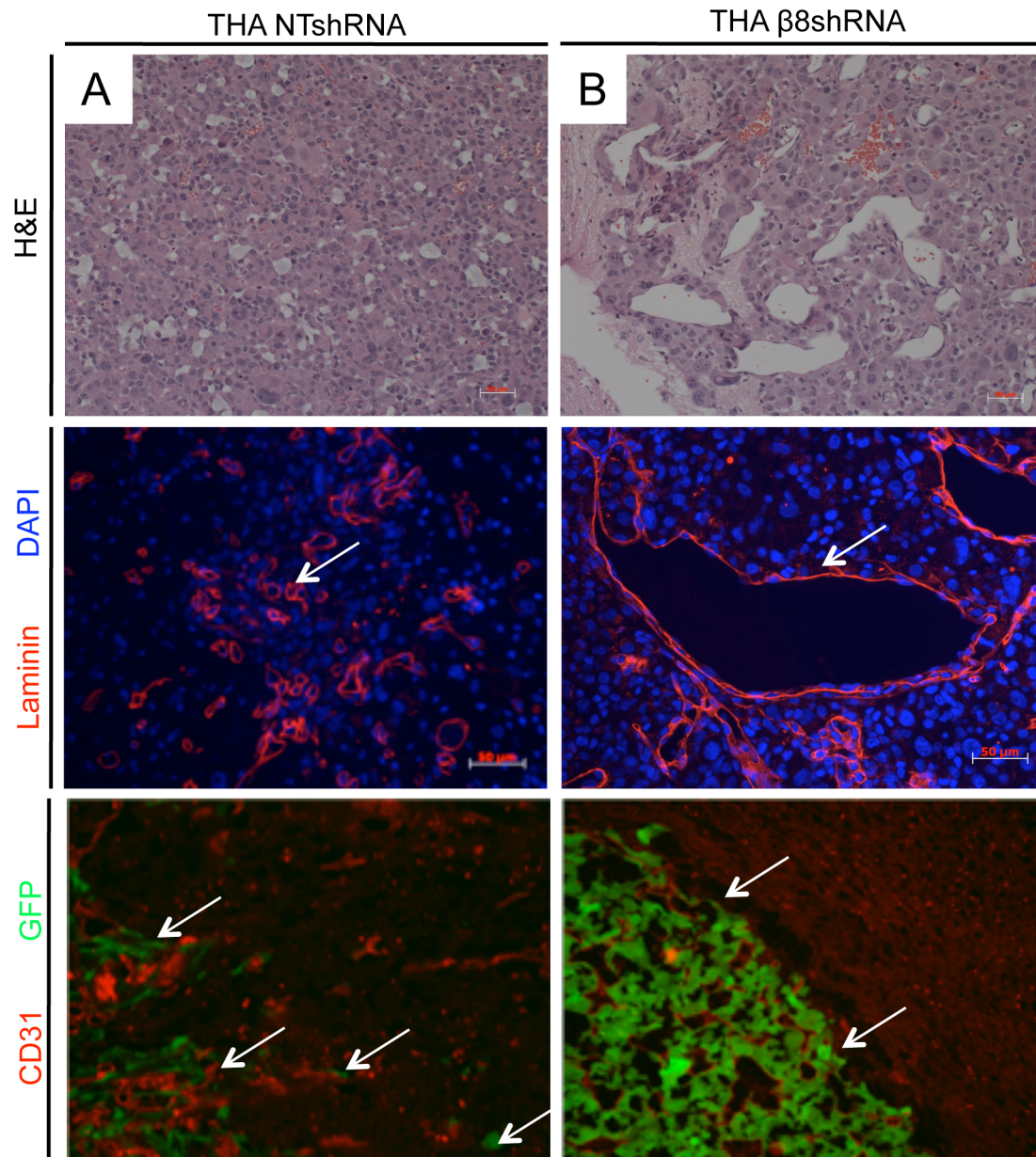


Figure 33

Elucidating the Mechanism Behind the $\beta 8$ shRNA Tumor Pathologies

Similar to the data for VEGF protein levels in conditioned media from wild type and $\beta 8^{-/-}$ transformed mouse astroglia, nearly identical results were found in conditioned media from NTshRNA and $\beta 8$ shRNA THAs. Both THAs lines were plated (n=3) and allowed to grow and condition media for 48 hours after which a human-specific ELISA was used to measure VEGF-A production. NTshRNA THAs produced significantly more VEGF than $\beta 8$ shRNA THAs, *in vitro* (Figure 34a). Substantial increase in VEGF production would most likely drive tumorigenesis and increase the severity of the tumor, although Sonoda et al. showed the exact opposite. THAs that are forced to overexpress VEGF did not convert grade III anaplastic astrocytomas to GBM (120). Perhaps, the loss of $\alpha v\beta 8$ integrin leads to tumor progression to grade IV, suggested by the differences in blood vessel characteristics among the $\beta 8$ shRNA lentiviral-infected THAs.

Next, a TGF β activation assay was performed on the NT- and $\beta 8$ shRNA THAs. Cells were transiently transfected with the truncated PAI-1L promoter plasmid (106). Next, both cell lines were exposed to 10ng/ml LAP-TGF β 1 for 18 hours. The following day, cells were lysed and firefly luciferase activity was assessed. There was significantly less TGF β activation in the $\beta 8$ shRNA THAs versus the NTshRNA THAs (Figure 34b, black bars). Furthermore, endogenously produced latent TGF β s produced by the THAs was unable to be activated in those cells stably transduced with the $\beta 8$ shRNA lentivirus (Figure 34b, gray bars). Taken together, these data further suggest a role for $\alpha v\beta 8$ integrin-mediated activation of latent TGF β s, similarly observed in the orthotopic mouse model.

Lastly, a Kaplan-Meier survival study was initiated to determine if the β 8shRNA tumors would cause early lethality. 50,000 cells (NT- and β 8shRNA THAs) were stereotactically injected in the striatum of immunocompromised mice (n=7 mice/cell line). Tumors were allowed to grow until the mice succumbed to tumor burden. β 8shRNA tumor bearing animals survived significantly less than NTshRNA tumor bearing animals (Figure 34c). Increased time to lethality in the knockdown tumor bearing mice was likely due to the severe hydrocephaly and enhanced tumor size.

Figure 34: Mechanism and Survival Analyses of NTshRNA and β 8shRNA Tumors.

(A) NTshRNA transformed human astrocytes condition media contained significantly more VEGF than β 8shRNA transformed human astrocytes, as assessed by ELISA (n=3/cell line) (*p<0.001). (B) NTshRNA and β 8shRNA transformed human astrocytes were transiently transfected with the PAI1-L vector to measure TGF β activity. Conditioned media from NTshRNA cells, pre-treated with LAP-TGF β 1, induced significantly more luciferase activity as compared to β 8shRNA cells (n=3/cell line) (*p<0.001). (C) Kaplan Meier survival analysis reveals a significant overall reduction in survival in β 8shRNA tumor bearing mice (n=7) versus NTshRNA tumor bearing mice (n=7) (*p<0.04 at 50% survival).

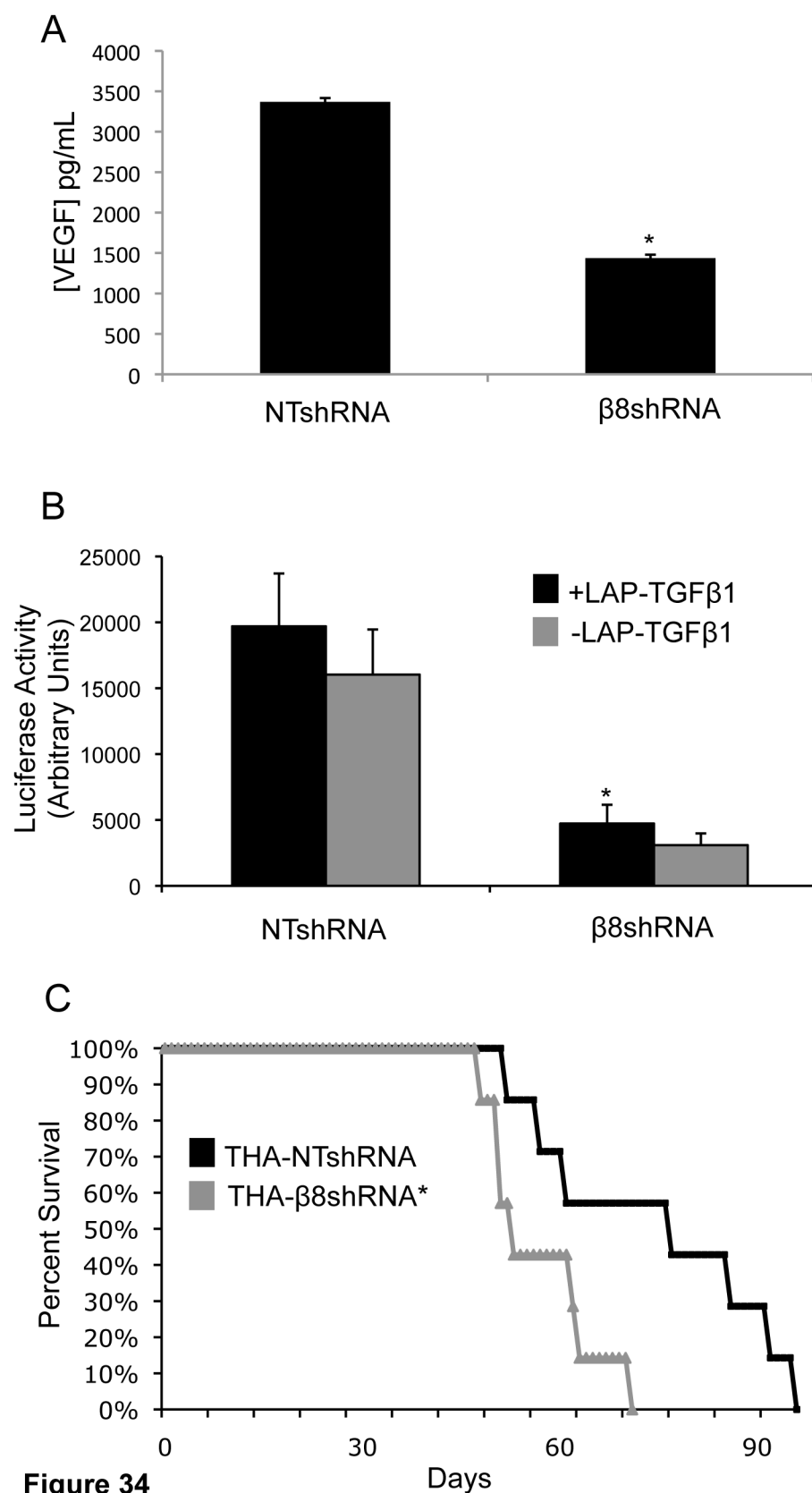


Figure 34

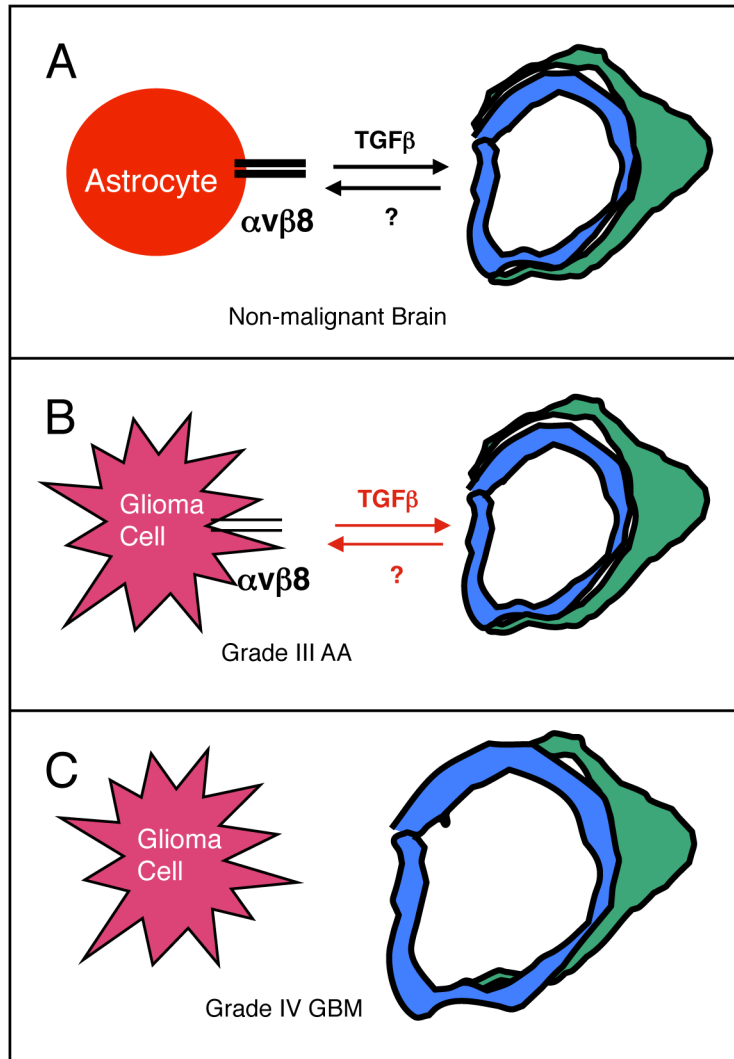


Figure 35: A Model for $\alpha v \beta 8$ Integrin-mediated Regulation of Tumorigenesis in the Brain.

(A) Perivascular astrocytes expressing $\alpha v \beta 8$ regulate cerebral blood vessel growth and stability by adhesion to ECM proteins, i.e. latent TGF β s. (B) Upon cell transformation, $\alpha v \beta 8$ integrin expression is down-regulated, thus ‘priming’ cells to exploit the vascular niche to promote tumor growth and survival. (C) As lower grade astrocytomas acquire more genetic mutations, these tumors progress to GBM status while $\alpha v \beta 8$ integrin expression and function is lost in the perivascular tumor niche, thus promoting angiogenesis pathologies commonly identified in GBM. Decreased tumor cell invasion and robust tumor growth are also evident.

Discussion

In this chapter, we extended our studies of $\alpha v\beta 8$ integrin in mouse gliomas to human gliomas. A previous report has documented increased $\beta 8$ integrin mRNA expression in human GBM samples (103), although their focus was on primary *de novo* GBMs as oppose to secondary GBMs, which resemble the mouse model described in the previous chapter. In addition, they analyzed bulk tumor masses rather than distinct tumor cells, as they harbor stromal infiltrative reactive astrocytes that may serve as a false positive. Secondly, our lab has concluded that the ' $\beta 8$ -specific' antibody used in these studies lacks specificity, as complete $\beta 8^{-/-}$ mouse brains show similar staining patterns to wild type mouse brains. Furthermore, their non-malignant brain tissue used to compare with human GBMs was cultured from cerebral cortices rather than neurogenic regions of the brain, such as the subventricular zone, which harbor neural stem cells, which are putative cells of origin for GBMs (84, 149).

This aim has revealed a significant role for $\alpha v\beta 8$ integrin in human gliomas beginning with the evaluation of expression in adherent cell lines. Although a majority of the samples expressed the integrin, the ones that did not exhibited robust intratumoral hemorrhage and other vascular pathologies (Figure 21b, 22c) that were largely resolved upon forced expression of $\beta 8$ integrin protein (Figure 22b). In addition, microvascular density and vessel size were largely reduced in those $\beta 8$ integrin expressing U87 tumors (Figure 22f). Interestingly, the U87+ $\beta 8V5$ tumor cells produced significantly more VEGF into the conditioned media compared to empty vector U87 cells (data not shown), similarly observed in wild type

transformed mouse astroglia. Further mechanistic investigation confirmed the role of $\alpha\text{v}\beta 8$ integrin in endothelial cell growth control based upon the significantly reduced bioactivation of latent TGF β s in low $\beta 8$ integrin expressing tumor cells (Figure 23).

Evaluation of $\alpha\text{v}\beta 8$ integrin expression in freshly resected human glioma samples revealed limited differences in total $\beta 8$ integrin expression levels (Figure 24a). However, these data are likely skewed by the stromal infiltrates, e.g. astrocytes, and non-malignant brain tissue present in the tumor specimens. Resected GBM samples gave us ample opportunity to culture primary cells in order to study the integrin's role in glioma progression. However, upon successful knockdown of αv and $\beta 8$ integrin subunits using lentiviral-delivered shRNAs, differences in tumor phenotypes were not obvious (Figure 26, 28). Although limited pathological differences were observed, it was most likely not due to alternate integrin compensation following $\beta 8$ integrin knockdown. Subpopulations of cells still expressing the integrin may be the primary cause for a lack of pathologies in the αv and $\beta 8$ integrin knockdown primary GBM cell line tumors. Perhaps, spatial patterning of those cells have a tendency to grow in a perivascular manner, similarly seen by neural stem cells in the vascular niche (150). Furthermore, the residual $\alpha\text{v}\beta 8$ integrin expression after lentiviral knockdown may not be sufficient to generate a difference in pathological outcomes and these cells may populate the tumor at a faster rate than the knockdown cells. In addition, the primary GBM cell lines used in this study could have more potent oncogenic potential that may mask presence or absence of $\alpha\text{v}\beta 8$ integrin expression, *in vivo*. Lastly, upon sorting αv integrin low

and high expressing sub-populations, the most convincing results towards our understanding of the integrin's role in the human disease with regard to the primary GBM cell line tumor model, became evident. A significant increase in tumor volume was revealed in those tumors expressing low levels of αv integrin, suggesting a suppressive role for this integrin in tumor progression. Although the angiogenic profiles of the αv integrin low tumors were no different than the αv integrin high tumors, many tumor cells have been known to upregulate integrins that are pro-tumorigenic while down regulating ones that are growth inhibitory (151). Furthermore, αv integrin's presence may have an autocrine role in growth inhibition upon the activation of latent TGF β s leading to the expression of CDK inhibitors and perturbing cell cycle progression (152). In addition, upon successful sorting of high and low αv integrin expressing sub-populations, $\beta 8$ integrin proteins levels remained unchanged (Figure 29c). The αv subunit is responsible for the binding of the RGD tri-peptide domain in latent TGF β s, therefore αv integrin low expressing tumors could exhibit TGF β growth inhibition, but the residual αv integrin expression, coupled with unchanged $\beta 8$ integrin expression, may inhibit expected vascular pathologies.

In a more genetically tractable model, normal human astrocytes were transformed and these formed intracranial lesions, indicative of grade III anaplastic astrocytomas (80). Utilizing this model provided us with better control of the genetic modifications to the cell line being studied. Surprisingly, lentiviral RNAi technology targeting of $\beta 8$ integrin resulted in nearly 100% knockdown (Figure 31b). Furthermore, stereotactic intracranial tumors formed significantly larger, and

strikingly, more hemorrhagic tumors than control tumors (Figure 32a, b). These pathologies led to a significant decrease in overall survival, which correlated with impaired TGF β activation and signaling in endothelial cells. In this model, the near complete silencing of β 8 integrin expression led to the significant decrease in autocrine TGF β signaling, which would suggest a pro-proliferative environment, even though α v integrin expression remained unchanged. Resulting vascular pathologies resembled those found in the mouse model discussed in Chapter 3, whereby impaired paracrine TGF β activation was determined to be a possible mechanism. In this model, the same idea would hold true. Collectively, defective TGF β activation would reduce growth inhibition and promote angiogenesis as evidenced in the silenced THA tumors.

Another significant finding in the THA mouse model was the substantial decrease in migration and invasion upon β 8 integrin gene silencing. Wound healing and matrigel invasion assays provided data that were very obvious *in vitro*. Silenced tumors grew in a similar manner to U87 parental tumors exhibiting large lesions with non-invasive margins. Bello and colleagues have described α v β 3 and α v β 5 integrins as being prominent proteins expressed on the tumor periphery responsible for migration and invasion (97); therefore, α v β 8 integrin could have the same effect in this model, as the data would suggest. Furthermore, control tumor cells invade and migrate faster, which carries over to the *in vivo* setting. Stimulation of adherent glioma cell lines with TGF β has promoted migration (153), which could be a result of α v β 8 integrin expression and therefore explain the non-invasive tendencies of the silenced tumors.

Collectively, these data identify an important role for $\alpha\text{v}\beta 8$ integrin in human gliomagenesis. Vascular and invasive pathologies highlight those processes regulated by $\alpha\text{v}\beta 8$ integrin in this chapter. In the normal brain, $\alpha\text{v}\beta 8$ integrin acts in concert with TGF β activation homeostatically regulating the cerebral blood vasculature. Upon accumulation of somatic mutations, $\alpha\text{v}\beta 8$ integrin is down-regulated setting up the vascular niche for aggressive tumor growth and survival. As lower grade astrocytomas gain additional genetic mutations, $\alpha\text{v}\beta 8$ integrin expression is lost promoting robust angiogenesis and tumor growth commonly observed in GBM (Figure 35).

Summary

This investigation is the first to link $\alpha v\beta 8$ integrin to pathologies associated with astrocytomas, particularly GBM. Several key observations were made and are detailed below:

1. Wild type transformed astroglia formed intracranial tumors that were indicative of grade III anaplastic astrocytomas, whereas $\beta 8^{-/-}$ transformed astroglia gave rise to tumors that were more similar to grade IV GBMs.
2. $\beta 8^{-/-}$ mouse tumors exhibited hemorrhagic pathologies and enhanced vascular density that resulted in premature lethality.
3. Forced $\beta 8$ integrin protein expression in $\beta 8^{-/-}$ transformed astroglia largely resolved *in vivo* vascular pathologies in $\beta 8^{-/-}$ mouse tumors.
4. $\beta 8^{-/-}$ tumor pathologies were due, in part, to impaired integrin-mediated TGF β activation and signaling in blood vessels.
5. U87 human glioma cell lines, expressing low levels of $\beta 8$ integrin, recapitulated $\beta 8^{-/-}$ mouse tumor pathologies and were resolved upon forced expression of $\beta 8$ integrin protein.
6. Primary GBM αv^{LO} cells produced significantly larger tumors than αv^{HI} cells.
7. Stable lentiviral silencing of $\beta 8$ integrin protein in transformed human astrocytes (THAs) resulted in significantly larger and more hemorrhagic intracranial tumors resulting in premature lethality.
8. $\beta 8$ silenced THA tumors displayed minimal invasiveness evidenced by *in vitro* and *in vivo* studies.

9. Stark differences in tumor growth and angiogenesis in control versus silenced THA tumors were, in part, due to impaired integrin-mediated TGF β activation.

Identifying $\alpha\beta 8$ integrin's involvement in brain tumor-associated vessel pathologies further establishes integrin biology as a key determinant in low- versus high-grade human gliomas. This knowledge could provide insights into the development of more targeted therapies to reduce tumor severity, thus resulting in increased patient survival. Unfortunately, current treatment for GBM is highly ineffective, only extending survival 5-10 months longer with an aggressive regime of concomitant radio- and chemotherapies that compromises quality of life. Anti-vascular agents have begun to show promise in the clinic as bevacizumab as recently been FDA-approved for the treatment of recurrent gliomas. Unfortunately, these agents are not used during primary treatment of newly diagnosed patients because of a poor benefit to risk ratio shortly after initial tumor resection. Therefore, more targeted therapies are necessary in the clinic in order to improve dismal median survival rates of GBM-diagnosed patients, which have not significantly changed over the past several decades.

This is the first investigation of $\alpha\beta 8$ integrin in GBM; however, there are many interesting future directions that should be pursued as a result of the data presented. First, further inquiry into $\alpha\beta 8$ integrin's involvement in human glioma invasion should be studied as obvious differences were seen in the transformed human astrocyte mouse model. Additionally, mice harboring control and integrin-

silenced tumors should be sacrificed earlier, i.e. 14 days post-injection, to determine whether the significant growth differences were a result of increased angiogenesis or tumor cell proliferation. Moreover, this same study should be performed analyzing the α^{LO} and α^{HI} sub-population tumors. Lastly, additional exploration of other mechanisms behind those pathologies presented should be further analyzed. The integrin's role in endothelial cell homeostasis was clear, although a more detailed analysis should be researched in order to determine if the TGF β bioactivation has more consequences in a para- or autocrine manner.

Further analysis of intracellular signaling within the tumor cells could also provide insights into the striking vascular pathological differences evidenced in this investigation. There is limited intracellular knowledge about how genetic ablation or stable silencing of $\beta 8$ integrin in tumor cells affects tumorigenesis. Perhaps, dissecting the auto- and paracrine molecular pathways as a result of this loss may further provide understanding in regard to $\alpha\beta 8$ integrin during gliomagenesis. Additional co-culture assays involving tumor cells and endothelial cells, such as tube formation or transwell assays, could reveal added mechanistic understanding behind the pathologies observed.

In addition to the various mouse models presented, the RCAS-N-tva mouse model could be valuable, commonly known for its initiation of 'endogenous' tumor formation upon retroviral delivery of potent oncogenes. Upon RCAS-PDGF β overexpression in the glial-specific N-tva model, low-grade III oligodendrogliomas appear (154). It is possible an endogenous tumor microenvironment devoid of $\alpha\beta 8$ integrin expression could push the tumors pass the threshold, classifying them as

grade IV GBMs. Furthermore, additional potent RCAS vectors such as myristoylated-Akt, K-Ras or VEGF concomitant with $\beta 8$ integrin loss could increase tumor severity as well. Other brain cancers could also be investigated, such as pediatric brain tumors, e.g. medulloblastoma.

Taken together, this thesis has provided a potential therapeutic target to further investigate based upon $\alpha v\beta 8$ integrin's involvement in glioma-induced angiogenesis, which could contribute to possible increased prevention (lower grade to high grade) and early diagnosis of GBM.

References Cited:

1. Iadecola, C. 2004. Neurovascular regulation in the normal brain and in Alzheimer's disease. *Nat Rev Neurosci* 5:347-360.
2. Carmeliet, P., and M. Tessier-Lavigne. 2005. Common mechanisms of nerve and blood vessel wiring. *Nature* 436:193-200.
3. Ek, C. J., K. M. Dziegielewska, H. Stolp, and N. R. Saunders. 2006. Functional effectiveness of the blood-brain barrier to small water-soluble molecules in developing and adult opossum (*Monodelphis domestica*). *J Comp Neurol* 496:13-26.
4. McCarty, J. H. 2005. Cell biology of the neurovascular unit: implications for drug delivery across the blood-brain barrier. *Assay Drug Dev Technol* 3:89-95.
5. Grieb, P., R. E. Forster, D. Strome, C. W. Goodwin, and P. C. Pape. 1985. O₂ exchange between blood and brain tissues studied with ¹⁸O₂ indicator-dilution technique. *J Appl Physiol* 58:1929-1941.
6. Tam, S. J., and R. J. Watts. Connecting vascular and nervous system development: angiogenesis and the blood-brain barrier. *Annu Rev Neurosci* 33:379-408.
7. Lee, J., C. Lund-Smith, A. Borboa, A. M. Gonzalez, A. Baird, and B. P. Eliceiri. 2009. Glioma-induced remodeling of the neurovascular unit. *Brain Res* 1288:125-134.

8. Stewart, P. A., and M. J. Wiley. 1981. Developing nervous tissue induces formation of blood-brain barrier characteristics in invading endothelial cells: a study using quail--chick transplantation chimeras. *Dev Biol* 84:183-192.
9. McCarty, J. H. 2009. Integrin-mediated regulation of neurovascular development, physiology and disease. *Cell Adh Migr* 3:211-215.
10. Takada, Y., X. Ye, and S. Simon. 2007. The integrins. *Genome Biol* 8:215.
11. Hynes, R. O. 1987. Integrins: a family of cell surface receptors. *Cell* 48:549-554.
12. Burke, R. D. 1999. Invertebrate integrins: structure, function, and evolution. *Int Rev Cytol* 191:257-284.
13. Ginsberg, M. H., A. Partridge, and S. J. Shattil. 2005. Integrin regulation. *Curr Opin Cell Biol* 17:509-516.
14. Mobley, A. K., J. H. Tchaicha, J. Shin, M. G. Hossain, and J. H. McCarty. 2009. $\beta 8$ integrin regulates neurogenesis and neurovascular homeostasis in the adult brain. *J Cell Sci* 122:1842-1851.
15. Rathinam, R., and S. K. Alahari. Important role of integrins in the cancer biology. *Cancer Metastasis Rev* 29:223-237.
16. Ginsberg, M. H., X. Du, and E. F. Plow. 1992. Inside-out integrin signalling. *Curr Opin Cell Biol* 4:766-771.
17. Barczyk, M., S. Carracedo, and D. Gullberg. Integrins. *Cell Tissue Res* 339:269-280.

18. Tanentzapf, G., and N. H. Brown. 2006. An interaction between integrin and the talin FERM domain mediates integrin activation but not linkage to the cytoskeleton. *Nat Cell Biol* 8:601-606.
19. Moser, M., B. Nieswandt, S. Ussar, M. Pozgajova, and R. Fassler. 2008. Kindlin-3 is essential for integrin activation and platelet aggregation. *Nat Med* 14:325-330.
20. Gahmberg, C. G., S. C. Fagerholm, S. M. Nurmi, T. Chavakis, S. Marchesan, and M. Gronholm. 2009. Regulation of integrin activity and signalling. *Biochim Biophys Acta* 1790:431-444.
21. Hynes, R. O. 1992. Integrins: versatility, modulation, and signaling in cell adhesion. *Cell* 69:11-25.
22. Belkin, A. M., and M. A. Stepp. 2000. Integrins as receptors for laminins. *Microsc Res Tech* 51:280-301.
23. Nishiuchi, R., J. Takagi, M. Hayashi, H. Ido, Y. Yagi, N. Sanzen, T. Tsuji, M. Yamada, and K. Sekiguchi. 2006. Ligand-binding specificities of laminin-binding integrins: a comprehensive survey of laminin-integrin interactions using recombinant alpha3beta1, alpha6beta1, alpha7beta1 and alpha6beta4 integrins. *Matrix Biol* 25:189-197.
24. Eble, J. A., K. W. Wucherpfennig, L. Gauthier, P. Dersch, E. Krukonis, R. R. Isberg, and M. E. Hemler. 1998. Recombinant soluble human alpha 3 beta 1 integrin: purification, processing, regulation, and specific binding to laminin-5 and invasin in a mutually exclusive manner. *Biochemistry* 37:10945-10955.

25. White, D. J., S. Puranen, M. S. Johnson, and J. Heino. 2004. The collagen receptor subfamily of the integrins. *Int J Biochem Cell Biol* 36:1405-1410.
26. Tulla, M., O. T. Pentikainen, T. Viitasalo, J. Kapyla, U. Impola, P. Nykvist, L. Nissinen, M. S. Johnson, and J. Heino. 2001. Selective binding of collagen subtypes by integrin alpha 1I, alpha 2I, and alpha 10I domains. *J Biol Chem* 276:48206-48212.
27. Kern, A., J. Eble, R. Golbik, and K. Kuhn. 1993. Interaction of type IV collagen with the isolated integrins alpha 1 beta 1 and alpha 2 beta 1. *Eur J Biochem* 215:151-159.
28. Heino, J. 2000. The collagen receptor integrins have distinct ligand recognition and signaling functions. *Matrix Biol* 19:319-323.
29. Hynes, R. O. 2002. Integrins: bidirectional, allosteric signaling machines. *Cell* 110:673-687.
30. Denucci, C. C., J. S. Mitchell, and Y. Shimizu. 2009. Integrin function in T-cell homing to lymphoid and nonlymphoid sites: getting there and staying there. *Crit Rev Immunol* 29:87-109.
31. Abram, C. L., and C. A. Lowell. 2009. The ins and outs of leukocyte integrin signaling. *Annu Rev Immunol* 27:339-362.
32. Humphries, J. D., A. Byron, and M. J. Humphries. 2006. Integrin ligands at a glance. *J Cell Sci* 119:3901-3903.
33. Mu, D., S. Cambier, L. Fjellbirkeland, J. L. Baron, J. S. Munger, H. Kawakatsu, D. Sheppard, V. C. Broaddus, and S. L. Nishimura. 2002. The

- integrin $\alpha(v)\beta 8$ mediates epithelial homeostasis through MT1-MMP-dependent activation of TGF- $\beta 1$. *J Cell Biol* 157:493-507.
34. Brooks, P. C., R. A. Clark, and D. A. Cheresh. 1994. Requirement of vascular integrin $\alpha v \beta 3$ for angiogenesis. *Science* 264:569-571.
 35. Bader, B. L., H. Rayburn, D. Crowley, and R. O. Hynes. 1998. Extensive vasculogenesis, angiogenesis, and organogenesis precede lethality in mice lacking all αv integrins. *Cell* 95:507-519.
 36. McCarty, J. H., A. Lacy-Hulbert, A. Charest, R. T. Bronson, D. Crowley, D. Housman, J. Savill, J. Roes, and R. O. Hynes. 2005. Selective ablation of αv integrins in the central nervous system leads to cerebral hemorrhage, seizures, axonal degeneration and premature death. *Development* 132:165-176.
 37. Fassler, R., and M. Meyer. 1995. Consequences of lack of $\beta 1$ integrin gene expression in mice. *Genes Dev* 9:1896-1908.
 38. Hodivala-Dilke, K. M., K. P. McHugh, D. A. Tsakiris, H. Rayburn, D. Crowley, M. Ullman-Cullere, F. P. Ross, B. S. Coller, S. Teitelbaum, and R. O. Hynes. 1999. $\beta 3$ -integrin-deficient mice are a model for Glanzmann thrombasthenia showing placental defects and reduced survival. *J Clin Invest* 103:229-238.
 39. Tronik-Le Roux, D., V. Roullot, C. Poujol, T. Kortulewski, P. Nurden, and G. Marguerie. 2000. Thrombasthenic mice generated by replacement of the integrin $\alpha(IIb)$ gene: demonstration that transcriptional activation of this megakaryocytic locus precedes lineage commitment. *Blood* 96:1399-1408.

40. Huang, X., M. Griffiths, J. Wu, R. V. Farese, Jr., and D. Sheppard. 2000. Normal development, wound healing, and adenovirus susceptibility in beta5-deficient mice. *Mol Cell Biol* 20:755-759.
41. Breuss, J. M., J. Gallo, H. M. DeLisser, I. V. Klimanskaya, H. G. Folkesson, J. F. Pittet, S. L. Nishimura, K. Aldape, D. V. Landers, W. Carpenter, and et al. 1995. Expression of the beta 6 integrin subunit in development, neoplasia and tissue repair suggests a role in epithelial remodeling. *J Cell Sci* 108 (Pt 6):2241-2251.
42. Huang, X. Z., J. F. Wu, D. Cass, D. J. Erle, D. Corry, S. G. Young, R. V. Farese, Jr., and D. Sheppard. 1996. Inactivation of the integrin beta 6 subunit gene reveals a role of epithelial integrins in regulating inflammation in the lung and skin. *J Cell Biol* 133:921-928.
43. Nishimura, S. L., K. P. Boylen, S. Einheber, T. A. Milner, D. M. Ramos, and R. Pytela. 1998. Synaptic and glial localization of the integrin alphavbeta8 in mouse and rat brain. *Brain Res* 791:271-282.
44. Zhu, J., K. Motejlek, D. Wang, K. Zang, A. Schmidt, and L. F. Reichardt. 2002. beta8 integrins are required for vascular morphogenesis in mouse embryos. *Development* 129:2891-2903.
45. Milner, R., and I. L. Campbell. 2002. The integrin family of cell adhesion molecules has multiple functions within the CNS. *J Neurosci Res* 69:286-291.
46. Moyle, M., M. A. Napier, and J. W. McLean. 1991. Cloning and expression of a divergent integrin subunit beta 8. *J Biol Chem* 266:19650-19658.

47. Nishimura, S. L., D. Sheppard, and R. Pytela. 1994. Integrin alpha v beta 8. Interaction with vitronectin and functional divergence of the beta 8 cytoplasmic domain. *J Biol Chem* 269:28708-28715.
48. Venstrom, K., and L. Reichardt. 1995. Beta 8 integrins mediate interactions of chick sensory neurons with laminin-1, collagen IV, and fibronectin. *Mol Biol Cell* 6:419-431.
49. Cambier, S., S. Gline, D. Mu, R. Collins, J. Araya, G. Dolganov, S. Einheber, N. Boudreau, and S. L. Nishimura. 2005. Integrin alpha(v)beta8-mediated activation of transforming growth factor-beta by perivascular astrocytes: an angiogenic control switch. *Am J Pathol* 166:1883-1894.
50. McCarty, J. H., A. A. Cook, and R. O. Hynes. 2005. An interaction between {alpha}v{beta}8 integrin and Band 4.1B via a highly conserved region of the Band 4.1 C-terminal domain. *Proc Natl Acad Sci U S A* 102:13479-13483.
51. Calinisan, V., D. Gravem, R. P. Chen, S. Brittin, N. Mohandas, M. C. Lecomte, and P. Gascard. 2006. New insights into potential functions for the protein 4.1 superfamily of proteins in kidney epithelium. *Front Biosci* 11:1646-1666.
52. Proctor, J. M., K. Zang, D. Wang, R. Wang, and L. F. Reichardt. 2005. Vascular development of the brain requires beta8 integrin expression in the neuroepithelium. *J Neurosci* 25:9940-9948.
53. Holland, E. C. 2001. Gliomagenesis: genetic alterations and mouse models. *Nat Rev Genet* 2:120-129.

54. Ohgaki, H., and P. Kleihues. 2007. Genetic pathways to primary and secondary glioblastoma. *Am J Pathol* 170:1445-1453.
55. Ohgaki, H. 2005. Genetic pathways to glioblastomas. *Neuropathology* 25:1-7.
56. Louis, D. N., H. Ohgaki, O. D. Wiestler, W. K. Cavenee, P. C. Burger, A. Jouvett, B. W. Scheithauer, and P. Kleihues. 2007. The 2007 WHO classification of tumours of the central nervous system. *Acta Neuropathol* 114:97-109.
57. Sanai, N., A. Alvarez-Buylla, and M. S. Berger. 2005. Neural stem cells and the origin of gliomas. *N Engl J Med* 353:811-822.
58. Shih, A. H., and E. C. Holland. 2004. Developmental neurobiology and the origin of brain tumors. *J Neurooncol* 70:125-136.
59. Fomchenko, E. I., and E. C. Holland. 2006. Origins of brain tumors--a disease of stem cells? *Nat Clin Pract Neurol* 2:288-289.
60. Hadjipanayis, C. G., and E. G. Van Meir. 2009. Brain cancer propagating cells: biology, genetics and targeted therapies. *Trends Mol Med* 15:519-530.
61. Lantos, P. L., and D. J. Cox. 1976. The origin of experimental brain tumours: a sequential study. *Experientia* 32:1467-1468.
62. Quigley, M. R., C. Post, and G. Ehrlich. 2007. Some speculation on the origin of glioblastoma. *Neurosurg Rev* 30:16-20; discussion 20-11.
63. Odoux, C., H. Fohrer, T. Hoppe, L. Guzik, D. B. Stolz, D. W. Lewis, S. M. Gollin, T. C. Gamblin, D. A. Geller, and E. Lagasse. 2008. A stochastic

- model for cancer stem cell origin in metastatic colon cancer. *Cancer Res* 68:6932-6941.
64. Shih, A. H., C. Dai, X. Hu, M. K. Rosenblum, J. A. Koutcher, and E. C. Holland. 2004. Dose-dependent effects of platelet-derived growth factor-B on glial tumorigenesis. *Cancer Res* 64:4783-4789.
 65. Holland, E. C., J. Celestino, C. Dai, L. Schaefer, R. E. Sawaya, and G. N. Fuller. 2000. Combined activation of Ras and Akt in neural progenitors induces glioblastoma formation in mice. *Nat Genet* 25:55-57.
 66. Reilly, K. M., D. A. Loisel, R. T. Bronson, M. E. McLaughlin, and T. Jacks. 2000. Nf1;Trp53 mutant mice develop glioblastoma with evidence of strain-specific effects. *Nat Genet* 26:109-113.
 67. Kyritsis, A. P., M. L. Bondy, J. S. Rao, and C. Sioka. Inherited predisposition to glioma. *Neuro Oncol* 12:104-113.
 68. Wechsler-Reya, R., and M. P. Scott. 2001. The developmental biology of brain tumors. *Annu Rev Neurosci* 24:385-428.
 69. Bunney, T. D., and M. Katan. Phosphoinositide signalling in cancer: beyond PI3K and PTEN. *Nat Rev Cancer* 10:342-352.
 70. Holland, E. C., W. P. Hively, R. A. DePinho, and H. E. Varmus. 1998. A constitutively active epidermal growth factor receptor cooperates with disruption of G1 cell-cycle arrest pathways to induce glioma-like lesions in mice. *Genes Dev* 12:3675-3685.
 71. Parsons, D. W., S. Jones, X. Zhang, J. C. Lin, R. J. Leary, P. Angenendt, P. Mankoo, H. Carter, I. M. Siu, G. L. Gallia, A. Olivi, R. McLendon, B. A.

- Rasheed, S. Keir, T. Nikolskaya, Y. Nikolsky, D. A. Busam, H. Tekleab, L. A. Diaz, Jr., J. Hartigan, D. R. Smith, R. L. Strausberg, S. K. Marie, S. M. Shinjo, H. Yan, G. J. Riggins, D. D. Bigner, R. Karchin, N. Papadopoulos, G. Parmigiani, B. Vogelstein, V. E. Velculescu, and K. W. Kinzler. 2008. An integrated genomic analysis of human glioblastoma multiforme. *Science* 321:1807-1812.
72. Yan, H., D. W. Parsons, G. Jin, R. McLendon, B. A. Rasheed, W. Yuan, I. Kos, I. Batinic-Haberle, S. Jones, G. J. Riggins, H. Friedman, A. Friedman, D. Reardon, J. Herndon, K. W. Kinzler, V. E. Velculescu, B. Vogelstein, and D. D. Bigner. 2009. IDH1 and IDH2 mutations in gliomas. *N Engl J Med* 360:765-773.
 73. Stupp, R., W. P. Mason, M. J. van den Bent, M. Weller, B. Fisher, M. J. Taphoorn, K. Belanger, A. A. Brandes, C. Marosi, U. Bogdahn, J. Curschmann, R. C. Janzer, S. K. Ludwin, T. Gorlia, A. Allgeier, D. Lacombe, J. G. Cairncross, E. Eisenhauer, and R. O. Mirimanoff. 2005. Radiotherapy plus concomitant and adjuvant temozolomide for glioblastoma. *N Engl J Med* 352:987-996.
 74. Clarke, J., N. Butowski, and S. Chang. Recent advances in therapy for glioblastoma. *Arch Neurol* 67:279-283.
 75. Stupp, R., M. E. Hegi, W. P. Mason, M. J. van den Bent, M. J. Taphoorn, R. C. Janzer, S. K. Ludwin, A. Allgeier, B. Fisher, K. Belanger, P. Hau, A. A. Brandes, J. Gijtenbeek, C. Marosi, C. J. Vecht, K. Mokhtari, P. Wesseling, S. Villa, E. Eisenhauer, T. Gorlia, M. Weller, D. Lacombe, J. G. Cairncross, and

- R. O. Mirimanoff. 2009. Effects of radiotherapy with concomitant and adjuvant temozolomide versus radiotherapy alone on survival in glioblastoma in a randomised phase III study: 5-year analysis of the EORTC-NCIC trial. *Lancet Oncol* 10:459-466.
76. de Vries, N. A., J. H. Beijnen, W. Boogerd, and O. van Tellingen. 2006. Blood-brain barrier and chemotherapeutic treatment of brain tumors. *Expert Rev Neurother* 6:1199-1209.
77. Khasraw, M., and A. B. Lassman. Advances in the treatment of malignant gliomas. *Curr Oncol Rep* 12:26-33.
78. Holash, J., S. Davis, N. Papadopoulos, S. D. Croll, L. Ho, M. Russell, P. Boland, R. Leidich, D. Hylton, E. Burova, E. Ioffe, T. Huang, C. Radziejewski, K. Bailey, J. P. Fandl, T. Daly, S. J. Wiegand, G. D. Yancopoulos, and J. S. Rudge. 2002. VEGF-Trap: a VEGF blocker with potent antitumor effects. *Proc Natl Acad Sci U S A* 99:11393-11398.
79. Miletic, H., S. P. Niclou, M. Johansson, and R. Bjerkvig. 2009. Anti-VEGF therapies for malignant glioma: treatment effects and escape mechanisms. *Expert Opin Ther Targets* 13:455-468.
80. Sonoda, Y., T. Ozawa, Y. Hirose, K. D. Aldape, M. McMahon, M. S. Berger, and R. O. Pieper. 2001. Formation of intracranial tumors by genetically modified human astrocytes defines four pathways critical in the development of human anaplastic astrocytoma. *Cancer Res* 61:4956-4960.
81. Holland, E. C., W. P. Hively, V. Gallo, and H. E. Varmus. 1998. Modeling mutations in the G1 arrest pathway in human gliomas: overexpression of

- CDK4 but not loss of INK4a-ARF induces hyperploidy in cultured mouse astrocytes. *Genes Dev* 12:3644-3649.
82. Cespedes, M. V., I. Casanova, M. Parreno, and R. Mangués. 2006. Mouse models in oncogenesis and cancer therapy. *Clin Transl Oncol* 8:318-329.
 83. Llaguno, S. A., J. Chen, C. H. Kwon, and L. F. Parada. 2008. Neural and cancer stem cells in tumor suppressor mouse models of malignant astrocytoma. *Cold Spring Harb Symp Quant Biol* 73:421-426.
 84. Alcantara Llaguno, S., J. Chen, C. H. Kwon, E. L. Jackson, Y. Li, D. K. Burns, A. Alvarez-Buylla, and L. F. Parada. 2009. Malignant astrocytomas originate from neural stem/progenitor cells in a somatic tumor suppressor mouse model. *Cancer Cell* 15:45-56.
 85. Weiss, W. A., M. J. Burns, C. Hackett, K. Aldape, J. R. Hill, H. Kuriyama, N. Kuriyama, N. Milshteyn, T. Roberts, M. F. Wendland, R. DePinho, and M. A. Israel. 2003. Genetic determinants of malignancy in a mouse model for oligodendroglioma. *Cancer Res* 63:1589-1595.
 86. Gladson, C. L. 1999. The extracellular matrix of gliomas: modulation of cell function. *J Neuropathol Exp Neurol* 58:1029-1040.
 87. Gingras, M. C., E. Roussel, J. M. Bruner, C. D. Branch, and R. P. Moser. 1995. Comparison of cell adhesion molecule expression between glioblastoma multiforme and autologous normal brain tissue. *J Neuroimmunol* 57:143-153.
 88. Reardon, D. A., L. B. Nabors, R. Stupp, and T. Mikkelsen. 2008. Cilengitide: an integrin-targeting arginine-glycine-aspartic acid peptide with promising

- activity for glioblastoma multiforme. *Expert Opin Investig Drugs* 17:1225-1235.
89. Reardon, D. A., K. L. Fink, T. Mikkelsen, T. F. Cloughesy, A. O'Neill, S. Plotkin, M. Glantz, P. Ravin, J. J. Raizer, K. M. Rich, D. Schiff, W. R. Shapiro, S. Burdette-Radoux, E. J. Dropcho, S. M. Wittemer, J. Nippgen, M. Picard, and L. B. Nabors. 2008. Randomized phase II study of cilengitide, an integrin-targeting arginine-glycine-aspartic acid peptide, in recurrent glioblastoma multiforme. *J Clin Oncol* 26:5610-5617.
90. Tabatabai, G., M. Weller, B. Nabors, M. Picard, D. Reardon, T. Mikkelsen, C. Ruegg, and R. Stupp. Targeting integrins in malignant glioma. *Target Oncol*.
91. Wesseling, P., J. A. van der Laak, H. de Leeuw, D. J. Ruiter, and P. C. Burger. 1994. Quantitative immunohistological analysis of the microvasculature in untreated human glioblastoma multiforme. Computer-assisted image analysis of whole-tumor sections. *J Neurosurg* 81:902-909.
92. Goldbrunner, R. H., J. J. Bernstein, and J. C. Tonn. 1999. Cell-extracellular matrix interaction in glioma invasion. *Acta Neurochir (Wien)* 141:295-305; discussion 304-295.
93. Tucker, G. C. 2006. Integrins: molecular targets in cancer therapy. *Curr Oncol Rep* 8:96-103.
94. Francis, S. E., K. L. Goh, K. Hodivala-Dilke, B. L. Bader, M. Stark, D. Davidson, and R. O. Hynes. 2002. Central roles of alpha5beta1 integrin and fibronectin in vascular development in mouse embryos and embryoid bodies. *Arterioscler Thromb Vasc Biol* 22:927-933.

95. Kita, D., T. Takino, M. Nakada, T. Takahashi, J. Yamashita, and H. Sato. 2001. Expression of dominant-negative form of Ets-1 suppresses fibronectin-stimulated cell adhesion and migration through down-regulation of integrin alpha5 expression in U251 glioma cell line. *Cancer Res* 61:7985-7991.
96. Uhm, J. H., C. L. Gladson, and J. S. Rao. 1999. The role of integrins in the malignant phenotype of gliomas. *Front Biosci* 4:D188-199.
97. Bello, L., M. Francolini, P. Marthyn, J. Zhang, R. S. Carroll, D. C. Nikas, J. F. Strasser, R. Villani, D. A. Cheresh, and P. M. Black. 2001. Alpha(v)beta3 and alpha(v)beta5 integrin expression in glioma periphery. *Neurosurgery* 49:380-389; discussion 390.
98. Chatterjee, S., A. Matsumura, J. Schradermeier, and G. Y. Gillespie. 2000. Human malignant glioma therapy using anti-alpha(v)beta3 integrin agents. *J Neurooncol* 46:135-144.
99. Kanamori, M., S. R. Vanden Berg, G. Bergers, M. S. Berger, and R. O. Pieper. 2004. Integrin beta3 overexpression suppresses tumor growth in a human model of gliomagenesis: implications for the role of beta3 overexpression in glioblastoma multiforme. *Cancer Res* 64:2751-2758.
100. Cheng, S. Y., M. Nagane, H. S. Huang, and W. K. Cavenee. 1997. Intracerebral tumor-associated hemorrhage caused by overexpression of the vascular endothelial growth factor isoforms VEGF121 and VEGF165 but not VEGF189. *Proc Natl Acad Sci U S A* 94:12081-12087.
101. Deeken, J. F., and W. Loscher. 2007. The blood-brain barrier and cancer: transporters, treatment, and Trojan horses. *Clin Cancer Res* 13:1663-1674.

102. Jain, R. K., E. di Tomaso, D. G. Duda, J. S. Loeffler, A. G. Sorensen, and T. T. Batchelor. 2007. Angiogenesis in brain tumours. *Nat Rev Neurosci* 8:610-622.
103. Riemenschneider, M. J., W. Mueller, R. A. Betensky, G. Mohapatra, and D. N. Louis. 2005. In situ analysis of integrin and growth factor receptor signaling pathways in human glioblastomas suggests overlapping relationships with focal adhesion kinase activation. *Am J Pathol* 167:1379-1387.
104. Calabrese, C., H. Poppleton, M. Kocak, T. L. Hogg, C. Fuller, B. Hamner, E. Y. Oh, M. W. Gaber, D. Finklestein, M. Allen, A. Frank, I. T. Bayazitov, S. S. Zakharenko, A. Gajjar, A. Davidoff, and R. J. Gilbertson. 2007. A perivascular niche for brain tumor stem cells. *Cancer Cell* 11:69-82.
105. Rietze, R. L., and B. A. Reynolds. 2006. Neural stem cell isolation and characterization. *Methods Enzymol* 419:3-23.
106. Abe, M., J. G. Harpel, C. N. Metz, I. Nunes, D. J. Loskutoff, and D. B. Rifkin. 1994. An assay for transforming growth factor-beta using cells transfected with a plasminogen activator inhibitor-1 promoter-luciferase construct. *Anal Biochem* 216:276-284.
107. Kissler, S., P. Stern, K. Takahashi, K. Hunter, L. B. Peterson, and L. S. Wicker. 2006. In vivo RNA interference demonstrates a role for Nramp1 in modifying susceptibility to type 1 diabetes. *Nat Genet* 38:479-483.
108. Furnari, F. B., T. Fenton, R. M. Bachoo, A. Mukasa, J. M. Stommel, A. Stegh, W. C. Hahn, K. L. Ligon, D. N. Louis, C. Brennan, L. Chin, R. A. DePinho,

- and W. K. Cavenee. 2007. Malignant astrocytic glioma: genetics, biology, and paths to treatment. *Genes Dev* 21:2683-2710.
109. McCarty, J. H., R. A. Monahan-Earley, L. F. Brown, M. Keller, H. Gerhardt, K. Rubin, M. Shani, H. F. Dvorak, H. Wolburg, B. L. Bader, A. M. Dvorak, and R. O. Hynes. 2002. Defective associations between blood vessels and brain parenchyma lead to cerebral hemorrhage in mice lacking α v integrins. *Mol Cell Biol* 22:7667-7677.
 110. Mu, Z., Z. Yang, D. Yu, Z. Zhao, and J. S. Munger. 2008. TGF β 1 and TGF β 3 are partially redundant effectors in brain vascular morphogenesis. *Mech Dev* 125:508-516.
 111. Hall, P. E., J. D. Lathia, M. A. Caldwell, and C. French-Constant. 2008. Laminin enhances the growth of human neural stem cells in defined culture media. *BMC Neurosci* 9:71.
 112. Mori, T., A. Buffo, and M. Gotz. 2005. The novel roles of glial cells revisited: the contribution of radial glia and astrocytes to neurogenesis. *Curr Top Dev Biol* 69:67-99.
 113. Stipursky, J., and F. C. Gomes. 2007. TGF- β 1/SMAD signaling induces astrocyte fate commitment in vitro: implications for radial glia development. *Glia* 55:1023-1033.
 114. Liu, X., A. Clements, K. Zhao, and R. Marmorstein. 2006. Structure of the human Papillomavirus E7 oncoprotein and its mechanism for inactivation of the retinoblastoma tumor suppressor. *J Biol Chem* 281:578-586.

115. Uhrbom, L., C. Dai, J. C. Celestino, M. K. Rosenblum, G. N. Fuller, and E. C. Holland. 2002. Ink4a-Arf loss cooperates with KRas activation in astrocytes and neural progenitors to generate glioblastomas of various morphologies depending on activated Akt. *Cancer Res* 62:5551-5558.
116. Uchida, N., D. W. Buck, D. He, M. J. Reitsma, M. Masek, T. V. Phan, A. S. Tsukamoto, F. H. Gage, and I. L. Weissman. 2000. Direct isolation of human central nervous system stem cells. *Proc Natl Acad Sci U S A* 97:14720-14725.
117. O'Brien, C. A., A. Pollett, S. Gallinger, and J. E. Dick. 2007. A human colon cancer cell capable of initiating tumour growth in immunodeficient mice. *Nature* 445:106-110.
118. Bachoo, R. M., E. A. Maher, K. L. Ligon, N. E. Sharpless, S. S. Chan, M. J. You, Y. Tang, J. DeFrances, E. Stover, R. Weissleder, D. H. Rowitch, D. N. Louis, and R. A. DePinho. 2002. Epidermal growth factor receptor and Ink4a/Arf: convergent mechanisms governing terminal differentiation and transformation along the neural stem cell to astrocyte axis. *Cancer Cell* 1:269-277.
119. Sonoda, Y., T. Ozawa, K. D. Aldape, D. F. Deen, M. S. Berger, and R. O. Pieper. 2001. Akt pathway activation converts anaplastic astrocytoma to glioblastoma multiforme in a human astrocyte model of glioma. *Cancer Res* 61:6674-6678.
120. Sonoda, Y., M. Kanamori, D. F. Deen, S. Y. Cheng, M. S. Berger, and R. O. Pieper. 2003. Overexpression of vascular endothelial growth factor isoforms

- drives oxygenation and growth but not progression to glioblastoma multiforme in a human model of gliomagenesis. *Cancer Res* 63:1962-1968.
121. Adams, R. H., and K. Alitalo. 2007. Molecular regulation of angiogenesis and lymphangiogenesis. *Nat Rev Mol Cell Biol* 8:464-478.
 122. Benjamin, L. E., and E. Keshet. 1997. Conditional switching of vascular endothelial growth factor (VEGF) expression in tumors: induction of endothelial cell shedding and regression of hemangioblastoma-like vessels by VEGF withdrawal. *Proc Natl Acad Sci U S A* 94:8761-8766.
 123. Khalil, N. 1999. TGF-beta: from latent to active. *Microbes Infect* 1:1255-1263.
 124. Aluwihare, P., Z. Mu, Z. Zhao, D. Yu, P. H. Weinreb, G. S. Horan, S. M. Violette, and J. S. Munger. 2009. Mice that lack activity of α v β 6- and α v β 8-integrins reproduce the abnormalities of Tgfb1- and Tgfb3-null mice. *J Cell Sci* 122:227-232.
 125. Massague, J. 2008. TGFbeta in Cancer. *Cell* 134:215-230.
 126. Oka, N., A. Soeda, A. Inagaki, M. Onodera, H. Maruyama, A. Hara, T. Kunisada, H. Mori, and T. Iwama. 2007. VEGF promotes tumorigenesis and angiogenesis of human glioblastoma stem cells. *Biochem Biophys Res Commun* 360:553-559.
 127. Ramsauer, M., and P. A. D'Amore. 2007. Contextual role for angiopoietins and TGFbeta1 in blood vessel stabilization. *J Cell Sci* 120:1810-1817.
 128. Petersen, M., E. Pardali, G. van der Horst, H. Cheung, C. van den Hoogen, G. van der Pluijm, and P. Ten Dijke. Smad2 and Smad3 have opposing roles

- in breast cancer bone metastasis by differentially affecting tumor angiogenesis. *Oncogene* 29:1351-1361.
129. McCarty, J. H., M. Barry, D. Crowley, R. T. Bronson, A. Lacy-Hulbert, and R. O. Hynes. 2008. Genetic ablation of α v integrins in epithelial cells of the eyelid skin and conjunctiva leads to squamous cell carcinoma. *Am J Pathol* 172:1740-1747.
 130. Bogler, O., H. J. Huang, and W. K. Cavenee. 1995. Loss of wild-type p53 bestows a growth advantage on primary cortical astrocytes and facilitates their in vitro transformation. *Cancer Res* 55:2746-2751.
 131. Giese, A., B. Laube, S. Zapf, U. Mangold, and M. Westphal. 1998. Glioma cell adhesion and migration on human brain sections. *Anticancer Res* 18:2435-2447.
 132. Conti, J. A., T. J. Kendall, A. Bateman, T. A. Armstrong, A. Papa-Adams, Q. Xu, G. Packham, J. N. Primrose, R. C. Benyon, and J. P. Iredale. 2008. The desmoplastic reaction surrounding hepatic colorectal adenocarcinoma metastases aids tumor growth and survival via α v integrin ligation. *Clin Cancer Res* 14:6405-6413.
 133. Liu, B., D. Tian, W. Yi, L. Wu, Q. Cai, H. Dong, H. Shen, B. Ji, L. Wang, S. Zhang, D. Ruan, and Q. Chen. Effect of Bone Morphogenetic Protein 4 in the Human Brain Glioma Cell Line U251. *Cell Biochem Biophys*.
 134. Schittenhelm, J., M. Mittelbronn, T. D. Nguyen, R. Meyermann, and R. Beschorner. 2008. WT1 expression distinguishes astrocytic tumor cells from normal and reactive astrocytes. *Brain Pathol* 18:344-353.

135. Bonnet, D., and J. E. Dick. 1997. Human acute myeloid leukemia is organized as a hierarchy that originates from a primitive hematopoietic cell. *Nat Med* 3:730-737.
136. Ricci-Vitiani, L., D. G. Lombardi, E. Pilozzi, M. Biffoni, M. Todaro, C. Peschle, and R. De Maria. 2007. Identification and expansion of human colon-cancer-initiating cells. *Nature* 445:111-115.
137. Prince, M. E., R. Sivanandan, A. Kaczorowski, G. T. Wolf, M. J. Kaplan, P. Dalerba, I. L. Weissman, M. F. Clarke, and L. E. Ailles. 2007. Identification of a subpopulation of cells with cancer stem cell properties in head and neck squamous cell carcinoma. *Proc Natl Acad Sci U S A* 104:973-978.
138. Singh, S. K., C. Hawkins, I. D. Clarke, J. A. Squire, J. Bayani, T. Hide, R. M. Henkelman, M. D. Cusimano, and P. B. Dirks. 2004. Identification of human brain tumour initiating cells. *Nature* 432:396-401.
139. Yang, Z. J., and R. J. Wechsler-Reya. 2007. Hit 'em where they live: targeting the cancer stem cell niche. *Cancer Cell* 11:3-5.
140. Miller, F. D., and A. Gauthier-Fisher. 2009. Home at last: neural stem cell niches defined. *Cell Stem Cell* 4:507-510.
141. Tan, B. T., C. Y. Park, L. E. Ailles, and I. L. Weissman. 2006. The cancer stem cell hypothesis: a work in progress. *Lab Invest* 86:1203-1207.
142. Skuli, N., S. Monferran, C. Delmas, G. Favre, J. Bonnet, C. Toulas, and E. Cohen-Jonathan Moyal. 2009. α 3 β 5 integrins-FAK-RhoB: a novel pathway for hypoxia regulation in glioblastoma. *Cancer Res* 69:3308-3316.

143. Cheng, J. X., B. L. Liu, and X. Zhang. 2009. How powerful is CD133 as a cancer stem cell marker in brain tumors? *Cancer Treat Rev* 35:403-408.
144. Singh, S. K., I. D. Clarke, M. Terasaki, V. E. Bonn, C. Hawkins, J. Squire, and P. B. Dirks. 2003. Identification of a cancer stem cell in human brain tumors. *Cancer Res* 63:5821-5828.
145. Pohl, A., G. Lurje, M. Kahn, and H. J. Lenz. 2008. Stem cells in colon cancer. *Clin Colorectal Cancer* 7:92-98.
146. Woodward, W. A., and E. P. Sulman. 2008. Cancer stem cells: markers or biomarkers? *Cancer Metastasis Rev* 27:459-470.
147. Nilsson, C. L., R. Dillon, A. Devakumar, S. D. Shi, M. Greig, J. C. Rogers, B. Krastins, M. Rosenblatt, G. Kilmer, M. Major, B. J. Kaboord, D. Sarracino, T. Rezai, A. Prakash, M. Lopez, Y. Ji, W. Priebe, F. F. Lang, H. Colman, and C. A. Conrad. Quantitative phosphoproteomic analysis of the STAT3/IL-6/HIF1alpha signaling network: an initial study in GSC11 glioblastoma stem cells. *J Proteome Res* 9:430-443.
148. Rich, J. N., C. Guo, R. E. McLendon, D. D. Bigner, X. F. Wang, and C. M. Counter. 2001. A genetically tractable model of human glioma formation. *Cancer Res* 61:3556-3560.
149. Zheng, H., H. Ying, H. Yan, A. C. Kimmelman, D. J. Hiller, A. J. Chen, S. R. Perry, G. Tonon, G. C. Chu, Z. Ding, J. M. Stommel, K. L. Dunn, R. Wiedemeyer, M. J. You, C. Brennan, Y. A. Wang, K. L. Ligon, W. H. Wong, L. Chin, and R. A. DePinho. 2008. p53 and Pten control neural and glioma stem/progenitor cell renewal and differentiation. *Nature* 455:1129-1133.

150. Tavazoie, M., L. Van der Veken, V. Silva-Vargas, M. Louissaint, L. Colonna, B. Zaidi, J. M. Garcia-Verdugo, and F. Doetsch. 2008. A specialized vascular niche for adult neural stem cells. *Cell Stem Cell* 3:279-288.
151. Guo, W., and F. G. Giancotti. 2004. Integrin signalling during tumour progression. *Nat Rev Mol Cell Biol* 5:816-826.
152. Derynck, R., R. J. Akhurst, and A. Balmain. 2001. TGF-beta signaling in tumor suppression and cancer progression. *Nat Genet* 29:117-129.
153. Wick, W., M. Platten, and M. Weller. 2001. Glioma cell invasion: regulation of metalloproteinase activity by TGF-beta. *J Neurooncol* 53:177-185.
154. Dunlap, S. M., J. Celestino, H. Wang, R. Jiang, E. C. Holland, G. N. Fuller, and W. Zhang. 2007. Insulin-like growth factor binding protein 2 promotes glioma development and progression. *Proc Natl Acad Sci U S A* 104:11736-11741.

Vita

Jeremy Hatem Tchaïcha was born in Paris, France, on March 10, 1980, the son of Josef Pavlic and Jane Tchaïcha. After graduating from Needham High School in Needham, Massachusetts in May 1998, he began his undergraduate studies at Lafayette College in Easton, Pennsylvania. In May 2002, he graduated with his Bachelor of Science degree in Biology. Shortly after undergraduate school, Jeremy worked at Pfizer Inc., in the protein biochemistry department followed by a two-year tenure at Merrimack Pharmaceuticals in Cambridge, MA. In August 2005, Jeremy entered the Ph.D. graduate program at the University of Texas Health Science Center at the Houston Graduate School of Biomedical Sciences. In May 2006, he joined the laboratory of Dr. Joseph H. McCarty at the University of Texas M.D. Anderson Cancer Center to study the role of $\alpha\beta 8$ integrin in glioma-induced angiogenesis.